

LENS - European Laboratory for Non-linear Spectroscopy  
Università degli studi di Firenze



PhD Thesis  
in Atomic and molecular spectroscopy

XXIV Cycle - FIS/03

## **Experiments with interacting bosons in a disordered lattice**

Presented by:

Eleonora Lucioni

*Supervisor:* Prof. Giovanni Modugno

*Coordinator:* Prof. Francesco Pavone



*A Elio, il mio papà.*



# Contents

<b>Introduction</b>	<b>1</b>
<b>1 Bosonic atoms in disordered optical lattices: tuning the interactions</b>	<b>5</b>
1.1 The Bose Hubbard model . . . . .	6
1.1.1 Introducing disorder . . . . .	9
1.2 Anderson Localization . . . . .	10
1.3 Delocalization by weak interaction . . . . .	12
1.4 Mott insulator . . . . .	15
1.5 Bose glass . . . . .	20
<b>2 A <math>^{39}\text{K}</math> Bose-Einstein condensate with tunable interaction in a quasiperiodic potential</b>	<b>25</b>
2.1 Optical lattices . . . . .	26
2.1.1 Lattice calibration: Raman-Nath spectroscopy . . . . .	28
2.2 Interaction energy in a Bose-Einstein condensate . . . . .	31
2.2.1 Tuning the interactions: Feshbach resonances . . . . .	31
2.3 Disordered optical potential . . . . .	34
2.3.1 Quasiperiodic lattice . . . . .	35
2.4 Experimental realization of the $^{39}\text{K}$ BEC with tunable interaction	38
2.5 Imaging techniques . . . . .	41
2.5.1 In situ images . . . . .	42
2.5.2 Time of flight images . . . . .	43
2.6 One-dimensional systems . . . . .	44
2.6.1 1D optical lattice on a 3D BEC . . . . .	46
2.6.2 Three-Dimensional optical lattice . . . . .	47
<b>3 Experimental investigation of weakly-interacting bosons in a dis- ordered lattice</b>	<b>49</b>

---

3.1	Observed disordered regime: from the localized to the superfluid phase . . . . .	50
3.1.1	Experimental procedure . . . . .	51
3.1.2	Local shape of the wavefunction . . . . .	55
3.1.3	Phase fluctuations . . . . .	57
3.1.4	Correlation properties . . . . .	59
3.2	Subdiffusive expansion in the disordered lattice . . . . .	62
3.2.1	Perturbative model . . . . .	68
3.2.2	Numerical simulations for the quasiperiodic potential . . . . .	73
3.2.3	Finite temperature and radial degrees of freedom effect . . . . .	76
3.2.4	Time evolution of the density profiles . . . . .	80
3.3	Noise-induced delocalization . . . . .	87
3.3.1	Non-interacting diffusive expansion . . . . .	89
3.3.2	Combined effect of noise and weak interactions . . . . .	92
<b>4</b>	<b>Experimental investigation of strongly-interacting bosons in a disordered lattice</b>	<b>97</b>
4.1	Experimental realization of the one-dimensional system with tunable interactions . . . . .	98
4.2	Correlation measurements . . . . .	101
4.2.1	Analysis of the momentum distributions . . . . .	101
4.2.2	$\Delta - U$ Phase diagram . . . . .	105
4.3	Transport measurements . . . . .	111
4.4	Excitation spectra measurements . . . . .	113
	<b>Conclusions</b>	<b>119</b>
	<b>Bibliography</b>	<b>123</b>

# Introduction

The interplay between disorder and interactions lies at the heart of many physical phenomena and its study has recently attracted more and more interest. Although it is present in any real physical system, disorder is difficult to control, to tune, and therefore to study. Even more challenging is the investigation of the combined effect of disorder and interactions. The possibility of tuning independently and in a large range of values these two parameters, is in fact a rare feature for both real and experimental systems.

Since the first experimental realization of a degenerate atomic quantum gas, they have revealed to be extremely versatile tools and have provided important contributions in many physical areas. In particular the possibility to trap ultracold atoms in perfectly periodical potentials by means of optical lattices, has allowed the experimental study of fundamental problems related to condensed matter physics.

During the last few years, experiments with Bose-Einstein condensates have also produced remarkable results in the field of the physics of disorder. Laser light can in fact provide, not only an ideal lattice, but also a controllable and tunable disordered potential. Furthermore in ultracold atomic gases, by means of Feshbach resonances, it is also possible to tune the interparticle interaction in a wide range of strengths. This gives the possibility to manage non-interacting, weakly interacting and strongly correlated samples.

In the experiments reported in this thesis, a degenerate Bose gas of Potassium-39 atoms is employed to investigate the different quantum phases arising from the complex competition between disorder and interactions. We performed our studies on both the equilibrium and the transport properties of the system. In the weakly interacting regime we detected and characterized the crossover from Anderson glass, to weakly-interacting Bose glass to superfluid by analyzing, in particular, the correlation properties of the atomic wavefunction. We then studied the expansion dynamics of the atomic cloud in the disordered potential when either

interactions or dynamical noise are present in the system. Anomalous diffusion evidences are shown. In the strongly-correlated regime we studied the correlation and transport properties and the excitation spectra of the system aiming to experimentally characterize the Bose glass phase. We provide the first full experimental phase diagram which shows a complex structure with different insulating and non-insulating regions for a wide range of disorder and interaction.

In the following we briefly summarize the structure of the thesis. In the first chapter we introduce the disordered Bose-Hubbard model to describe (interacting) bosonic atoms in a (disordered) optical lattice. We then consider the different regimes that the system undergoes when varying the relative strength of interaction and disorder. We describe the features of the different quantum phases and we report and discuss the main experiments with ultracold atoms so far performed in the different regimes.

In the second chapter we introduce the main ingredients that characterize the experimental realization of the tunable disordered system. The chapter opens in fact with showing how the lattice potential is realized and characterized. After a short description of the broad magnetic Feshbach resonance that allows to finely tune interactions between Potassium atoms, we then turn to describe the disordered potential. Disorder is provided by a quasiperiodic lattice obtained by the superposition over the main lattice of a weaker incommensurate secondary lattice. The height of the secondary lattice determines the disorder strength. We then briefly summarize the experimental sequence to produce the Bose-Einstein condensate and, since we aim to study a one-dimensional disordered lattice, we describe how we produce a one-dimensional system. The chapter ends with a short description of the detection image techniques.

The third and the fifth chapters of the thesis report the experimental results. In the third chapter we concentrate on the weakly interacting regime. Weak repulsive interactions serve to screen the disordered potential and the system undergoes a crossover from a disordered-induced localized phase (Anderson glass) to a superfluid one. This crossover is experimentally characterized by considering the local shape of the wavefunction and its correlation properties. We show that in the non-interacting situation the wavefunctions are localized and no coherence is observed. By adding controlled weakly interactions we gradually restore coherence over the entire system and the wavefunctions result to be extended. The second part of the chapter is devoted to the study of the dynamical properties. We characterize the expansion dynamics of the atomic cloud in the quasiperiodic potential. In the non-interacting case localization results in absence of expansion. Conversely,

---

when a weak interaction between atoms is added, a slow expansion is observed. We provide the first experimental observation of the subdiffusive expansion of a wavepacket in a non-linear disordered potential. We also extend the study of the out of equilibrium expansion to the case in which the potential is perturbed by a controlled temporal noise. Noise destroys disorder induced localization resulting in a diffusive expansion. The combination of weakly interaction and noise is also studied.

In the last chapter we report the experiments performed in the strongly correlated regime. In absence of disorder the system undergoes the transition from a superfluid phase to an interaction induced insulator (Mott insulator). When disorder is added, cooperation between disorder and interactions results in a new glassy phase (Bose glass). This phase is characterized by the presence of islands of superfluid not connected together. This results in a globally insulating phase with a gapless excitation spectrum conversely to the Mott insulator phase. Exploiting the possibility to independently tune disorder and interactions over a large range of parameters, we trace a complete phase diagram of the system measuring the correlation length of the atomic wavefunction. The crossovers between superfluid and insulator phases is also confirmed by transport measurements. Preliminary measurements of the excitation spectrum of the system are also presented.



## Chapter 1

# Bosonic atoms in disordered optical lattices: tuning the interactions

During the last years experiments with cold atoms have offered new possibilities to understand the physics of interacting quantum particles in the presence of disorder. Using laser light it is in fact possible to shape conservative potentials for neutral atoms at will, exploiting the dipole interaction between atoms and the electromagnetic field. In particular a standing wave provides a perfect periodical potential and different possibilities have been found to engineer disordered potential in a very controllable way. Also the two-body interaction in a dilute cold atom sample is easy to model and, for some atomic species, to tune.

We will provide more details about optical potentials and interactions between atoms in the next chapter. In this chapter we derive the Hamiltonian which describes interacting bosonic atoms in periodic potential following the *Bose-Hubbard model*. We show how it is possible, in the same framework, to model also disordered systems. We then analyze the regimes in which disorder or interaction dominate and determine the physical properties of the system showing some results obtained in the cold atoms field. The regimes in which both interaction and disorder are relevant in determining the atomic behavior are finally considered. Also in this context we show how experiments with cold atoms are giving a strong contribution to better understand the interplay between disorder and interactions.

## 1.1 The Bose Hubbard model

The quantum state of interacting bosonic atoms in a periodic potential can be described [1, 2] by the second quantization Hamiltonian for the boson field operator  $\hat{\psi}$ <sup>1</sup>:

$$\hat{H} = \int dr \hat{\psi}^\dagger \left[ -\frac{\hbar^2 \nabla^2}{2m} + V_{ext}(r) + V_L \right] \hat{\psi} + \frac{g}{2} \int dr \hat{\psi}^\dagger \hat{\psi}^\dagger \hat{\psi} \hat{\psi} \quad (1.1)$$

where  $g$  is the non-linear coupling term which quantifies the interaction strength between two particles. The two-body interaction potential can in fact be written in terms of a contact pseudo-potential:

$$v(r - r') = g \delta(r - r') \quad \text{with} \quad g = \frac{4\pi\hbar^2}{m} a \quad (1.2)$$

where  $a$  is the s-wave scattering length and  $m$  is the atomic mass.  $V_{ext}$  is a generic external potential superimposed on the periodic one,  $V_L$ , that in cold atoms experiments is usually provided by an optical lattice and it is of the form:

$$V_L(r) = V_0 \sin^2(kr). \quad (1.3)$$

As we will better describe in the next chapter, using laser light it is possible to create potentials for neutral atoms by exploiting the dipole interaction between the atom and the electromagnetic field. In particular an optical lattice of the form given by Eq.(1.3) is obtained with a stationary wave created by a retroreflected laser beam with wavevector  $k = 2\pi/\lambda$ . The periodicity of the potential is therefore  $d = \lambda/2$ . More details on how the lattice is created and characterized in the experiment are given in the next chapter (section 2.1).

According to the Bloch theorem the wavefunctions of a particle moving in a periodic potential correspond to plane waves  $e^{iqr}$  modulated by a function  $u_{n,q}(r)$  having the same periodicity  $d$  of the potential:

$$\psi_{n,q}(r) = e^{iqr} u_{n,q}(r) \quad \text{with} \quad u_{n,q}(r) = u_{n,q}(r + d). \quad (1.4)$$

The Bloch functions  $\psi_{n,q}(r)$  are labeled by two quantum numbers:  $n$  that is the band index, and  $q$  that indicates the quasi-momentum of the particle. We limit the description of the system at the first band (*single band approximation*). In the following we thus fix  $n = 1$  and omit the  $n$  index. In cold atoms experiments the energies involved in the system, starting from the temperature, are small enough to not induce inter-band excitation, therefore this approximation applies. In the

---

<sup>1</sup>The normalization of the field operator is given by:  $\int dr \hat{\psi}^\dagger \hat{\psi} = N_{tot}$ , where  $N_{tot}$  is the total number of particle in the system.

weak potential limit the Bloch functions are almost plane waves. As the potential depth  $V_0$  increases they become more and more localized around the lattice sites. In this regime, which is known as *tight binding regime*, it is thus convenient to express the Bloch wavefunctions as a sum of orthogonal and normalized set of wavefunctions maximally localized at each lattice site:

$$\psi_q(r) = \sum_j e^{iqr_j} w(r - r_j) \quad (1.5)$$

where  $j$  is the lattice site index.  $w(r - r_j) = w_j(r)$  is the *Wannier function* localized at  $j$ -th site. The Wannier functions are usually well approximated by a Gaussian function and form a orthonormal basis:

$$\int dr w_j^*(r) w_{j'}(r) = \delta_{jj'} \quad (1.6)$$

The field operator  $\hat{\psi}$  in Eq.(1.1) can thus be written as the superposition of Wannier function localized at the lattice sites:

$$\hat{\psi}(r) \equiv \sum_j \hat{a}_j w_j(r) \quad (1.7)$$

being  $\hat{a}_j$  the annihilation operator of one boson at the  $j$ -th site which satisfies the canonical commutation relation:  $[\hat{a}_j^\dagger, \hat{a}_{j'}] = \delta_{jj'}$ . This kind of description is very convenient when one wants to describe atom-atom on-site interactions. Using Eq.(1.7) we can rewrite the Hamiltonian in Eq.(1.1) in the following way:

$$\begin{aligned} \hat{H} = & \int dr \sum_j \hat{a}_j^\dagger w_j^*(r) \left[ -\frac{\hbar^2 \nabla^2}{2m} + V_L(r) + V_{ext}(r) \right] \sum_{j'} \hat{a}_{j'} w_{j'}(r) \\ & + \frac{g}{2} \sum_{jj' ll'} \hat{a}_j^\dagger \hat{a}_l^\dagger \hat{a}_{j'} \hat{a}_{l'} \int dr w_j^*(r) w_l^*(r) w_{l'}(r) w_{j'}(r) \end{aligned} \quad (1.8)$$

We can define:

$$\hat{H} = \hat{H}_L + \hat{H}_{ext} + \hat{H}_{int} \quad (1.9)$$

with

$$\hat{H}_L = \sum_{jj'} \hat{a}_j^\dagger \hat{a}_{j'} \int dr w_j^*(r) \left[ -\frac{\hbar^2 \nabla^2}{2m} + V_L(x) \right] w_{j'}(r) \quad (1.10)$$

$$\hat{H}_{ext} = \sum_{jj'} \hat{a}_j^\dagger \hat{a}_{j'} \int dr w_j^*(r) V_{ext}(x) w_{j'}(r) \quad (1.11)$$

$$\hat{H}_{int} = \frac{g}{2} \sum_{jj' ll'} \hat{a}_j^\dagger \hat{a}_l^\dagger \hat{a}_{j'} \hat{a}_{l'} \int dr w_j^*(r) w_l^*(r) w_{l'}(r) w_{j'}(r) \quad (1.12)$$

We now consider one by one the terms here defined and simplify them by applying appropriate approximations. Let us start with the term given by the

external potential. We can take into account a potential which varies smoothly across the lattice such that it can be assumed to be constant on the lattice site distance. In this approximation we can define  $\epsilon_j$  to be the external potential inside the  $j$ -th site and rewrite Eq.(1.11):

$$\begin{aligned}\hat{H}_{ext} &\simeq \sum_{jj'} \hat{a}_j^\dagger \hat{a}_{j'} V_{ext}(r_j) \int dr w_j^*(r) w_{j'}(r) = \\ &= \sum_{jj'} \epsilon_j \hat{a}_j^\dagger \hat{a}_{j'} \delta_{jj'} = \sum_j \epsilon_j \hat{a}_j^\dagger \hat{a}_j = \\ &= \sum_j \epsilon_j \hat{n}_j\end{aligned}\tag{1.13}$$

where we define the number operator  $n_j = \hat{a}_j^\dagger \hat{a}_j$  which gives the number of particles at the  $j$ -th lattice site.

Let us now consider the term given by the lattice potential. Here we can consider the tight binding regime neglecting the superposition of the Wannier functions centered more than one lattice site apart and write:

$$\hat{H}_L \simeq \epsilon_0 \sum_j \hat{n}_j - J \sum_{\langle j, j' \rangle} \hat{a}_j^\dagger \hat{a}_{j'}\tag{1.14}$$

where the symbol  $\langle j, j' \rangle$  indicates that the sum has to be considered only between the first neighbor sites. The single site energy  $\epsilon_0$  is constant for all the lattice sites and it is given by the this expression:

$$\epsilon_0 = \int dr w_j^*(r) \left[ -\frac{\hbar^2 \nabla^2}{2m} + V_L(x) \right] w_j(r)\tag{1.15}$$

The *tunneling energy*  $J$  is essentially the superposition of the Wannier function centered in two neighboring lattice sites  $j$  and  $j'$ :

$$J = - \int dr w_j^*(r) \left[ -\frac{\hbar^2 \nabla^2}{2m} + V_L(x) \right] w_{j'}(r).\tag{1.16}$$

$J$  represents the energy scale for the kinetic energy of the particles in the lattice. The energy dispersion given by the lattice potential is indeed  $\epsilon(q) = -2J \cos(qd)$ .

We finally consider the term due to the interaction between particles. Since the interaction is local, we need to consider only the on-site interaction term. The Wannier functions  $w_j$  are all identical except that they are centered in different lattice sites. We thus have:

$$\begin{aligned}\hat{H}_{int} &\simeq \sum_j \hat{a}_j^\dagger \hat{a}_j^\dagger \hat{a}_j \hat{a}_j \frac{g}{2} \int dr |w_j(r)|^4 \\ &= \frac{U}{2} \sum_j \hat{a}_j^\dagger \hat{a}_j^\dagger \hat{a}_j \hat{a}_j\end{aligned}\tag{1.17}$$

where we defined

$$U = g \int dr |w(r)|^4. \quad (1.18)$$

$U$  quantifies the strength of the interaction in the system and gives the second important energy scale. By using the canonical commutation relation we can rewrite the interaction Hamiltonian in term of the number operator:

$$\hat{H}_{int} = \frac{U}{2} \sum_j \hat{n}_j(\hat{n}_j - 1). \quad (1.19)$$

We can now put the three terms together obtaining the well known Bose-Hubbard Hamiltonian:

$$\hat{H}_{BH} = -J \sum_{\langle j,j' \rangle} \hat{a}_j^\dagger \hat{a}_{j'} + \sum_j (\epsilon_0 + \epsilon_j) \hat{n}_j + \frac{U}{2} \sum_j \hat{n}_j(\hat{n}_j - 1). \quad (1.20)$$

### 1.1.1 Introducing disorder

In this framework of the Bose-Hubbard Hamiltonian it is also possible to model a disordered system. The presence of a disordered external potential can in fact be taken into account. Disorder can in principle affect each of the three terms of the Hamiltonian. In general one could consider the strength of the on-site repulsion, the hopping term between neighboring sites and the on-site energy changing in a disordered way from site to site. In this work we will consider only the effect of a disordered energetic landscape below the regular optical lattice. In this case one can see that if the lattice is deep enough and the disorder potential is not too strong the Wannier function shape and the position of the lattice wells are not perturbed too much by the presence of the disorder:  $J$  and  $U$  can thus be taken as constant. We can therefore assume only  $\epsilon_j$ , the on-site energy given by the external potential, to vary in a disordered way across the lattice. We can thus rewrite the Hamiltonian in the following way<sup>2</sup>:

$$\hat{H}_{DBH} = -J \sum_{\langle j,j' \rangle} \hat{a}_j^\dagger \hat{a}_{j'} + \Delta \sum_j e_j \hat{n}_j + \frac{U}{2} \sum_j \hat{n}_j(\hat{n}_j - 1). \quad (1.21)$$

where  $\epsilon_j = \Delta e_j$  changes from site to site. Here  $\Delta$  represents the characteristic energy of the disorder and  $e_j$  is a number in the interval  $[-1,1]$ . The actual distribution of  $\epsilon_j$  across the lattice depends on the details of the disorder. As we will see in the following, details like the energy distribution of the  $\epsilon_j$  or their spatial correlation properties affect in a very strong way the exact behavior of the system.

---

<sup>2</sup>Here we omit the  $\epsilon_0$  term, since it is constant and does not change the properties of the system.

From the interplay between the kinetic energy, the interaction energy and the disorder strength, quantified in this picture respectively by  $J$ ,  $U$  and  $\Delta$ , many interesting phenomena appear in a physical system. In some circumstances one of these energies dominates over the other ruling the behavior of the particles. In more intriguing cases they have comparable strength and compete or cooperate in determining the different quantum phases and dynamical properties of the system. Cold atoms experiments offer the possibility to control with high degree of tunability the three terms independently. In the following we consider different regimes when varying the amplitude of the three terms and, in each case, we trace the main properties of the system.

## 1.2 Anderson Localization

Let us start by considering the case of non interacting particles ( $U = 0$ ) and analyzing the effect of the presence of disorder on the wavefunction and on the transport properties of bosons in a lattice. The quantum transport properties of a system are intimately related to the underlying symmetries of the Hamiltonian. In a perfect periodic system all the eigenstate are extended Bloch waves and the system is in a conducting phase. For a random potential, where there is no trace of translational symmetry, we instead expect to have an opposite behavior. The eigenfunction of the particles are expected to be localized and the transport inhibited. The very interesting and general phenomenon of localization of particles and waves in random media was first studied by P.A. Anderson in 1958 [3]. Anderson studied the transport of generic “entities”, originally electrons, in a crystal by using a single particle tight-binding model with random on site energy similar to the one introduced in the previous section in the case of non-interacting particles. Nevertheless Anderson localization is a wave phenomenon which relies on destructive interference of several multiple scattering paths which results in absence of diffusion and in wavefunctions exponentially localized in space. The Anderson’s idea has thus been extended to electromagnetic waves and many experiments have been performed over the last twenty years [4, 5, 6, 7].

Going back to the case of particles, we can use the Hamiltonian (1.21) to describe the disordered system. If we consider the non-interacting case it takes the form:

$$\hat{H}_A = -J \sum_{\langle j,j' \rangle} \hat{a}_j^\dagger \hat{a}_{j'} + \Delta \sum_j e_j \hat{n}_j, \quad (1.22)$$

being  $e_j$  a number which randomly varies in the interval  $[-1,1]$  from site to site.

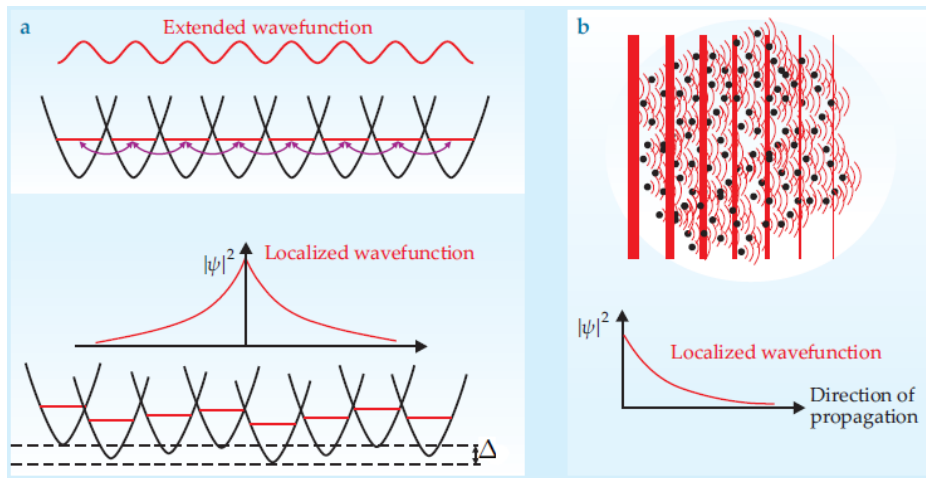


Figure 1.1: Schematic representation of the Anderson localization phenomenon [8]. Anderson localization can be thought in term of tunneling of particle (a). In an ordered lattice particles are allowed to tunnel between neighboring sites and freely propagate across the lattice. If the regularity of the lattice is broken by randomly changing the depth of the potential at each lattice site, tunneling is suppressed and particle become localized with an exponential decaying wavefunction. From another point of view, Anderson localization can also be understood in term of destructive interference of waves propagating in a medium with large concentration of randomly distributed scatterers (b).

Already in his original work, Anderson showed that the transport, i.e. the diffusion of an initially localized wavepacket, is suppressed if the disordered amplitude  $\Delta$  exceeds a critical value of the order of the tunneling energy  $J$ . The original studies by Anderson were performed for a three-dimensional lattice. In one-dimension, in the case of a pure random potential, all the eigenstates are localized for any value of the disorder  $\Delta$ . On the contrary, in the case in which the disordered potential has non-vanishing spatial correlations, the system shows a transition from extended to localized states for a finite value of  $\Delta$  similar to what occurs in pure random three-dimensional systems. Anderson localization can be thought as both a disordered induced suppression of the tunneling of particle across a lattice and a destructive interference of waves as schematically represented in Fig.1.1.

The first observation of Anderson localization of matter waves either in a random potential [9] or in a perturbed periodic potential (quasiperiodic lattice) [10, 11] has been achieved in 2008 in two complementary experiments with bosonic ultracold atoms. Both experiments showed the suppression of the matter transport across the system due to disorder and the exponential shape of the tails the atomic spatial distribution as shown in Fig.1.2. These experiments have been performed in one-dimensional disordered potential. More recent experiments ob-

served Anderson localization in the three-dimensional case [12, 13].

When the disorder can be neglected, and the kinetic energy is the dominant energy term, each atom is free to move from site to site across the lattice, i.e. each atom is delocalized throughout the lattice and the system is *superfluid*. As already pointed out, the ground state in this case is a Bloch wave and can be written as the superposition  $\sum_j \hat{a}_j^\dagger |0\rangle$  of the Wannier functions with the same phase. If we consider  $N$  atoms we can write the many-body state as the product of identical single-particle states,

$$|\psi_{SF}\rangle \propto \left(\sum_j \hat{a}_j^\dagger\right)^N |0\rangle \quad (1.23)$$

and can thus be described by a single macroscopic wavefunction, which is equivalent to a coherent state whose phase is well defined and constant across the lattice. As a consequence the momentum distribution of the atoms in the lattice is characterized by narrow peaks  $2\hbar k_1$  apart. When disorder is introduced particles begin to localize in certain lattice site and there is no more coherence across the whole lattice. This results in a broadening of the momentum distribution. Roughly speaking a localization in the real space corresponds to a “delocalization” in the momentum space. The experimental observation by Roati *et al.* [10] of the broadening of the momentum distribution for increasing disorder strength is shown in Fig.1.3.

### 1.3 Delocalization by weak interaction

The presence of interaction between particles can strongly affect the system and in particular can destroy the disorder induced localization. For this reason Anderson localization has never been observed in atomic crystals, where electron-electron interaction represent a deviation from the Anderson model and prevent the system from localizing. Here we take into account the situation in which a repulsive interaction is introduced between the particles in a system that is localized by disorder. It is known that interactions themselves can induce the localization of each particle in a certain lattice site suppressing the tunneling from site to site. This happens when interactions are strong enough to overcome kinetic energy. We describe this situation, called *Mott insulator* phase, in the next section. Instead we now consider the case  $U < J$ . What is interesting in this situation is the competing effect of the disorder which tends to localize the bosons in the absolute lowest energy state and the weak repulsive interaction which can counteract this effect drastically changing the feature of the system. In particular a weak repulsion

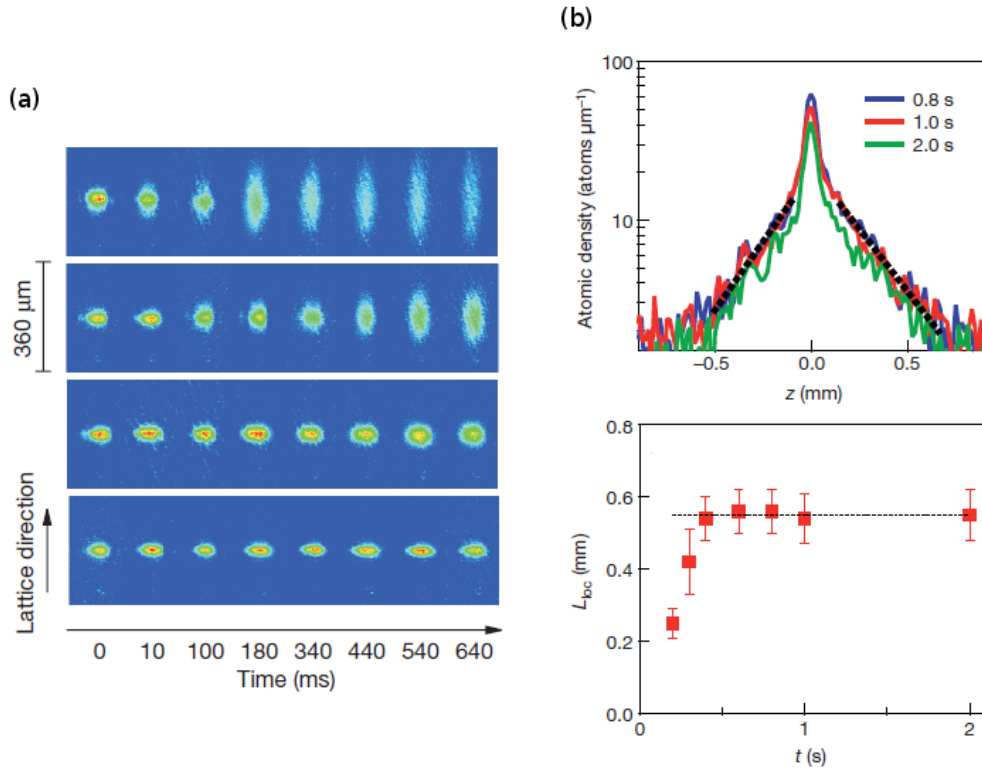


Figure 1.2: Experimental observation of Anderson localization with cold atoms. Left panel (a) shows the result of the experiment performed in Florence by Roati *et al.* [10]. The expansion of the atomic cloud along an optical lattice is inhibited by the presence of disorder. From top to bottom the pictures show the time evolution of the atomic cloud for increasing value of the disorder strength  $\Delta$ . We note that when the disorder is strong enough the cloud does not expand in the lattice since the atoms are localized and the transport is completely suppressed. Right panel (b) refers to the results obtained in Paris by Billy *et al.* [9]. Also in this case we see that, after an initial expansion due to residual interaction between atoms, the atomic sample does not expand in the disordered potential as shown in the plot of the localization length in function of the time. In the top panel we can also see the typical exponential shape of the tails of the atomic distribution characterizing Anderson localization

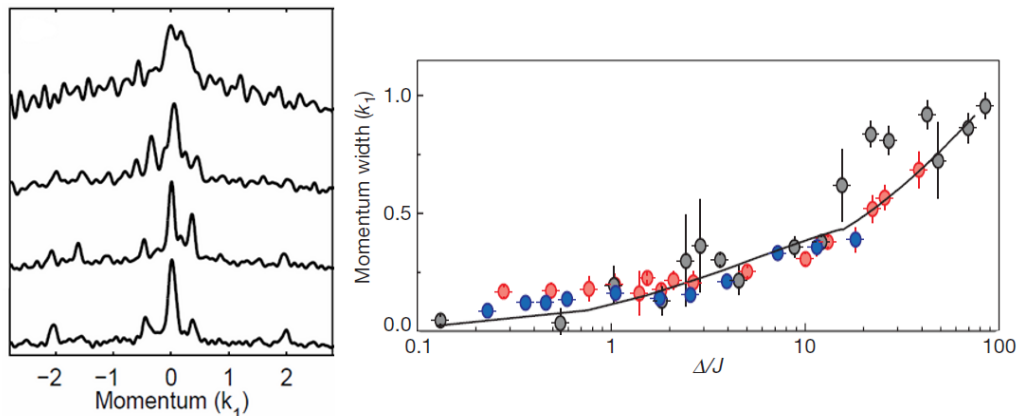


Figure 1.3: Momentum distribution of a cold atoms sample in a quasiperiodic lattice [10], for varying disorder strength. The left panel shows the momentum distribution profiles of atoms. From top to bottom we note that the peaks broaden for increasing value of the disorder, which destroys the coherence in the system. The right panel plots the dependence of the width of the central peak on the disorder strength  $\Delta$ . Different colors represents data taken for different values of the tunneling energy  $J$ .

can “screen” the disorder [14] and bring the system back to a coherent extended superfluid, as in the clean lattice, passing through an intermediate glassy phase. Interactions allow the coupling between localized states centered in different lattice sites.

A detailed study of the properties of a disordered bosonic system in the weakly interacting regime is actually one of the goals of this thesis and we will describe the experimental results we achieved in chapter 3. Here we just give a brief qualitative description on how a weak repulsive interaction can destroy the disorder-induced localization. We refer to Fig.1.4. In the non-interacting case, for strong enough disorder, only the absolute lowest energy level is populated, the many-body state coincide with the single particle one and the wavefunction is exponentially localized. A very weak interaction pushes the bosons out of the lowest localized state. The many-body states are however very close to the single particle ones and there is no coherence between atoms in different lattice sites. This regime is often addressed in literature as *Anderson* (or *Lifshitz*) *glass*. For larger interaction energies but still smaller than  $\Delta$ , the many-body state are substantially deformed and start to occupy more than one single particle state, creating islands of superfluid. However, the coherence across the entire system is not yet restored. This regime is addressed in literature as *fragmented BEC* or *weakly interacting Bose Glass*. Finally when the interaction strength is comparable with the disorder one,

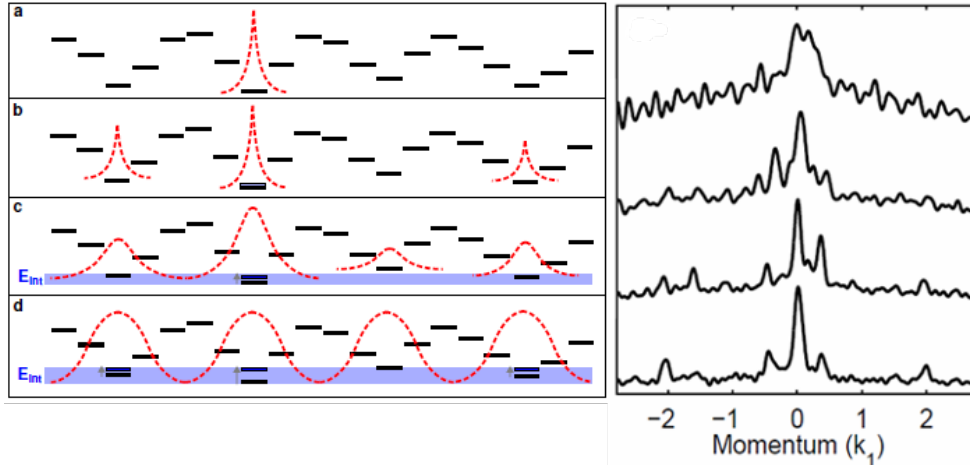


Figure 1.4: Left: schematic of the interaction-induced delocalization. In the non-interacting case ( $U = 0$ ) the system is Anderson localized in the lowest energy state (a). For increasing interaction energy the system tends to occupy more than one single particle state, *Anderson glass* (b), and to create coherent islands of superfluid, *weakly interacting Bose glass* (c). When the interaction energy is comparable with the disorder ( $U \sim \Delta$ ) the coherence is restored across the entire system (d). Right: Experimental momentum distribution of atoms in a disordered lattice for increasing interaction energy [15]. Coherence is gradually restored in the system and this results in narrower and narrower peaks until the full coherence is restored and the momentum distribution resemble the one of atoms in a regular lattice.

a coherent state can form on the entire system. The coherence increasing across the transition has been experimentally proved by looking for example at the momentum distribution [15]. When a large enough interaction energy is present in the disordered system, a coherent state is recovered. This shows the same momentum distribution as in the regular lattice as can be seen by comparing Fig.1.4 and Fig.1.3.

## 1.4 Mott insulator

We have described in the previous section the delocalizing effect of a weak repulsive interaction against disorder. We can now trace out the role of the interaction in a clean system (without disorder) before moving to the more complex case in which disorder and interaction have comparable strength and drive the system to more complex phases. The Hamiltonian (1.21) in this case simplifies and reads:

$$\hat{H}_{HBH} = -J \sum_{\langle j,j' \rangle} \hat{a}_j^\dagger \hat{a}_{j'} + \frac{U}{2} \sum_j \hat{n}_j (\hat{n}_j - 1). \quad (1.24)$$

We have already observed that the many body ground state of  $N$  particle in a lattice without interaction is a superfluid state (Eq.(1.23)) characterized by full coherence across the lattice. In a superfluid the phase is perfectly defined for each site whereas the number of particles is not determined and exhibits Poissonian fluctuations in agreement with the Heisenberg uncertainty principle, according to which the phase operator and the number operator are conjugate variables. This assumption continues to hold also for interacting particles, as long as the first term in Eq.(1.24) is the dominant one, i.e. until  $U \ll J$ . In this case in fact it is energetically favorable for the system to enhance the tunneling processes of the atoms from site to site.

On the contrary when  $U \gg J$ , interactions dominate the Hamiltonian (1.24). Under this condition, the Poissonian fluctuations in atom number become energetically very costly and tunneling from site to site is suppressed. The ground state of the system will therefore consist of localized atomic wavefunctions with a fixed number of atoms per site that minimize the interaction energy. The strong repulsive interaction in fact forces the atoms to not share the same lattice sites. This system takes the name of *Mott insulator*. The many-body ground state is a product of local Fock states which are the eigenstate of the number operator of each lattice site. In this limit, the ground state of the many-body system for a commensurate filling of  $n$  atoms per lattice site in the homogeneous case is:

$$|\psi_{MI}\rangle \propto \prod_j (\hat{a}_j^\dagger)^n |0\rangle. \quad (1.25)$$

The homogeneous site filling  $n$  is determined by the chemical potential  $\mu$ . In strong contrast with the superfluid phase, the number of particle per site is perfectly determined. On the contrary, the conjugate variable, that is the phase, has the maximum uncertainty. For this reason in a Mott insulator there is not coherence across the lattice.

### Quantum phase transition

Increasing the strength of the interaction energy the systems undergoes a quantum phase transition between a superfluid and an insulating phase when the interaction energy becomes the dominant energy  $U > J$ . The exact critical value  $(J/U)_c$  at which the transition occurs depends on the chemical potential  $\mu$  as shown in the phase diagram in Fig.1.5 [1]. This transition is induced by quantum fluctuation and it is present also at zero temperature, where the thermal fluctuation is suppressed. For two and three-dimensional lattices the mean field approach to

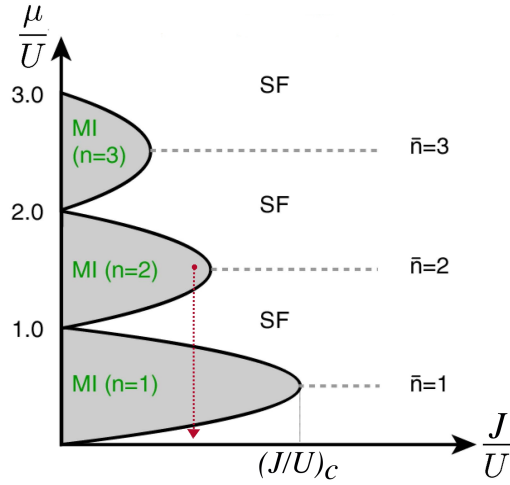


Figure 1.5: Phase diagram of the superfluid (SF) to Mott insulator (MI) transition for a clean homogeneous Bose-Hubbard model. The MI lobes are characterized by constant site filling  $n$ . Note that the larger the average occupancy  $\bar{n}$ , the larger the critical interaction energy to enter the Mott insulator phase. In an inhomogeneous case, for a fix interaction atoms alternate different phases according to the local chemical potential as one can get by moving along the red arrow.

calculate the quantum critical point has been shown to be in good agreement with more sophisticate calculation which nevertheless result to be necessary in the one dimensional case. For a given average occupation  $\bar{n} = N/M$  (where  $M$  is the number of lattice sites), the estimates for the critical energy  $(U/J)_c$  result to be:

$$(U/J)_c = \begin{cases} 3.84, & \text{if } \bar{n} = 1 \\ 2.2\bar{n}, & \text{if } \bar{n} \gg 1 \end{cases} \quad (1.26)$$

in the one-dimensional case, and

$$(U/J)_c = \begin{cases} 5.8z, & \text{if } \bar{n} = 1 \\ 4\bar{n}z, & \text{if } \bar{n} \gg 1 \end{cases} \quad (1.27)$$

in higher dimensions, being  $z$  the number of nearest neighbors.

### Experimental observation of the superfluid-Mott insulator transition with ultracold atoms

The transition from a superfluid phase to a Mott insulator phase for increasing value of the interaction energy with respect to the kinetic one has been probed during the last years in different cold atoms experiments. The first observation was made by Greiner *et al.* in 2002 [16] by looking at the momentum distribution

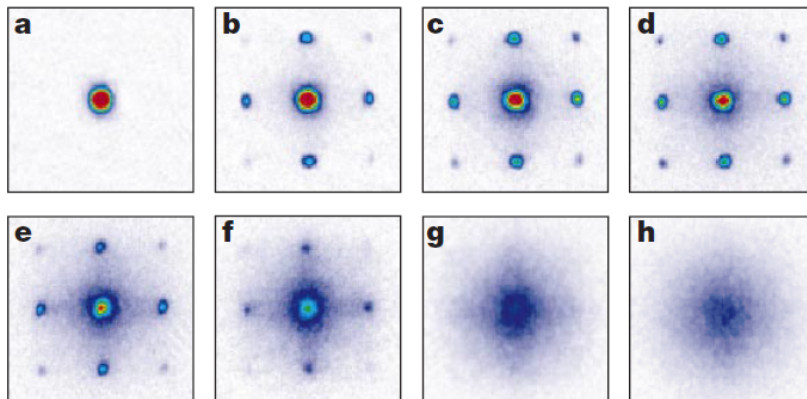


Figure 1.6: Observation of the superfluid to Mott insulator transition by measuring the momentum distribution [16]. Images are taken for increasing value of  $U/J$ . In the superfluid case (a) a clear interference pattern indicates phase coherence across the entire system. Conversely, when the system enters the Mott insulator phase, atoms are localized in single lattice sites and phase coherence is lost. This results in a broadening of the momentum distribution and eventually the peaks completely disappear. These picture refer to a three-dimensional optical lattice.

of the atoms (see Fig.1.6). When the system is superfluid in fact the momentum distribution is given by a clear interference pattern with narrow peaks. On the contrary in the Mott insulator there is not phase coherence in the system and the interference is lost similarly to what happens in the Anderson's case.

Another experimental prove of the appearance of a Mott insulator phase in an atomic system is given by the measurement of the excitation spectrum. In the Mott insulator state in fact, the excitation spectrum is substantially modified compared to the one of the superfluid state: it shows an energy gap. In the limit  $U \gg J$  the energy gap is equal to the on-site interaction energy. This can be understood within a simplified picture as follows. We consider a Mott insulator state with exactly one atom per lattice site. The lowest lying excitation for such a state is the creation of a particle-hole pair, where an atom is removed from a lattice site and added to a neighboring one. Due to the on-site repulsion between two atoms, the energy of the state describing two atoms in a single lattice site is raised by an amount  $U$  in energy above the state with only a single atom in this lattice site. Therefore in order to create an excitation the amount of energy  $U$  is required. It can be shown that this is also true for number states with exactly  $n$  atoms per lattice site. Also here  $U$  is the energy required to make a particle-hole excitation<sup>3</sup>. Through this picture one can also get a better idea of why hopping of

<sup>3</sup>Actually  $U$  depends on the number of particles that occupy a single lattice site since the

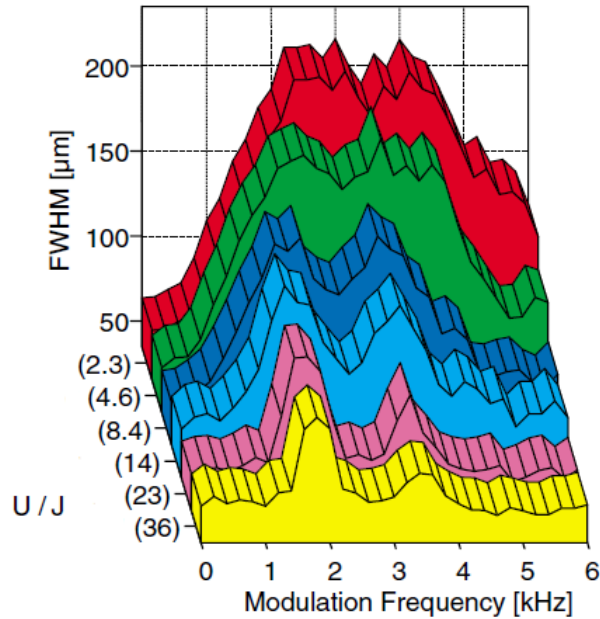


Figure 1.7: Measured excitation spectrum of atoms in a one dimensional lattice for different values of the ratio  $U/J$  [18]. For small value of  $U/J$  the system is in the superfluid phase and its spectrum is gapless (red curve): any amount of energy can be transfer in the system. On the contrary when the interaction energy become the dominant energy, the system enters in the Mott Insulator phase and an amount of energy equal to  $U$  is required in order to excite the system. When the excitation energy is equal to  $U$  in fact a particle-hole excitation can be created in the lattice. If the perturbation is strong enough also double particle-hole excitation can occur: this happens for an excitation energy equal to  $2U$ . The excitation spectrum is thus characterized by two narrow peaks (yellow curve).

particles throughout the lattice is suppressed in the Mott insulator phase. In the superfluid case instead any amount of energy can be transfer in the system and the excitation spectrum is gapless. Fig.1.7 [18] shows the excitation spectrum for an atomic gas undergoing the superfluid-Mott insulator transition.

The different microscopic occupation of the lattice sites which determines the two quantum phases, translates in drastically different properties of the entire system as many experiments showed. The more recent experiments were also able to observe the single site occupation across the lattice and measure the vanishing atom number fluctuations across the transition to Mott insulator [19, 20].

---

wavefunction of interacting atoms is also dependent on the atom number. Then the excitation energy needed to move one atom from a site to another one depends, in turn, on how many atoms were occupying the two involved lattice sites. A precise measurement of the excitation spectrum allows to resolve number-dependent shift in the excitation energy caused by effective multi-body interactions[17].

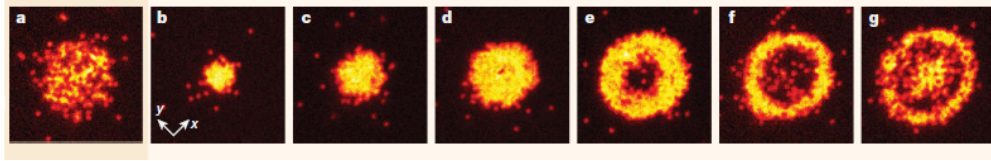


Figure 1.8: Fluorescence images of atoms in a two-dimensional lattice in the Mott insulator regime  $U \gg J$ . The typical wedding-cake structure is observed. Moving from the center towards the edges an alternation of Mott insulator shells with even (full) and odd (empty) site occupation is shown. Images are taken for increasing number of atom [20].

### Inhomogeneous case: shell structure

In cold atoms experiment an external potential is always present and the ideal homogeneous case is never realized. The typical confinements in the experiment are given by harmonic potential and can be included in the Bose-Hubbard model in the term  $\sum_j \epsilon_j \hat{n}_j$  of the Hamiltonian (1.20). This confinement helps the system to achieve in some region of the lattice the commensurate filling necessary for the Mott insulator to form. The system can be thought to be characterized by a local chemical potential which slowly varies from site to site and reaches its maximum at the center of the harmonic potential. For a constant  $J/U < (J/U)_c$  the atoms alternate different phases according to the local chemical potential as one can get by moving along a vertical line in Fig.1.5 (red arrow in the picture). Moving from the center of the trapping potential towards the edges, Mott Insulator shells with decreasing occupation filling alternate with superfluid ones. In the limiting case of  $U \gg J$  only Mott insulator shells remain and the density profile of the trapped atoms shows the so called wedding-cake shape. This peculiar distribution of the atoms in the lattice has been experimentally observed as shown in Fig.1.8 [20].

## 1.5 Bose glass

Let us now come to consider the more complex and by far more debated regime of strong interaction and disorder. In section 1.3 we have seen how a weak interaction can delocalize a disordered localized system and in section 1.4 we have instead spoken about the Mott insulator regime in which interaction itself is strong enough to compete against the kinetic energy and have a localizing effect in a regular lattice. We can now discuss the interplay between disorder and interaction in the strongly interacting regime. Do the two effects cooperate in creating an insulating phase or, on the contrary, inhomogeneities induced in the system by disorder tend to destroy the ordered Mott Insulator phase leading to a more coherent state?

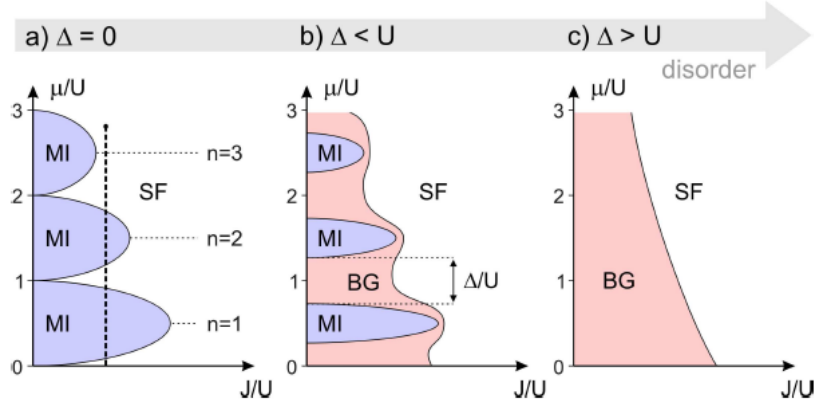


Figure 1.9: Phase diagram for disordered interacting bosons. Depending on the relative strength of the tunneling energy  $J$ , the interaction energy  $U$  and the disorder  $\Delta$ , the system is in a superfluid (SF), Mott insulator (MI) or Bose glass (BG) phase.

Many theoretical and numerical works predict, in this regime, the appearance of a glassy phase called *Bose glass*, which is not too different from the glassy phase of the weakly interacting regime introduced in section 1.3. A clear experimental characterization of this complex phase is still missing.

The fourth chapter of this thesis will be devoted to the analysis of experimental studies performed in this thesis' work in the strongly interacting regime. Here we simply summarize the main properties of the Bose glass phase and briefly describe the transition that the system undergoes from Mott insulator when disorder is gradually added in the system.

As discussed in the previous section, when the system is ordered, its properties are totally determined by the competition between the tunneling energy  $J$  and the interaction energy  $U$ . In particular in the limit of strong interaction ( $U \gg J$ ), the system is characterized by Mott insulator domains, each of them with an integer site occupation  $n$  determined by the local effective chemical potential (Fig.1.9a). When weak disorder ( $\Delta < U$ ) is added in the system, the Mott insulator lobes are expected to shrink, and give room to another quantum phase, known as *Bose glass* (Fig.1.9b) [1]. For larger disorder, when  $\Delta \geq U$ , the Mott insulator lobes completely disappear and, for sufficiently small  $J$ , only the Bose glass phase should hold (Fig.1.9c).

The Bose glass phase is an insulating although compressible phase. Like the Mott insulator, the Bose Glass is insulating since it does not have long-range phase coherence. Like a superfluid, it has a gapless excitation spectrum and consequently a finite compressibility. We note that the coexistence of these two properties is not in contradiction: despite the absence of a gap in the excitation spectrum, excitations

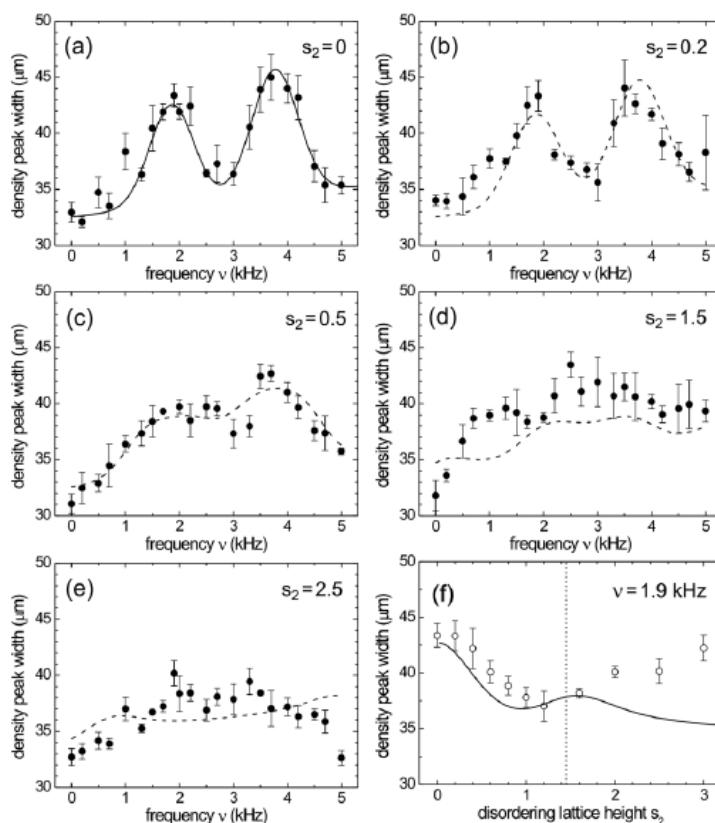


Figure 1.10: Excitation spectra of an interacting bosonic gas for a fix value of interaction energy and increasing value of the disorder strength (a)-(e) [21]. Effect of excitation at a frequency of 1.9kHz as a function of the disorder (f). The progressive vanishing of the Mott insulator excitation peaks is clearly visible.

at low energy only occur locally in regions of superfluidity. The Bose glass phase is thus characterized by a short-range phase coherence given by these superfluid regions but, globally, it is insulating.

As already pointed out a clear experimental investigation of the Bose glass phase is, up to now, still missing. However few experiments with cold atoms have studied during the last years bosonic disordered systems in the strongly correlated regime. In the following we report on some of the main experimental results.

### Experimental investigation of the strongly interacting disordered regime with cold atoms

The first experiment towards the Bose glass was performed in Florence in 2007 [21]. In this experiment Fallani *et al.* demonstrated the progressive broadening and eventually flattening of the Mott insulator excitation energy peaks as the disorder amplitude  $\Delta$  increases as shown in Fig.1.10. The vanishing energy gap in the

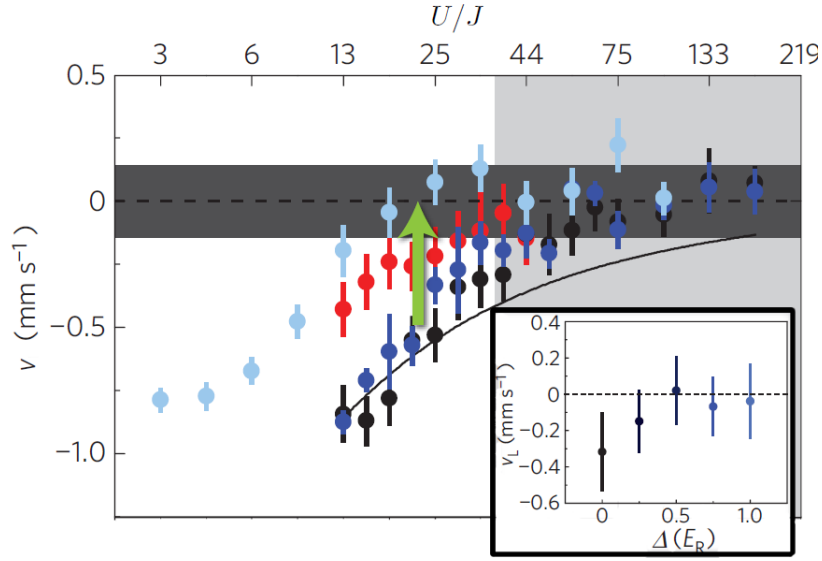


Figure 1.11: Effect of disorder on the transport of interacting bosons [22]. Dependence of the center of mass velocity on the interaction energy for increasing disorder strengths (black, dark blue, light blue). The conductor-insulator transition is shifted towards smaller value of  $U/J$  as the disorder increases. The inset shows how disorder affects the velocity for a fix value of the interaction ( $U/J \simeq 45$ ). Red points refer to high temperature transport in a clean (without disorder) lattice.

excitation spectrum of an insulating strongly-interacting gas of bosons is a strong indication of a new phase, different from a homogeneous Mott insulator. However these spectra are also compatible with the formation of a strongly inhomogeneous Mott insulator which is a conceptually different phase with respect to the Bose glass.

A more recent work performed in Urbana demonstrated how, by adding disorder in an interacting superfluid system, one observes a greater energy dissipation i.e. the appearance of an insulating phase [22, 23]. Pasienski *et al.* by measuring transport in a disordered lattice, experimentally proved a disorder-induced superfluid-insulator transition in an interacting system, compatible with the appearance of the expected Bose glass phase. The velocity of the center of mass of the bosonic gas after an impulse is applied decreases by increasing either the interaction or the disorder as shown in Fig.1.11. In a certain range of parameters disorder and interaction can thus cooperate in making the system an insulator conversely to what happens in the weakly-interacting regime where interactions screen the effects of disorder.



## Chapter 2

# A $^{39}\text{K}$ Bose-Einstein condensate with tunable interaction in a quasiperiodic potential

The experiments reported in this thesis have been performed by investigating the behavior of a Bose-Einstein condensate (BEC) of Potassium-39 atoms in a potential created by two incommensurate optical lattices in one dimension. The quasiperiodic potential created by the lattices provides a disordered distribution of the on-site energies and mimics the Anderson physics. The single-particle eigenstates feature a transition to a localized regime for a finite value of the disorder strength. In the experiment the three important energies introduced in the previous chapter following the Bose-Hubbard model,  $J$ ,  $U$  and  $\Delta$ , can be measured and independently tuned in a controlled way.

$^{39}\text{K}$ , in absence of any external magnetic field, has a negative scattering length which corresponds to an attractive interaction which would make the BEC to collapse. Nevertheless in its ground state it shows a broad magnetic Feshbach resonance (see sec.2.2.1). It is therefore possible to tune the scattering length to positive value to condense the atoms, and adjust it at will to access various regimes of interaction. Thanks to this high degree of tunability of the scattering length,  $^{39}\text{K}$  BEC is actually an excellent sample to study the physics of disordered systems in the non-interacting, weakly interacting and strongly correlated regimes.

In this chapter we first give a brief description of optical lattices, i.e. of the perfectly periodic potentials for neutral atoms created by light (sec.2.1). We also show how the kinetic energy  $J$  is measured and controlled in the experiment. In sec.2.2 we characterize the interaction energy in the condensate and give a

qualitative idea on how it can be tuned by an external magnetic field. We then speak about disordered optical potential and in particular about quasiperiodic lattices (sec.2.3). We show how the disorder strength  $\Delta$  can also be easily measured and tuned. After a short description of the experimental procedure to create the  $^{39}\text{K}$  Bose-Einstein condensate (sec.2.4) we then explain how we use imaging techniques to investigate its behavior (sec.2.5). The chapter ends with sec.2.6 about the experimental realization of one-dimensional systems for ultracold atoms.

## 2.1 Optical lattices

Laser light can be exploited to trap neutral atoms in attractive or repulsive conservative potentials, the shape and depth of which can be easily engineered and dynamically controlled. Optical traps are commonly realized in cold atoms experiment focusing a gaussian laser beam on the atomic cloud. The trap depth is typically in the millikelvin range, orders of magnitude smaller than the thermal energy of atoms at room temperature. Anyway, once the gas has been driven to the ultralow temperatures necessary to reach Bose-Einstein condensation at moderate density, it can be easily trapped in these weak potentials. We now focus our attention particularly on the possibility to create with light a perfect periodic lattice where atoms are axially confined in the nodes or antinodes of a standing wave. Bosonic atoms in this kind of potential are thus perfect candidates to study the physics described by the Bose-Hubbard model introduced in the previous chapter.

Optical lattices rely on the *dipole force* that is the conservative force that arises from the dispersive interaction between the intensity gradient of a light field  $\mathbf{E}$  and the induced atomic dipole moment  $\mathbf{d}$ . We consider a far-off resonance laser beam. This means that the detuning  $\Delta = \omega - \omega_0$  between the field frequency  $\omega$  and the atomic resonance frequency  $\omega_0$  is much larger than the atomic radiative linewidth  $\Gamma$ . It can be shown from a semiclassical approach [24], that in this case the dipolar potential generated by the beam can be expressed as follow:

$$V_{dip}(\mathbf{x}) = \frac{3\pi c^2}{2\omega_0^2} \frac{\Gamma}{\Delta} I(\mathbf{x}) \quad (2.1)$$

being  $c$  the speed of light in vacuum and  $I(\mathbf{x}) = |\mathbf{E}(\mathbf{x})|^2$  the light intensity. The *scattering rate* due to the far-detuned photon absorbed and subsequently spontaneously remitted by the atoms, in the same semiclassical framework, results to be:  $\Gamma_{sc} = \frac{3\pi c^2}{2\omega_0^2} \left(\frac{\Gamma}{\Delta}\right)^2 I(\mathbf{x})$ . If, as it happens in the experiment,  $\Delta$  is chosen to be much larger than  $\Gamma$ ,  $\Gamma_{sc}$  can be neglected and the potential is conservative.

The method to create an optical lattice is in principle simple. A laser beam is retroreflected by a mirror in order to obtain a standing wave resulting from the interference of the two counter-propagating light fields. In our experiment we use a solid state Nd:YAG laser with wavelength  $\lambda \simeq 1064\text{nm}$ . Such a laser, which is optical pumped by a diode laser, is a very stable source characterized by a spectral linewidth  $\Delta\nu \leq 1\text{KHz}$ .

If we consider the two sinusoidal counterpropagating fields  $\mathbf{E}_1$  and  $\mathbf{E}_2$  having the same wave number  $k = 2\pi/\lambda$ , the same amplitude  $E_0$  and the same polarization, the time-averaged interference pattern is given by  $I(x) = |\mathbf{E}_1 + \mathbf{E}_2|^2 = I_0 \cos^2(kx)$  with  $I_0 = 2\epsilon_0 c E_0^2$ . Replacing this expression in Eq.(2.1) we obtain the potential exerted by the standing wave on the atoms:

$$V_{latt}(x) = V_0 \cos^2(kx) \quad \text{with} \quad V_0 = \frac{3\pi c^2}{2\omega_0^2} \frac{\Gamma}{\Delta} I_0 \quad (2.2)$$

This corresponds to a perfect sinusoidal optical lattice with spatial periodicity  $d = \lambda/2$ . Commonly the lattice depth  $V_0$  is expressed in terms of recoil energy as the dimensionless quantity:

$$s = \frac{V_0}{E_{rec}} \quad \text{with} \quad E_{rec} = \frac{\hbar^2 k^2}{2m} \quad (2.3)$$

$E_{rec}$  is the energy with which an atom of mass  $m$  recoils when it absorbs a photon with momentum  $\hbar k$  and it is the natural energy scale for atoms in an optical lattice. For  $s \geq 3$  the system is already in the *tight-binding* regime for which the Bose-Hubbard Hamiltonian applies.

### Calculation of the tunneling energy $J$

We now show how to calculate the tunneling energy between neighboring sites  $J$  given the lattice depth  $s$  [25].

If the lattice is deep enough it is possible to approximate the potential well of each lattice site with a harmonic well:

$$V_{latt}(x) = V_0 \cos^2(kx) \simeq s E_{rec} (kx)^2. \quad (2.4)$$

The oscillation frequency  $\omega_{latt}$  of a lattice site can then be obtained by solving the equation:

$$s E_{rec} (kx)^2 = \frac{1}{2} m \omega_{latt}^2 x^2, \quad (2.5)$$

and results to be:

$$\omega_{latt} = \frac{2E_{rec}}{\hbar} \sqrt{s}. \quad (2.6)$$

Under this approximation the Wannier function centered in the  $j$ -th lattice site can be written as the eigenfunction of the ground state of the harmonic oscillator with frequency  $\omega_{latt}$  and harmonic length:

$$a_{latt} = \sqrt{\hbar/(m\omega_{latt})}. \quad (2.7)$$

To estimate the tunneling energy we have to calculate the overlapping integral between the function centered in two neighbor sites as defined in Eq.(1.16). If we consider the Gaussian approximation introduced above we get:

$$\frac{J}{E_{rec}} = \frac{4}{\sqrt{\pi}} s^{0.75} e^{-2\sqrt{s}}. \quad (2.8)$$

We observe that the term  $J$  strongly depend on the overlapping of the tails of the Wannier functions where they differ more from the gaussian functions. For a more precise evaluation of the tunneling energy one has therefore to take into account the actual shape of the Wannier function and from a numerical fit one obtains [26]:

$$\frac{J}{E_{rec}} = 1.43s^{0.98} e^{-2.07\sqrt{s}}. \quad (2.9)$$

### 2.1.1 Lattice calibration: Raman-Nath spectroscopy

As discussed in the first chapter of this thesis, the kinetic energy scale is very important in determining the physical properties of the system. In order to have a good characterization of the physical system under investigation and a good interpretation of the experimental data it is thus fundamental to know, with high precision, the tunneling energy  $J$  of the optical lattice which can be calculated using Eq.(2.9) from the lattice depth  $s$ . However we have to note that Eq.(2.2) results to be only an approximation of the real potential felt by the atoms. In fact in a real experiment an unbalance between the powers of the two counter-propagating beams, a slight misalignment or a not completely parallel polarization of the beams field could result in an effective potential which differs from the one theoretically calculated. A direct measurement of the lattice depth is thus necessary in order to estimate  $J$  in a reliable way.

In the experiment we calibrate the height of the optical lattice by using an interferometric technique relying on the so-called Raman-Nath diffraction. The basic idea of this phenomenon is the following: as the light can be diffracted by a grating, in a similar way a Bose-Einstein condensate (which can be thought as a macroscopic matter wave) can be diffracted by an optical lattice. We shine on the BEC a short pulse of the laser light which creates the lattice. The duration of the

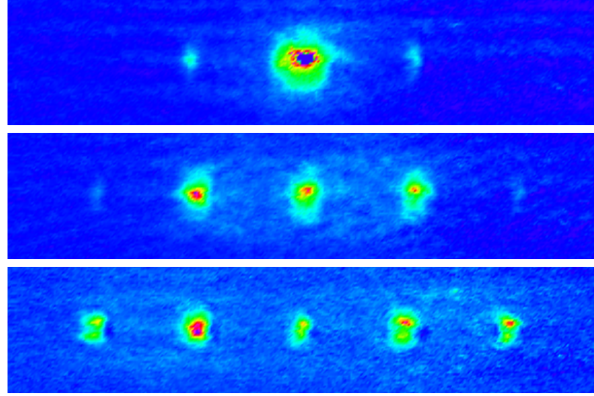


Figure 2.1: Absorption images of the BEC diffracted by the optical lattice in the Raman-Nath regime ( $T_{pulse}=10\mu\text{s}$ ) after a free expansion during  $t_{TOF}=16\text{ms}$ . A larger number of peaks corresponds to a deeper lattice. From the fit of the density profile integrated over the transversal axis with a sum of gaussian peaks we extrapolate the width of the central peak and the second momentum of the distribution. We can then calculate the lattice depth  $s$  with Eq.(2.17). From top to bottom the images correspond to  $s \simeq 0, 5, 15$

pulse  $T_{pulse}$  has to be short enough for not allowing the atoms to move along the lattice. The BEC diffracts and, after a free expansion during  $t_{TOF}$ , interference peaks appear in the density distribution. As shown in Fig.2.1 the number of peaks increases for increasing lattice depth.

Let us analyze this technique in a more quantitative way. Let us consider a standing wave potential of the form (2.2) and an atomic wavepacket, which can be treated as a plane wave with momentum  $p_0$ . The coupling between them will change the momentum of the atoms in  $p_0 \pm 2n\hbar k$ , where  $n$  is an integer number. If we now apply the standing wave only for a limited time  $T_{pulse}$  we can ask which is the probability of finding the atoms in the  $n$ -th plane wave. The calculation is straightforward if one can neglect the motion of the atomic center of mass along the lattice during the time  $T_{pulse}$ : in this case we are in the so called atomic Kapitza-Dirac regime, corresponding to the Raman-Nath light diffraction from a thin grating and the probability is given by [27]:

$$P_n = \left| J_n \left( \frac{V_0}{\hbar} t_{pulse} \right) \right| \quad (2.10)$$

being  $J_n$  the  $n$ -order Bessel function. The Raman-Nath regime applies when the kinetic energy of the involved plane wave is small with respect to the height of the optical potential. Taking as  $n_{max}$  the largest significant order of diffraction and neglecting the initial momentum  $p_0$ , one has that the condition to be satisfied is the following:

$$\frac{(2n_{max}\hbar k)^2}{2m} < sE_{rec} \quad (2.11)$$

An estimation of  $n_{max}$  can be done reminding that  $|J_n(z)|^2 < 1$  if  $|z| < n$ . We can thus assume  $n_{max} = (V_0/\hbar)T_{pulse}$  and rewrite the thin grating condition in terms of the duration of the pulse:

$$T_{pulse} < \frac{1}{\omega_{rec}\sqrt{s}}, \quad (2.12)$$

where we define  $\omega_{rec} = E_{rec}/\hbar$ . The typical value of the lattice depth in the experiment is  $s \simeq 10$ . In order to use this technique to calibrate the lattice we thus have to apply very short pulses  $T_{pulse} < 1ms$ .

In a more realistic situation in which the atomic plane wave is replaced by a Bose-Einstein condensate we can follow the same reasoning as above: the condensate get diffracted by the laser standing wave and atomic wavepackets with momenta spaced by  $2\hbar k$  are generated. These packets can be directly seen after the expansion as it is clearly shown in Fig. 2.1. If we indicate the condensate wavefunction as  $\psi_0(x)$ , the wave function after the interaction with the lattice in the thin grating approximation is given by

$$\psi(x) = \sum_n i^n J_n\left(\frac{s}{2}\omega_{rec}T_{pulse}\right)e^{-2inkx}\psi_0(x). \quad (2.13)$$

The corresponding momentum distribution is obtained with a simple Fourier transform:

$$\tilde{\psi}(p) = \sum_n i^n J_n\left(\frac{s}{2}\omega_{rec}T_{pulse}\right)\tilde{\psi}_0(p - 2n\hbar k). \quad (2.14)$$

With the assumption that  $\psi_0(x)$  extends over many lattice sites and therefore  $\tilde{\psi}_0(p)$  is narrow on the scale of  $\hbar k$ , it is possible to write the second moment of the momentum distribution as

$$\langle p^2 \rangle = \left(\sum_n P_n\right)\langle p^2 \rangle_0 + 4\hbar^2 k^2 \left(\sum_n n^2 P_n\right) \quad (2.15)$$

where we indicate with  $\langle p^2 \rangle_0$  the second moment of the momentum distribution of the trapped condensate. Using Eq.(2.10) and the sum rules for the Bessel function one finds:

$$\langle p^2 \rangle = \langle p^2 \rangle_0 + \frac{1}{2}(\hbar k)^2 (s\omega_{rec}T_{pulse})^2. \quad (2.16)$$

This quantity is simply proportional to the RMS width of the cloud after expansion  $\sigma_{RMS}$  provided that the original size in the trap can be neglected and that the atomic interactions play a negligible role during the expansion. Under these approximation in fact we have:

$$\sigma_{RMS}^2 = \frac{t_{TOF}}{m}\langle p^2 \rangle = \sigma_0^2 + \frac{1}{2}\left(\frac{kE_{rec}}{m}t_{TOF}T_{pulse}\right)^2 s^2. \quad (2.17)$$

Since  $\sigma_{RMS}$  and the width of the central peak  $\sigma_0$  can be obtained from the absorption images of the atoms, one can calculate  $s$  by using Eq.(2.17).

Besides measuring the lattice depth, this technique is also used in the daily procedure of alignment of the lattice: in fact it is easy to see that, for a given total intensity, the height of the optical lattice is maximum when the two beams are perfectly counterpropagating. We thus finely adjust the direction of the back-reflected beam in order to optimize the diffraction pattern.

## 2.2 Interaction energy in a Bose-Einstein condensate

In the previous section we have shown how it is possible to control and measure the kinetic energy of the atoms in the periodic optical lattice. We can now consider the interaction energy in the Bose-Einstein condensate and describe the way in which we are able to tune it. In an atomic gas in the dilute regime and at very low temperature only binary collisions are relevant and the two-body interaction potential can be written in terms of a contact pseudo-potential:

$$v(\mathbf{x} - \mathbf{x}') = g \delta(\mathbf{x} - \mathbf{x}') \quad \text{with} \quad g = \frac{4\pi\hbar^2}{m}a. \quad (2.18)$$

The strength of the interaction energy thus depends only on a single parameter:  $a$ , the s-wave scattering length. It is in fact possible to demonstrate that at low temperature s-wave scattering processes dominate over higher order ones which are strongly suppressed. The scattering length  $a$  depends on the details of the interaction potential. The sign of  $a$  determines the kind of interaction: positive values of the scattering length correspond to repulsive interaction and negative values to attractive one.

### 2.2.1 Tuning the interactions: Feshbach resonances

By means of a homogeneous magnetic field it is possible to tune  $a$  changing the intensity and the sign of the interactions. This phenomenon, known with the name of *magnetic Feshbach resonance*, has been first studied in nuclear physics [28, 29]. Successively Feshbach resonances found their application also in many atomic physics experiments [30] since they offer the possibility to tune the inter-atomic interactions in an easy and very controllable way.

The physical origin and the elementary properties of a Feshbach resonance can be understood from a simple picture. We consider two molecular potential curves  $V_{bg}(R)$  (ground state) and  $V_c(R)$  (excited state), corresponding to two spin

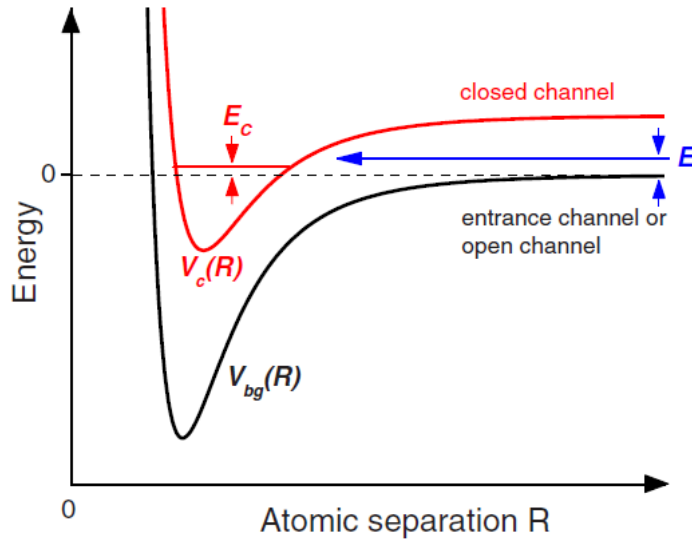


Figure 2.2: Basic two-channel model for a Feshbach resonance. The phenomenon occurs when two atoms colliding at energy  $E$  in the open channel resonantly couple to a molecular bound state with energy  $E_c$  supported by the closed channel potential. In the ultracold domain, collisions take place near zero energy,  $E \approx 0$ . When the magnetic moments corresponding to the two potentials differ, resonant coupling can therefore be conveniently realized by magnetically tuning  $E_c$  near 0.

configurations for atoms as shown in Fig. (2.2)<sup>1</sup>. For large the interatomic distance  $R$   $V_{bg}(R)$  corresponds to the energy of the two free atoms (dashed line), which is chosen as reference energy  $V_{bg}(\infty) = 0$ .

In ultracold gases two atoms can collide having small energy. The level  $V_{bg}(R)$ , called *open channel*, is accessible for a collisional process. The other potential  $V_c(R)$ , which is not accessible and is called *closed channel*, can however support a bound molecular state close to 0 energy. The two atoms have thus the energetically allowed possibility to make a (temporary) transition to this molecular state and their scattering cross section can extremely increase. Even a weak coupling can lead to strong mixing between the two channels. Provided that the states corresponding to the two channels have different magnetic moments, the relative energy difference can be controlled via a magnetic field  $B$  since they have a different response (Zeeman shift) to the applied  $B$ . This leads to a magnetically tunable Feshbach resonance. The dependence of the scattering length  $a$  on the

<sup>1</sup>In principle a molecule has several potential curves corresponding to the different hyperfine and Zeeman levels. For simplicity we consider only one excited state which is appropriate for an isolate resonance

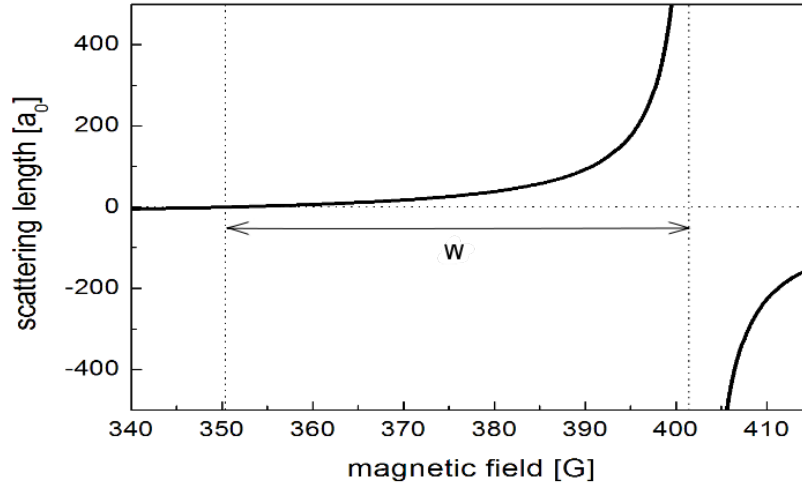


Figure 2.3: Magnetic field dependence of the scattering length  $a$  of  $^{39}\text{K}$  in the proximity of the Feshbach resonance centered at  $B_0 \simeq 400\text{G}$ .  $a$  vanishes at the zero-crossing magnetic field  $B_{zc} \simeq 350\text{G}$ .

magnetic field  $B$  can be described by a simple expression [31]:

$$a(B) = a_{bg} \left( 1 - \frac{W}{B - B_0} \right). \quad (2.19)$$

The *background scattering length*  $a_{bg}$ , which is the scattering length associated with  $V_{bg}(R)$ , represents the value far from resonance. The parameter  $B_0$  denotes the *resonance center*, where the scattering length diverges, and the parameter  $W$  is the *resonance width*. Note that both  $a_{bg}$  and  $W$  can be positive or negative. An important point in a Feshbach resonance is the zero crossing of the scattering length which occurs at a magnetic field  $B_{zc} = B_0 + W$ .

From Eq.(2.19) we can extrapolate the behavior of  $a$  around the magnetic field  $B_{zc}$  at which  $a$  vanishes:

$$a(B) \sim \frac{a_{bg}}{W} (B - B_{zc}). \quad (2.20)$$

The parameter that is important in order to control interaction around  $a=0$  is the ratio  $a_{bg}/W$ : the smaller it is, the better is the accuracy in tuning the interaction.

### Feshbach resonances of $^{39}\text{K}$

In the experiment we employ Potassium-39 atoms. This isotope is characterized by several magnetic Feshbach resonances [32]. In particular we exploit the broad one that  $^{39}\text{K}$  shows in its absolute ground state  $|F = 1, m_F = 1\rangle$  which is centered at  $B_0 \sim 400\text{ G}$ . The dependence of the scattering length  $a$  on the magnetic field in the proximity of a Feshbach resonance is given by (2.19). The resonance we

exploit in the experiment is shown in Fig. (2.3). For this resonance  $W \simeq 52\text{G}$  and  $a_{bg} \simeq -29a_0$ . The sensibility around  $B_{zc}=350\text{ G}$  is thus  $da/dB \simeq 0.56a_0/\text{G}$ . The stability of the Feshbach magnetic field in our experiment is of the order of  $0.1\text{ G}$ , which allows a fine tuning of the scattering length around zero and to achieve a good control up to few hundreds of  $a_0$ .

## 2.3 Disordered optical potential

We now turn to discuss the way in which disorder is realized in ultracold atoms experiments and, in particular, in our laboratory. In practice, two different possibilities have been exploited to create a disordered potential: a *laser speckles field* and a *quasiperiodic lattice*. Both configurations rely once more on the dipole force that light exerts on the atoms and that can be used to shape very different kind of well controllable and characterizable potentials. The possibility to add and to control the disorder in ultracold atoms systems is quite remarkable, especially as compared with real system in nature where, conversely, it is intrinsically present and can not be controlled.

A first way to create disorder with light is to shine a laser beam onto a diffuser rough surface, a speckle pattern is in fact created by the interference of the different paths of the light scattered by different facets of the surface [33]. Since the dipole potential is proportional to the laser intensity, the disordered spatial intensity produced by the speckles results in a spatially disordered potential for the atoms (fig. 2.4). The speckles induced disorder is constant in time and can be characterized by two parameters, its intensity standard deviation  $\sigma_I$  and its lengthscale  $\Delta_x$ , which is essentially the correlation length, i.e. the width of the autocorrelation function.

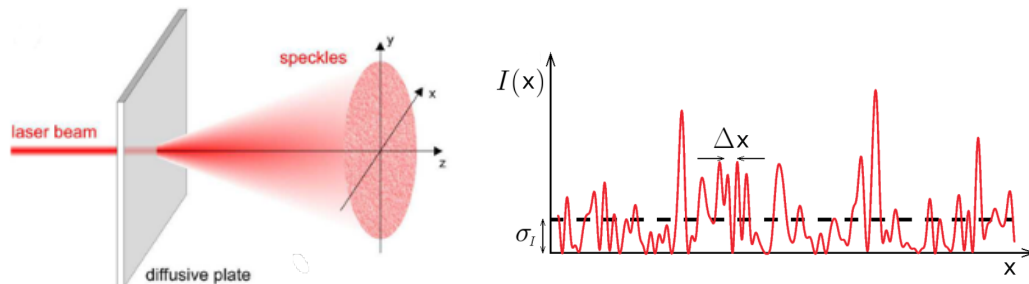


Figure 2.4: Speckles laser field. A laser beam is shined onto a diffusive plate to create a speckles interference pattern which provides a disordered potential for the atoms given by the random intensity distribution sketched on the left of the picture.

A quasiperiodic potential instead consists of two overlapping lattices with incommensurate wavelength (fig.2.5). The superposition over the main lattice of a second weaker one with incommensurate periodicity creates a potential which is described, according to Eq.(2.2) and (2.3), by the following expression:

$$V(x) = s_1 E_{rec1} \sin^2(k_1 x) + s_2 E_{rec2} \sin^2(k_2 x + \phi). \quad (2.21)$$

where  $k_i = 2\pi/\lambda_i$  ( $i=1,2$ ) are the lattice wavenumber and  $s_i$  are the lattice heights in unit of recoil energy  $E_{reci}$ . Provided that  $s_2 \ll s_1$  and  $\beta = k_2/k_1$  is an irrational number, the secondary lattice induces a perturbation on the main one resulting in an inhomogeneous and non-periodic shift of the energy minima. The quasiperiodic lattice is characterized by potential wells every  $D = 1/(\beta - 1)$  sites of the main lattice. In the experiment we use a Nd:YAG laser with wavelength  $\lambda_1 \simeq 1064$  nm to create the main lattice and a Ti:Sapphire laser with wavelength  $\lambda_2 \simeq 859$  nm for the secondary one. The quasiperiodic wells appear approximately every 4.2 lattice sites. We note that disorder introduced by the bichromatic lattice is not a random disorder since it has a quasiperiodic structure characterized by well defined incommensurate frequencies which results in a deterministic and spatially correlated distribution of the energy across the lattice sites. However the translational symmetry of a perfect lattice is broken in a non-trivial way and it is thus suitable for the study of disorder physics.

### 2.3.1 Quasiperiodic lattice

Using the expression for the quasiperiodic potential (2.21) in Eq.(1.21), one can rewrite the disordered Bose-Hubbard Hamiltonian in this form:

$$\hat{H}_{Quasiperiodic} = -J \sum_{\langle j,j' \rangle} \hat{a}_j^\dagger \hat{a}_{j'} + \Delta \sum_j \cos(2\pi\beta j + \phi) \hat{n}_j + \frac{U}{2} \sum_j \hat{n}_j (\hat{n}_j - 1). \quad (2.22)$$

For non-interacting atoms ( $U = 0$ ) the full Hamiltonian can be mapped onto that of the *Harper* or *Aubry-André model*. The disordered Bose-Hubbard model for the quasiperiodic potential is presented in ref.[34, 35]. It can be demonstrated that the perturbation induced by the secondary lattice does not change significantly the position of the lattice site, the tunneling energy from one site to the neighboring one  $J$  (which is given by the height of the primary lattice according to Eq.(2.9)) and the on-site interaction energy  $U$ .  $\Delta$  results to be proportional to  $s_2$ , the depth of the secondary lattice, and its expression can be obtained by numerical calculation [36] and results to be:

$$\frac{\Delta}{E_{rec}} = 0.5 s_2 \beta^2 e^{-2.18/s_1^{0.6}}, \quad (2.23)$$

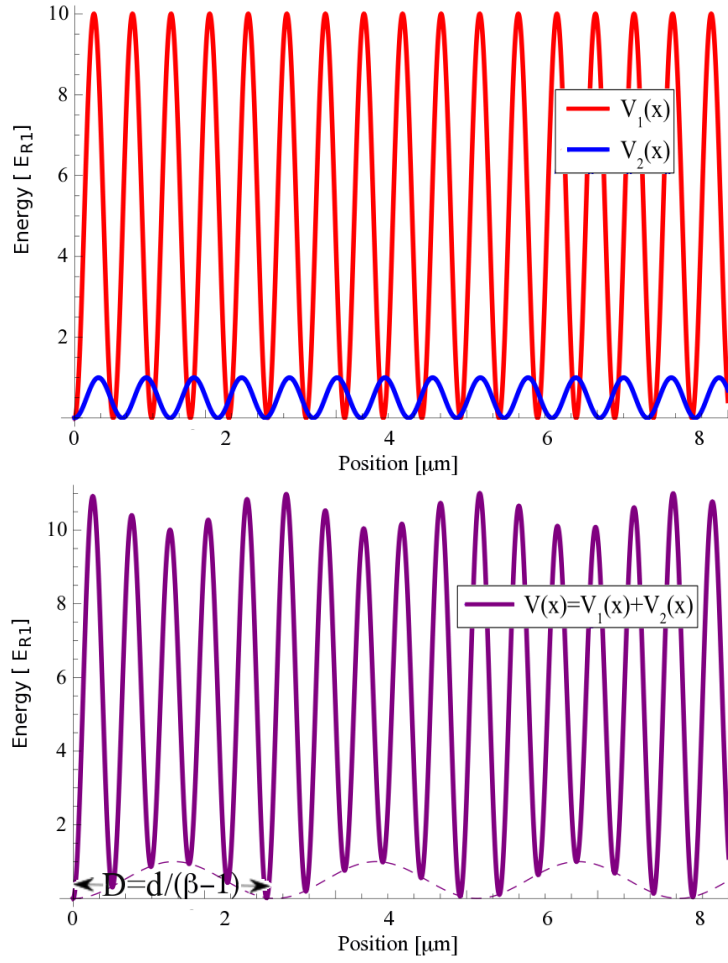


Figure 2.5: Bichromatic lattice. The superposition of two lattices with heights  $s_1 = 10$  and  $s_2 = 1$  created by laser beam with wavelengths  $\lambda_1 \simeq 1064\text{nm}$  (red line) and  $\lambda_2 \simeq 859\text{nm}$  (blu line), creates the quasiperiodic potential represented by the violet line in the bottom figure. The modulation (dashed line) introduced by the secondary lattice creates potential wells approximately every  $D = 1/(\beta - 1) \simeq 4.2$  sites of the main lattice.

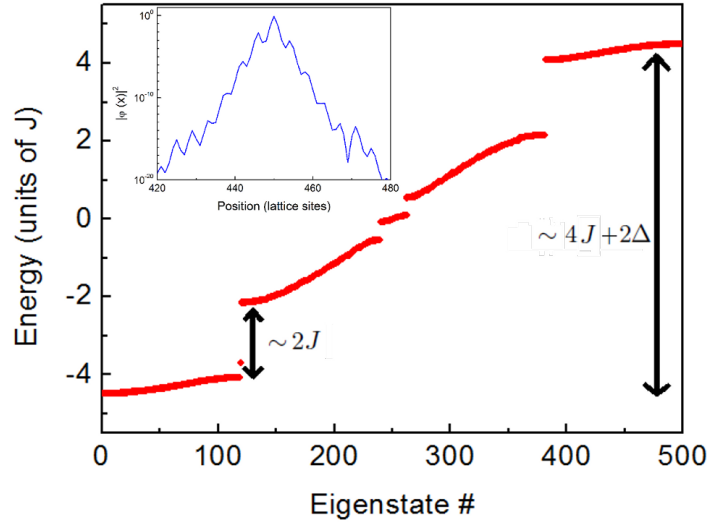


Figure 2.6: Energy of the eigenstates of the quasiperiodic potential with  $\Delta = 4J$  ordered for increasing energy. The minibands structure clearly appear in the spectrum. The shape of the eigenfunction in the first band is the same for each state. On the inset the profile of a typical eigenfunction is plotted: it shows the exponential shape characteristic of Anderson localization.

$E_{rec}$  is the recoil energy determined by the main lattice. The Aubry-André model displays a transition from extended to localized state for a finite value of the disorder  $\Delta/J = 2$ . This differs from the one dimensional pure random situation in which any amount of disorder is sufficient to localize the system. Above the localization threshold however all single particle eigenstates of the first band of the lattice are exponentially localized and the system behave similarly to the random case. The disorder dependent localization length  $\xi \approx d/\ln(\Delta/2J)$  (being  $d = \lambda_1/2$  the lattice site spacing) is the same for all the eigenstate. It should be notice that in the lowest band of a quasiperiodic lattice there are no mobility edges, i.e. all the states are either localized or extended. Conversely for the speckles potential effective mobility edges exist due to the spatial correlation of the disorder [37].

By diagonalizing the Hamiltonian, the spectrum of such a potential can be calculated<sup>2</sup>. A striking feature of the spectrum is the splitting of the first band of the lattice in many “minibands” besides a global spreading of the band width from  $4J$  in the regular lattice to approximately  $4J + 2\Delta$  in the bichromatic case. In Fig. 2.6 the spectrum for a fixed value of disorder ( $\Delta = 4J$ ) is shown. The quasiperiodic potential is correlated on all length scales, with maxima of its autocorrelation

<sup>2</sup>An additional harmonic confinement along the longitudinal axis of the lattice, typically present in the experiment, can be also taken into account in the calculation of the eigenvalues.

separated by  $D$ . The absolute lowest-energy eigenstates are those for which a lattice site coincides with a minimum of the potential well. These states populate the first miniband of the spectrum. When two neighbors lattice sites are nearly symmetric in potential energy in a well, the potential appear locally like a double well, for which the two lowest-lying eigenstate have a separation in energy of  $2J$ . The fact that the width of the first minigap is approximately  $2J$  for any value of the disorder can be justified by this simple consideration.

## 2.4 Experimental realization of the $^{39}\text{K}$ BEC with tunable interaction

$^{39}\text{K}$  BEC is a good candidate for the study of physical phenomena in which a non-interacting system is required and in which it is important to control and tune the interparticle interaction at will. Nevertheless, due to  $^{39}\text{K}$  level structure and collisional properties at zero magnetic field, the production of a BEC is not trivial. In our laboratory we employ  $^{87}\text{Rb}$ , which is easier to cool to the BEC regime, to sympathetic cool  $^{39}\text{K}$ . In spite of the small heteronuclear scattering length of  $^{87}\text{Rb}$ - $^{39}\text{K}$  collisions, the sympathetic cooling has been proven to work efficiently. A more recent experiment in Florence [38] shows however how it is possible to condense  $^{39}\text{K}$  without employing another atomic species by performing an efficient sub-doppler cooling and using a large and depth optical dipole trap.

The apparatus and experimental procedure used to produce the BEC has already been widely described in previous theses of our group [39, 40, 41, 42, 43]. In the following we only shortly list the steps performed to achieve the condensation:

1. **Laser cooling** in magneto-optical traps produces overlapped samples of K and Rb at a temperature  $T \approx 100\mu\text{K}$  and densities of about  $10^{10}\text{cm}^{-3}$ .
2. **Evaporative cooling in the magnetic trap:** The two atoms are prepared in their low-field seeking state  $|F = 2, m_F = 2\rangle$  and trapped in a QUIC magnetic trap. A forced, selective evaporation of Rb atoms on the microwave transition to the  $|F = 1, m_F = 1\rangle$  state cools both samples to about  $1.5\mu\text{K}$ .
3. **Optical trapping:** In order to further cool the sample and achieve condensation it is necessary to tune the scattering length by means of a magnetic Feshbach resonance. We thus need to transfer the atoms from the magnetic trap to an optical dipole trap which is compatible with the application of the Feshbach field. We employ a cross dipole trap realized by two focused red

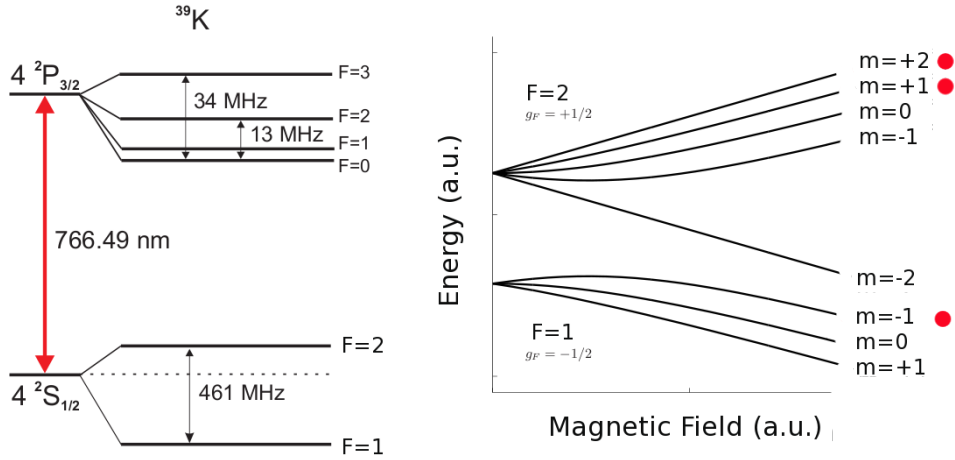


Figure 2.7: Left: Hyperfine structure of  $^{39}\text{K}$ . Right: Zeeman shift of the ground state levels. The red dots show magnetically trappable state at low magnetic field.

detuned laser beams at a wavelength  $\lambda=1032$  nm. The waist of the beams is around  $80 \mu\text{m}$  and we employ an initial power of around 800 mW for each beam. A schematic representation of the geometry in our experiment is given in Fig. 2.8.

4. **Transfer in the ground state** ( $|F = 1, m_F = 1\rangle$ ): The two species are transferred by two separate  $\mu$ -wave pulses from the  $|F = 2, m_F = 2\rangle$  state to the absolute ground state  $|F = 1, m_F = 1\rangle$ . Here  $^{87}\text{Rb}$ - $^{39}\text{K}$  have several interspecies Feshbach resonance and  $^{39}\text{K}$  has a broad intraspecies resonance at around 400 G. Residual Rb atoms in the  $|F = 2, m_F = 2\rangle$  state can cause a depolarization of the K sample and heating. For this reason we clean these atoms by a resonant light pulse.
5. **Evaporation in the optical trap**: The evaporation in the optical trap is performed in two steps by exponentially lowering the intensity of the two trap beams. Before starting the evaporation we ramp up a homogeneous magnetic field (Feshbach field).

- In the first part of the evaporation the magnetic field is tuned to one of the several interspecies Feshbach resonance at around 316 G, in this way we can enhance the collisional rate between  $^{87}\text{Rb}$  and  $^{39}\text{K}$  resulting in a more efficient thermalization among the two species. In this first part the evaporation ramps are shaped in such a way to obtain evaporation mostly on the vertical direction where the potential is shallower for the heavier Rb atoms. K atoms are sympathetically cooled.

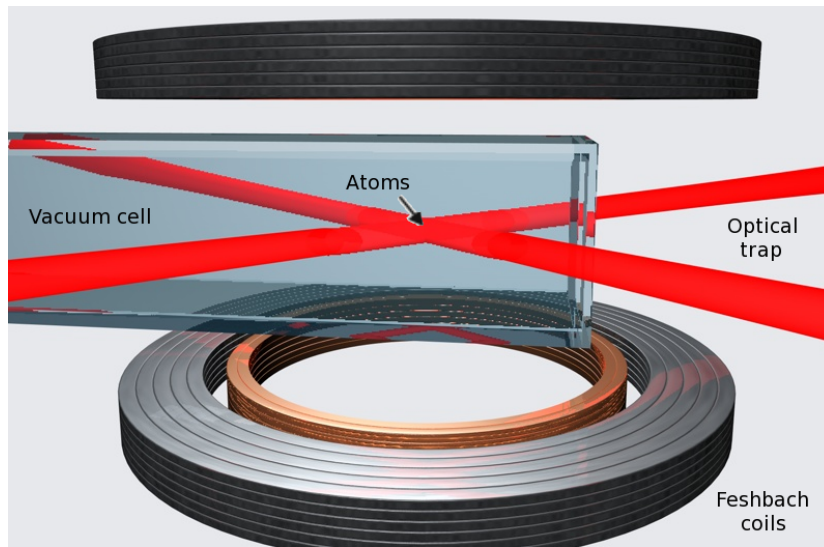


Figure 2.8: Schematic representation of the experimental setup. Bose-Einstein condensation of  $^{39}\text{K}$  atoms is reached in a crossed optical dipole trap obtained with two perpendicular focused laser beams. The laser wavelength,  $\lambda=1032\text{nm}$ , is red-detuned with respect to the atomic transition. A couple of coils in Helmholtz configuration provide an homogeneous magnetic field (Feshbach field) that we use to tune the interparticle scattering length. Another couple of coils create a magnetic field gradient which compensate for the gravity. This gradient prevent the atoms to fall down due to the gravity when the dipole confinement is turned off.

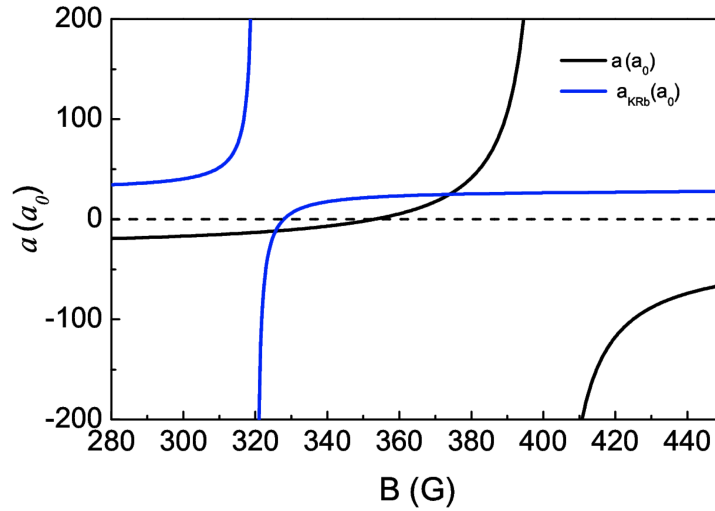


Figure 2.9: Magnetic field dependence of the heteronuclear scattering length between  $^{39}\text{K}$  and  $^{87}\text{Rb}$  atoms (blue line) and of the homonuclear scattering length  $^{39}\text{K}$ - $^{39}\text{K}$  (black line). During the first stage of the evaporation in the optical dipole trap we set the magnetic field at 316 G to exploit the heteronuclear Feshbach resonance and enhance the scattering  $^{39}\text{K}$ - $^{87}\text{Rb}$  providing a better thermalization between the two species. In the second step we switch to the K Feshbach resonance and we set the field at 395 G where the scattering length is good to condense, about  $180 a_0$ .

- In the second part of the evaporation the magnetic field is tuned to the homonuclear Feshbach resonance in order to get a positive scattering length, in this phase of the evaporation the cooling relies on the intraspecies collisions. The final vertical depth of the trap is not enough to compensate gravity for Rb atoms which are lost. We thus have a pure  $^{39}\text{K}$  condensate. The final average harmonic trap frequency is around 50 Hz. The typical number of atoms in condensate is around  $5 \times 10^4$  at a temperature of few tens of nK.

## 2.5 Imaging techniques

Our experiment consists of several stages with an overall duration of approximately one minute. The whole sequence is in cycles. After producing the BEC, we load it into the (disordered) optical potential, we perform the actual experiment and then we measure the result. The measurement is realized by absorption imaging, which is a destructive technique. The atoms are illuminated with a res-

onant light beam, and the shadow they cast in the beam by absorption is imaged through an appropriate lens system onto a CCD camera. Each atom scatters several photons during this process, and is therefore excited out of the trap. On the timescale of the imaging process, which is typically  $50\mu\text{s}$ , the atoms cannot move significantly and one therefore detects their density distribution.

### 2.5.1 In situ images

Some of the results presented in this thesis are extracted from *in situ* images. This means that we image the atoms while they are trapped in the optical potential. From these images one can directly get the spatial density distribution of the atomic cloud which is the modulus square of the atomic wavefunction  $\psi(x, y, z)$ :

$$\rho(x, y) = \int |\psi(x, y, z)|^2 dz \quad (2.24)$$

The main limitation of these techniques is the finite resolution of the imaging system. The typical size of the atomic cloud we study is in fact a few  $\mu\text{m}$  which is of the same order of magnitude of the imaging resolution given by the diffraction limit and aberrations. Our imaging system is basically constituted by a telescope. The magnification for this system is simply given by  $M = f_2/f_1$ , being  $f_1$  and  $f_2$  the focal lengths of the two lenses of the telescope which in our experiment are respectively 150 mm and 500 mm, giving  $M \sim 3$ . The diffraction limit can be estimated by the simple expression:

$$d = \frac{\lambda}{2 NA}, \quad \text{with } NA \sim \frac{r}{f_1}, \quad (2.25)$$

where  $r \sim 1.2\text{ cm}$  is the radius of the first lens and  $\lambda = 776\text{ nm}$  is the wavelength of the light resonant with the atomic transition of  $^{39}\text{K}$ . The best resolution we can get with this simple imaging system is therefore about  $4\mu\text{m}$ . The actual resolution is even lower (about  $10\mu\text{m}$ ) mostly due to spherical aberration introduced by the first lens of the telescope.

With this technique it is impossible to resolve structures in the spatial distribution of the atoms with typical dimension smaller than the resolution. For example it is impossible to observe the distribution of atoms in the single sites of an optical lattice. Sharp edges are also broadened by the imaging system since the actual density profile has to be convoluted with a Gaussian function with a width given by the resolution. A new generation of experiments with cold atoms are developing in the last few years imaging techniques with better resolution. These techniques are resulting to be very useful to study for example the physics of atoms in optical lattices since they are able to detect a single atom in a single lattice site [19, 20].

These methods are basically based on a microscope objective, which has a high NA and is almost free from any kind of aberration. A larger optical access on the atoms would be required in our experiment in order to implement this technique and at the moment this is impossible given the configuration of the coils we use to produce the magnetic field for the magnetic trap. However other methods exist to extract information about the atomic distribution in the trapping (disordered) potential as explained in the next section. The imaging resolution of our system is thus enough for our purposes.

We note that the atoms we want to detect are in the  $|F = 1, m_F = 1\rangle$  state at a magnetic field as large as 400 G. Even if at this strong field we are in the Paschen-Back limit where  $F$  and  $m_F$  are no more the good quantum number to describe the atomic state, we found convenient to keep the same label for the state along all the sequence. The imaging is performed using light near the  $^{39}\text{K}$  repumping transition at 767.1 nm on a partially open transition from  $|F = 1, m_F = 1\rangle$  to  $|F' = 1, m_{F'} = 0\rangle$ . The atoms pump to this excited state can either decay to the ground state or to the  $|F = 2, m_F = 2\rangle$  state. From here the close transition to  $|F' = 3, m_{F'} = 3\rangle$  can be exploited. The two transition have almost the same frequency at a magnetic field of 390 G. The same light is thus efficient for both transitions.

With this technique we are able to keep the magnetic field on during the imaging. This allows us to take images of the Bose-Einstein condensate in the trap where the density is high, avoiding the collapse due to the negative scattering length at zero magnetic field. With this technique we detect approximatively one third of the total number of atoms that we usual detect using the almost close cooling transition from  $|F = 2\rangle$  to  $|F' = 3\rangle$  at zero magnetic field. We take this limited efficiently into account when calculating the atom number from the images.

### 2.5.2 Time of flight images

Another possibility we have is to take an image of the atoms after releasing them from the trap confinement and letting them free to expand for a certain time of flight (TOF). At the time of the release, the scattering length is set below  $1 a_0$  in less than 1 ms and kept there until the Feshbach field is switched off 7 ms before taking the images. By this time the system has expanded by a sufficient amount to have a low density and thus neglect the effect of interactions. If the TOF is sufficiently large to be in the ‘far-field’ limit and the interactions can be neglected during the expansion, the image of the atoms that is acquired is approximatively the in-trap momentum distribution. To recover information about the in-trap

wavefunction, we can therefore use an inverse Fourier transform.

In this case at the moment of the imaging the Feshbach field is off. To image the atoms is just enough to pump the atoms from the  $|F = 1\rangle$  to the  $|F = 2\rangle$  state just before taking the picture with a short pulse of repumping light, and then use the cooling transition.

## 2.6 One-dimensional systems

In this thesis we aim to study the physics of disorder and in particular we focus our attention on the one-dimensional case. Generally speaking, besides being easier to be analytically and numerically studied than systems with higher dimensionality, 1D systems are also conceptually interesting since they present phenomena strictly related to the dimensionality. In the three-dimensional world, one-dimensional systems occur because of a confining potential along two directions which freezes the particles along these directions. In this case the interesting physical phenomena occur only along the third direction. In this section we show how a one-dimensional sample is obtained with cold atoms. The wavefunction of a particle free to move along the  $z$  direction and confined along the  $x$  and  $y$  directions can be written in the form:

$$\psi(r, z) = e^{ikz}\phi(r), \quad (2.26)$$

where we define  $r = \sqrt{x^2 + y^2}$ . The function  $\phi(r)$  depends on the shape of the confining potential. In cold atoms experiment this confinement is usually well described by harmonic approximation with frequency  $\omega_r$ . In this case  $\phi(r)$  is proportional to a Gaussian function:

$$\phi(r) \propto e^{-r^2/2a_{ho}^2}, \quad (2.27)$$

where  $a_{ho} = \sqrt{\hbar/m\omega_r}$  is the harmonic oscillator length,  $m$  being the mass of the particle. The energy of the system is quantized and can be written as the sum of the radial and axial part:

$$E = E_z + E_r = \frac{\hbar^2 k^2}{2m} + \hbar\omega_r(n_r + 1), \quad (2.28)$$

where  $n_r = n_x + n_y$  being  $n_x$  and  $n_y$  integer numbers. The system is thus characterized by transverse levels. If the separation in energy between these levels, i.e.  $\hbar\omega_r$ , is larger than the temperature and the interaction energy only the ground state is populated. The transverse degree of freedom is frozen and the dynamics of the system develops only along the axial direction. In the experiment an harmonic confinement is present also along the axial direction, this confinement is

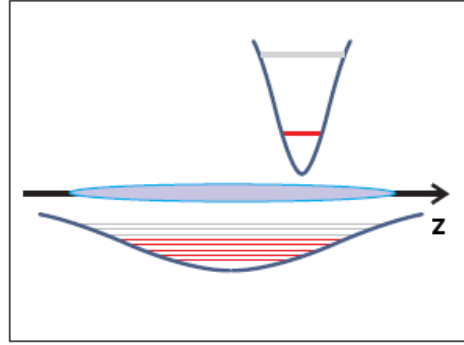


Figure 2.10: Schematic representation of a one dimensional system experimentally achievable. The radial harmonic confinement is very tight and atoms can occupy only the ground state. The radial degree of freedom are thus frozen. On the contrary the longitudinal harmonic trap is shallower. We represent in red the occupied state and in gray the empty ones.

usually much weaker than the transverse one satisfying the condition:  $\omega_z \ll \omega_r$ . In this case the longitudinal confinement does not invalidate the simple model we introduced so far even if in some circumstances it results in some important modifications in the physics of the system. Anyway if the temperature  $T$  and the interaction energy  $E_{int}$  fulfill the condition  $\hbar\omega_z \leq E_{int}, k_B T \ll \hbar\omega_r$ , the system still occupies the transverse ground state. A sketch of this situation is reported in Fig.2.10.

We would like to point out that an indefinite increase of the radial confinement would bring the gas into a regime of extreme interaction, the so called Tonks-Girardeau regime [44, 45, 46]. It is indeed possible to demonstrate [47] that if the length of the radial harmonic oscillator becomes comparable to the scattering length, the nature of the two-body collisions changes, since the collisional energy can no longer be distributed in the radial direction, but only in the axial one. This has in turn a drastic impact on the properties of the system, which can show a “fermionization” phenomenon where basically the individual bosons tend to avoid each other and get segregated in limited spatial regions along the 1D system. For the strongest radial confinement that we realize in the experiments reported in this work, the length of the radial harmonic oscillator is about  $3500a_0$ , indeed larger than the scattering length. For this reason, the experiments we have performed are however out of the Tonks-Girardeau regime and, therefore, we will not give a description of its properties. We just note that the parameters that is usually

defined to measure the closeness to such regime of very strong interactions is:

$$\gamma \approx \frac{2a}{a_r^2 n_{1D}} \quad (2.29)$$

where  $a$  is the scattering length, and  $a_r$  is the radial harmonic lengths, and  $n_{1D}$  is the one-dimensional atomic density. One enters the extreme-interactions one-dimensional regime when  $\gamma \gg 1$ . In our case  $\gamma$  is typically smaller than 1. We can thus say that the experiments here reported are performed in the quasi-1D regime, in which the dynamics along the radial direction is frozen though the nature of the collisional properties remains 3D.

### 2.6.1 1D optical lattice on a 3D BEC

In our experiment we study the ground state and the dynamics properties of bosons in a one-dimensional bichromatic optical lattice. At low temperature and for weak interaction one can realize a one-dimensional system by superimposing the disordered lattice along one of the axes of a 3D harmonic trap. One can study the physics which happens along the lattice independently on the radial degree of freedom. A part of the experiment presented in this thesis has been performed by using this simple technique. We have been able to characterize the ground state and the transport properties of a disordered system in the weakly interacting regime.

This technique fails when one wishes to study the strongly correlated regime. In this case in fact one wants to increase the interaction energy and make it larger than the hopping energy  $J$ , which, in this case, is comparable with the radial harmonic energy  $\hbar\omega_r$  given by the optical trap and the lattice beams themselves ( $\omega_r \simeq 2\pi \times 70\text{Hz}$ ). For these reason an increase of the interaction energy would lead the radial distribution in the Thomas-Fermi regime where the width of the sample depends on the interaction. The radial broadening of the radial distribution, in turn, lowers the density and the interaction energy itself. With this geometry it is actually impossible to achieve interaction energies larger than the radial harmonic quantum of radial energy. With this configuration is thus possible to study only the weakly interacting regime  $U < J$ . In order to get the strongly correlated regime one has to increase the radial confinement and make it larger than the hopping energy and the interaction energy. A very well known strategy to obtain this strong confinement is to employ an auxiliary 2D tight optical lattice, as we discuss in the following.

### 2.6.2 Three-Dimensional optical lattice

In the experiments intended to investigate atoms in the strongly correlated regime we realize a two-dimensional array of one dimensional tubes by loading the three-dimensional condensate into a pair of tight orthogonal optical lattices aligned along the  $x$  and the  $y$  directions. The bichromatic lattice is then produced along the vertical direction as shown in the schematic Fig. 2.11. Each single tube can be considered as an independent system since the tunneling rate from tube to tube is negligible on the experimental timescale. For the tight lattices we use ( $s_x \simeq s_y \simeq 30$ ) the tunneling rate is in fact about 2Hz. The frequency of the harmonic confinement in the tubes in this situation is much larger than before, in fact  $\omega_r \simeq 2\pi \times 50\text{kHz}$ . The radial energy thus becomes the dominant energy scale,  $\hbar\omega_r \gg U, J$ . Under these conditions the interaction energy can be made much larger than the tunneling one, and the regime of strong interaction,  $U \gg J$ , can be reached. This is the regime of interest for the last part of the experiments reported in this thesis.

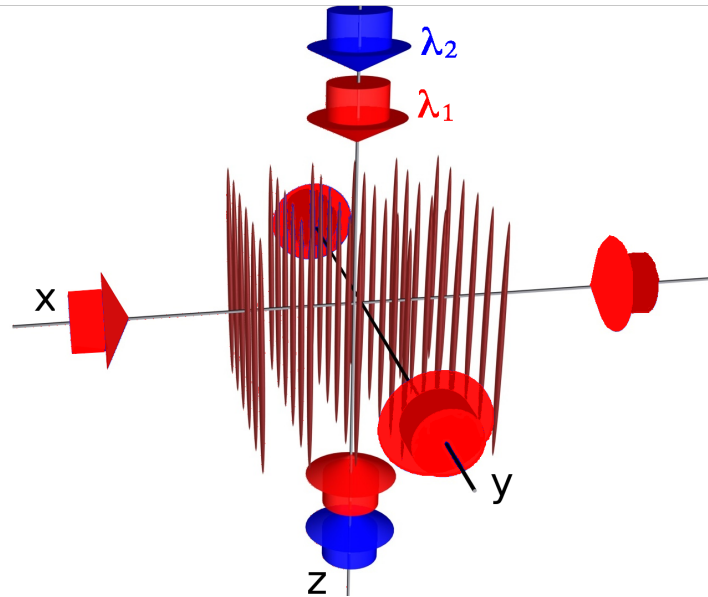


Figure 2.11: Schematic representation of the experimental configuration. Two tight lattices are aligned along the  $\hat{x}$  and  $\hat{y}$  directions of the system forming a two dimensional array of one dimensional tubes. The quasiperiodic lattice is aligned along  $\hat{z}$ , the axial direction of the tubes.



## Chapter 3

# Experimental investigation of weakly-interacting bosons in a disordered lattice

In the first chapter we described how the interplay between disorder and interaction strongly affects the behavior of bosons in a lattice. In fact, according to the relative strength of these two parameters, the system undergoes different phases that are characterized by drastically different properties. As discussed in the second chapter, ultracold atoms experiments offer a nicely controllable and tunable system to study the physics of disorder. Bose-Einstein condensate in disordered optical lattice can be described by the Bose-Hubbard Hamiltonian and the different phases predicted by the model can be experimentally investigated.

We now focus the attention on the weakly interacting regime and we show how we experimentally characterized the entire delocalization crossover of a disordered bosonic system caused by a weak repulsive interaction. In a first class of experiments we study the local shape of the states and the coherence and correlation properties in the different regimes (sec.3.1). Furthermore, in sec.3.2, we investigate the dynamical properties of the system by characterizing the expansion of the atomic cloud in the disordered potential when the localization is destroyed by interaction. In sec.3.3, we characterize the diffusive expansion of the atoms in the disordered lattice driven by a controlled noise and we show how a weak repulsive interaction cooperate with noise in the transport dynamics.

### 3.1 Observed disordered regime: from the localized to the superfluid phase

We concentrate in this section on the study of the properties of the ground state of weakly-interacting bosons in the disordered lattice. An overview on the effect of weak repulsive interactions on a disordered localized system has already been given in section 1.3. Here we review the delocalization caused by interaction considering the quasiperiodic nature of the disordered potential that we realize in the experiment.

Let us consider atoms in the quasiperiodic optical lattice above the localization threshold  $\Delta/J = 2$ . In section 2.3 we described the main features of the quasiperiodic lattice and in particular the minibands structure of the energy spectrum. A schematic representation of the energy level distribution along the lattice is shown in fig.1.4. Given the quasiperiodicity of the potential, the lowest energy eigenstates are  $D = 1/(\lambda_1/\lambda_2 - 1)$  lattice sites apart from each other, in the potential wells created by the beatnote of the two lattices. We remind that in our case the wavelengths of the laser beams are respectively  $\lambda_1 = 1064.4\text{nm}$  and  $\lambda_2 = 859.9\text{nm}$  and thus  $D \simeq 4.2$  lattice sites. Since in the experiment both temperature and interaction energy are small, only the states in the first “miniband” are populated. We can therefore restrict our analysis to these energies.

Let us outline the expected evolution of a disordered Bose-Einstein condensate when we vary the interaction strength. Non-interacting bosons would condense into the absolute lowest energy state of the quasiperiodic lattice. The single particle eigenstate of the system is an Anderson-like exponentially localized state. For very weak interactions, several low energy eigenstates of the non-interacting system, which seat in the potential wells created by the beatnote of the two lattices, can become populated. This phase is often called *Anderson glass* [48]. When enough interaction energy is present in the system, states sitting  $D$  lattice sites apart become degenerate, locally forming coherent fragments. This phase is called *weakly interacting Bose-glass* [49] or *fragmented BEC* [50]. Repulsive interactions indeed serve to smooth over the disordering potential in the occupied sites, providing a flatter energetic landscape on which more extended states can form. The number of independent fragments should decrease for larger interaction energies, until, for sufficiently large interaction, a single phase-coherent state is formed, and the extended BEC phase is recovered.

The center of the crossover from localized states to a coherent BEC is expected to occur when the interaction energy is comparable to the standard deviation

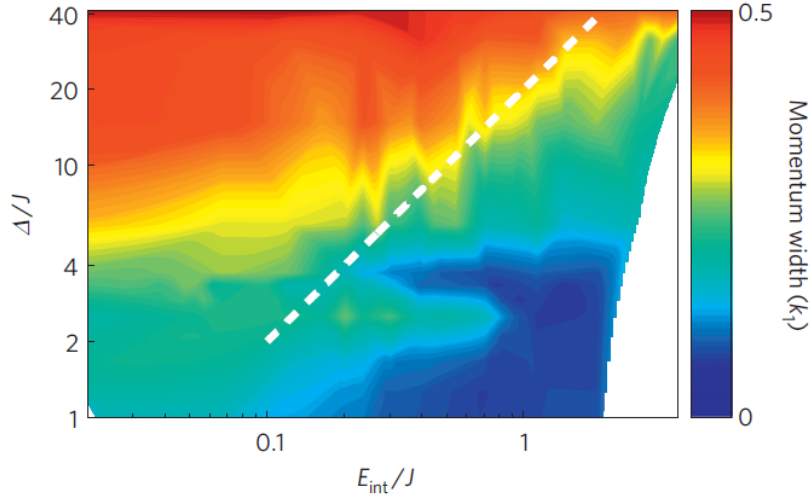


Figure 3.1: Phase diagram of a weakly interacting Bose gas in a quasiperiodic lattice, from the evolution of the momentum distribution [15]. The coherent phase is characterized by a narrow momentum distribution in contrast to the localized phase in which no coherence is present between states and the momentum distribution broadens. The position of the crossover is in good agreement with energetic arguments. The dashed white line indeed indicates where the interaction energy is equal to the standard deviation of the first “miniband” ( $E_{int} = 0.05\Delta$ )

of disordered energy distribution of the first “miniband” which is approximately  $0.05\Delta$ . All the lowest states should then be coupled together, forming an extended state, when the interaction energy becomes comparable with the full extension of the “miniband”  $E_{int} \approx 0.17\Delta$ .

In a previous work in our group [15], exploiting the independent and well controllable tunability of interaction and disorder, the phase diagram of weakly interacting bosons in the quasiperiodic lattice has been traced (fig.3.1). Those measurements show a clear transition from localized to extended state. The position of the crossover is in good agreement with such energetic consideration.

In the following we describe a more extensive study of the local shape of states and of the correlation properties of the system [51]. We have characterized the entire delocalization crossover across the three different regimes described here above (Anderson glass, Bose glass and extended Bose-Einstein condensate).

### 3.1.1 Experimental procedure

We produce a Bose Einstein condensate of about 40 000 atoms of  $^{39}\text{K}$  in a crossed optical dipole trap following the procedure previously summarized (sec.2.4). The scattering length during the last step of the evaporation in the optical trap is set

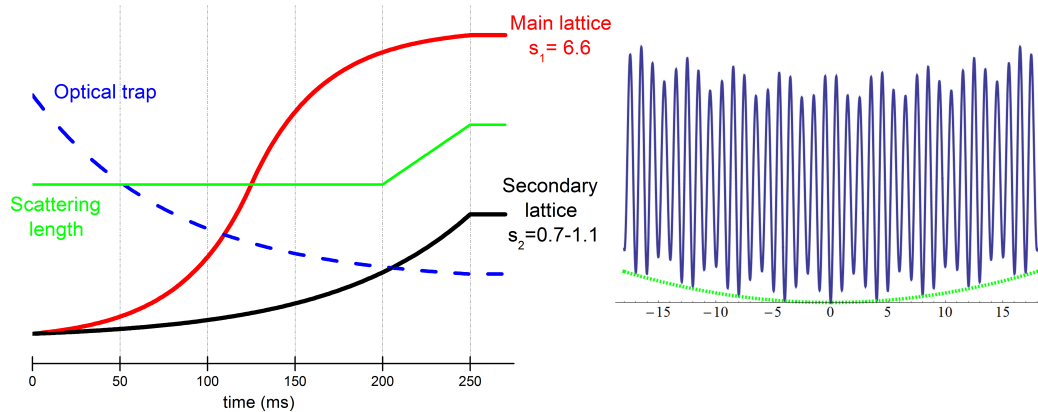


Figure 3.2: Left: Experimental sequence for the loading of the interacting atoms in the quasiperiodic lattice. Right: Sketch of the final optical potential. Green dashed line shows the residual longitudinal harmonic confinement given by the optical trap.

to  $250a_0$  and the final average harmonic trap frequency is around 50Hz.

The condensate is then loaded into the quasiperiodic lattice which is aligned along the vertical direction. At the same time the optical trap is decompressed to reduce the harmonic confinement and, during the last part of the loading of the quasiperiodic potential, also the scattering length  $a$  is changed to values ranging from  $a \leq 0.1a_0$  to about  $a = 300a_0$ . The experimental sequence is sketched in fig.(3.2). The main lattice is ramped up to the final height  $s_1 = 6.6$  (well inside the tight binding regime) in 250ms with a “S-shaped” ramp in order to minimize the heating of the atoms due to a non perfectly adiabatic process. The loading of the secondary lattice is less critical since its height is smaller compared to the primary lattice one, and it introduces less heating in the system. The final height of the secondary lattice is varied up to  $s_2 = 1.2$ , which corresponds to  $\Delta/J \simeq 10$ , well above the localization threshold. At the end of this procedure, the lattice lasers give a harmonic confinement of  $\omega_{\perp} = 2\pi \times 50\text{Hz}$  in the radial direction. In the vertical (axial) direction, a weak confinement of 5Hz is given by a weak remaining optical trap as well as by a curvature from the gravity-compensating magnetic field. A sketch of the final potential felt by the atoms is also shown in fig.(3.2).

Since many interacting particles populate the same site,  $U$ , as previously defined (sec.1.1), does not give a good estimation of the interaction energy per particle. In this experimental configuration the Bose gas has a three-dimensional geometry and there is coupling into the radial direction of the system; the shape of the on-site wavefunction thus depends on the interaction energy itself. We chose to quantify the relevant interaction energy per particle calculating the average

interaction energy per lattice site and dividing by the average number of particles per site. We define this quantity with the following expression:

$$E_{int} = \frac{g}{2} N \int \varphi^4 d^3x, \quad \text{with} \quad g = \frac{4\pi\hbar^2 a}{m}. \quad (3.1)$$

where  $\varphi$  is a 3D Gaussian approximation, normalized to have  $\int |\varphi(r)|^2 d^3x = 1$ , of the single site wavefunction<sup>1</sup> and  $N$  is the average atom number per occupied lattice site. We note that the  $E_{int}$  here defined does not scale linearly with the scattering length  $a$ , as in the canonical definition of  $U$ , since not only the coupling constant  $g$  depends on  $a$ , but also the on-site atomic distribution.

We estimate that around 30 lattice sites are populated during the loading of the lattice. This corresponds to about 7 adjacent localized states of the first “mini-band”. We therefore estimate  $N$  as the total number of atoms divided by 7. This is strictly valid only in the localized regime. In fact when the system delocalizes more sites are occupied and we thus overestimate the actual interaction energy since the number of atoms per occupied site decreases. Nevertheless, comparison with a numerical simulation of our experimental loading procedure has shown that the estimated  $N$  is a good approximation for all values of the scattering length up to an error of 30%.

The loading process is adiabatic for most of the parameter range explored until  $E_{int}$  becomes sufficiently low for the system to enter the fully localized regime. Here, several independent low-lying excited states are populated even when it would be energetically favorable to populate just the ground state. In the experiment we detect a loss of adiabaticity by measuring the energy transferred into the radial direction. We measure the radial temperature and the condensed fraction in time of flight, after having inversely repeated the loading procedure, and we compare the results with the case in which only the primary regular lattice is loaded. Throughout the parameter range explored, the radial temperature as well as the condensate fraction are approximately constant; we can therefore assume that the loading process is in good approximation adiabatic<sup>2</sup>.

<sup>1</sup>Along the lattice axis we consider the gaussian approximation of the Wannier function. Along the radial direction we consider the wavefunction of the ground state of the condensate in the harmonic confinement induced by the lattice beams. In the non-interacting case it corresponds to the single particle ground-state i.e. to the harmonic oscillator ground state. In the interacting case the BEC has a Thomas-Fermi profile [52]. In both cases we consider a Gaussian approximation of the wavefunction.

<sup>2</sup>In the previous work on our setup [15], a radial heating was seen to occur in the very weak interaction region for values of the disorder larger than what we consider here.

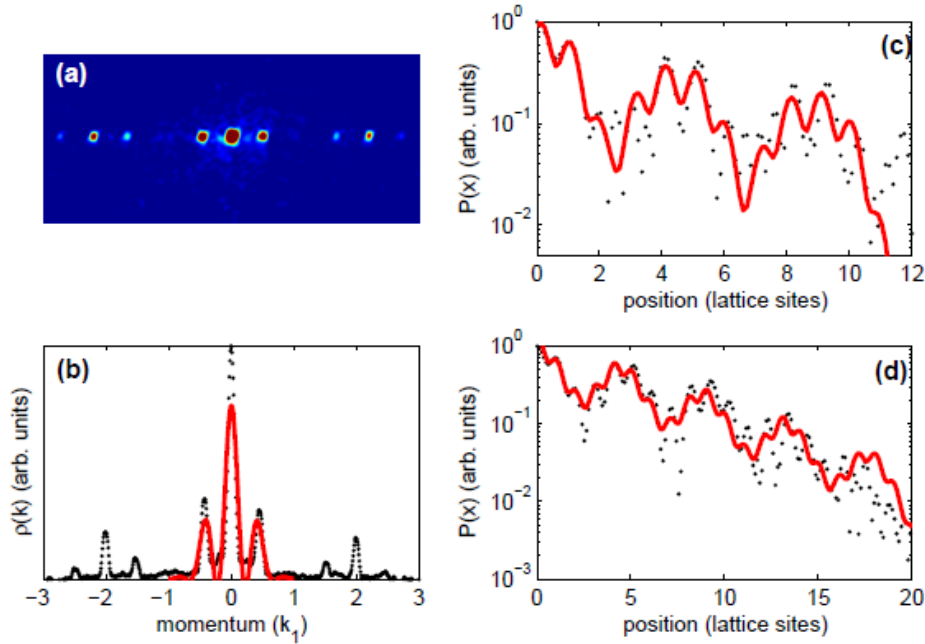


Figure 3.3: Example of image analysis. After integration along the radial direction of the acquired absorption image (a), the profile of the momentum distribution is fit with a cosine modulated Gaussian to recover the phase fluctuations (b). The Fourier transform of the square root of the profile can be fitted with three generalized exponential functions as in Eq.(3.4) to extract the exponent and local length of the localized states (c). The correlation function  $g(x)$  is given by the Fourier Transform of the momentum distribution itself, and can be fitted with three generalized exponentials, as in (c) in order to get  $g(4.2d)$  and  $g(8.4d)$ , or it can be fit with a generalized exponential decay up to 20 lattice sites (d).

### Analysis of the momentum distribution images

The system can be characterized by analyzing its momentum distribution and derived Fourier transforms. These techniques are used to extract information about the local shape of the wavefunction, the spatial correlations and the coherence properties of neighboring states. The momentum distribution of the atomic cloud is obtained from absorption images (Panel (a) in fig.3.3) taken after 46.5 ms of ballistic expansion<sup>3</sup> as explained in 2.5.2. Such a large time of flight is allowed by the gravitation-compensating magnetic gradient which prevents the atoms to fall out from the imaging beam once released from the optical confinements.

Due to the quasiperiodic nature of the employed potential, we expect that

<sup>3</sup>Such a large time of flight is permitted thanks to a gravity-compensating magnetic field gradient that prevents the atoms to fall out of the imaging beam during the expansion from the trap.

for a sufficiently homogeneous system like ours, the in-trap wavefunction can be decomposed into copies of the same state with real and non-negative envelope  $\xi(x)$ , spaced by  $D = 4.2d$ . The overall in-trap wavefunction along the lattice direction can therefore be approximated as:

$$\psi(x) = \sum_j a_j \xi(x - jD) e^{-i\phi_j}, \quad (3.2)$$

where  $\phi_j$  is the local phase, and  $\xi(x)$  can be taken as a generalized exponential function  $\exp(-|x/L|^\alpha)$ . By doing the Fourier transform of Eq.(3.2), we obtain that the magnitude of the overall wavefunction in momentum space, can be written as  $\sqrt{\rho(k)} = |\xi(k)|S(k)$ , where

$$S(k) = \left| \sum_j a_j e^{-i(jkD + \phi_j)} \right| \quad (3.3)$$

is an interference term. For many envelope functions  $\xi(x)$ , such as the generalized exponentials with  $0 < \alpha \leq 2$ , the Fourier transform  $\xi(k)$  itself is real and non-negative, so that the inverse Fourier transform of  $\sqrt{\rho(k)}$  can be written as  $\xi(x) \circ S(x)$ . This is simply the convolution of the envelope of a single state  $\xi(x)$  with the Fourier transform of the interference term,  $S(x)$ , which can be approximately described as a series of sharp peaks (approaching  $\delta$ -distributions) spaced by  $D$ , with a decreasing amplitude and phases that depend on the local phases  $\phi_j$  and amplitudes  $a_j$ .

The inverse Fourier transform of the square root of the momentum distribution  $\rho(k)$ , therefore allows an estimate of the average local shape of the (wave)function  $\xi(x)$ . On the other hand, the inverse Fourier transform of the momentum distribution itself can be employed to investigate the correlation properties of the system and in particular we can extract information about the extent of the coherence.

### 3.1.2 Local shape of the wavefunction

Information about the shape of the wavefunction of the occupied states can be obtained by analyzing the Fourier transform of the square root of the momentum distribution as justified here above. Due to the finite resolution of the imaging system the Fourier transform has an envelope with a width of about 10 lattice sites. This means that we can only distinguish easily up to three neighboring states. As shown in panel (c) of Fig.3.3, the averaged wavefunction is then analyzed by fitting to the sum of three generalized exponential functions modulated by the primary lattice:

$$f(x) = \left[ \sum_{j=0}^2 A_j \exp\left(-\left|\frac{x - jD}{L_s}\right|^\alpha\right) \right] \cdot [1 + B \cos(k_1 x + \delta)]. \quad (3.4)$$

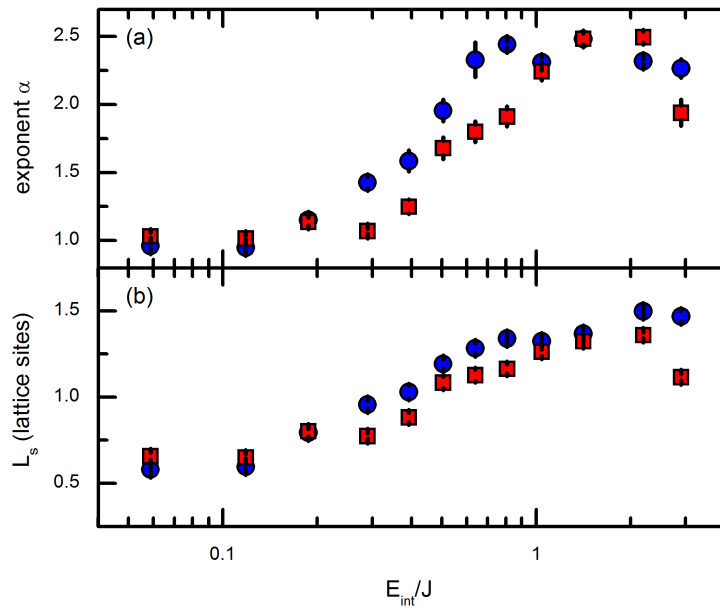


Figure 3.4: The exponent  $\alpha$  (a) and local extension of states  $L_s$  (b) are extracted from a fit of three generalized exponential states to the Fourier transform of the square root of the momentum distribution (Eq.(3.4)). The blue circles are for  $\Delta/J = 6.2$  and the red squares for  $\Delta/J = 9.5$ . In the localized regime the states are well fitted with an exponential function ( $\alpha = 1$ ) and their extension is small, less than the lattice site dimension. For increasing interaction the shape and the extension of the states change giving the indication of the crossover to the delocalized regime.

In Fig.3.4 we present the result of the analysis of localization properties of our system. We consider the evolution of the exponent  $\alpha$  and of the local extension of the states  $L_s$  as a function of the interaction energy  $E_{int}$ . We find that for very small  $E_{int}$ , the states are exponentially localized, since the exponent  $\alpha \simeq 1$ , and the local length  $L_s$  is small, consistent with the Anderson glass regime. The increase of  $E_{int}$  produces a growth of the local length and of the exponent up to  $\alpha > 2$ . Repulsive interactions therefore delocalize the system as expected, or alternatively, the localization crossover is shifted to higher values of the disorder strength  $\Delta/J$  when interactions are introduced into the system.

### 3.1.3 Phase fluctuations

As already pointed out, the restoration of an extended state can be understood in terms of phase lock of neighboring states to form coherent islands. An extensive study on the shot-to-shot fluctuations of the phase  $\phi$  of the interference in the momentum distribution gives indication on the degree of localization of the system. As shown in panel (c) of Fig.3.3, we extract this phase by fitting directly (without any Fourier transform) the momentum distribution within the first Brillouin zone with the following fitting function:

$$\rho_{fit}(k) = A \exp\left(-\frac{(k - k_c)^2}{2w^2}\right) \cdot [1 + B \cos(D(k - k_c) + \phi)], \quad (3.5)$$

where  $k_c$  is the center of the distribution, determined by fitting the average of all images of a given dataset.

If the states are not phase locked,  $\phi$  changes almost randomly at each repetition of the experimental sequence. In Fig.3.5 we show the standard deviation of  $\phi$ , estimated from a large number of repeated runs of the experiment with the same parameters. We see a decrease of the phase fluctuations by increasing  $E_{int}$ , that nevertheless remains relatively large in the crossover region and finally drop to the background value (i.e. the value measured in the case of a regular lattice) only when  $E_{int}$  is comparable to the full width of the lowest miniband of the non-interacting spectrum (dotted lines in figure). In this situation the system behaves as a single extended coherent state as in the regular lattice case. On the contrary in the localized regime the states are totally independent, which together with the localization properties summarized in Fig.3.4 indicates that the system can indeed be described as an Anderson glass.

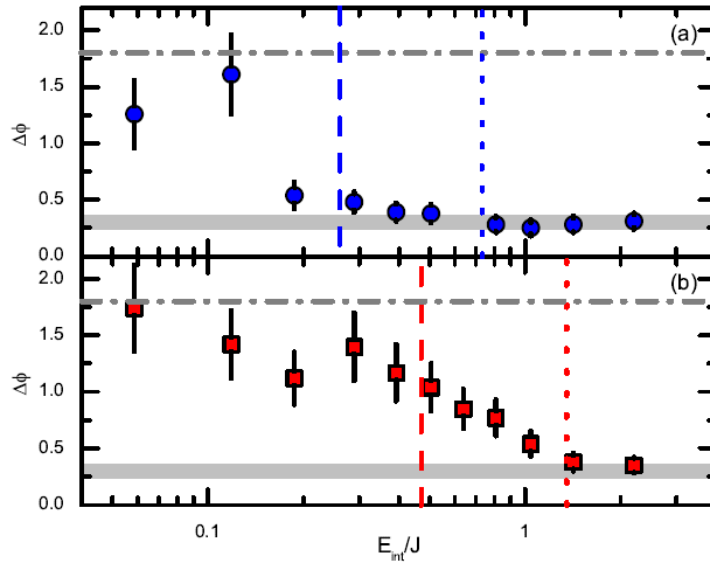


Figure 3.5: Standard deviation of the phase measured by repeating the experiment up to 26 times for a given set of parameters, for  $\Delta/J = 6.2$  (a) and  $\Delta/J = 9.5$  (b). The error is estimated as  $\Delta\phi/\sqrt{N}$ , where  $N$  is the number of images from which the phase was extracted. The gray shaded bar shows the phase fluctuations measured for an extended system below the localization threshold. The dashdotted line gives the standard deviation for a purely random distribution. The dashed (dotted) lines give the standard deviation (full extension) of energies in the lowest miniband.  $\Delta\phi$  reaches its background value when the interaction energy is comparable with the full extension of the miniband, i.e. when the system is expected to be in a single extended coherent state.

### 3.1.4 Correlation properties

We now report about the investigation of the correlation properties of our system. To directly determine the first-order correlation function  $G(x', x + x') = \langle \hat{\Psi}^\dagger(x') \hat{\Psi}(x + x') \rangle$  we would need to have explicit knowledge of the in-trap density distribution which is not possible in the experiment. Nevertheless using the Wiener-Khinchin theorem we can extract the *spatially averaged correlation function* from the Fourier transform of the momentum distribution, which is, conversely, experimentally accessible :

$$g(x) = \int G(x', x + x') dx' = \int \frac{dk}{2\pi} \rho(k) e^{ikx} \quad (3.6)$$

A first way to analyze the decay of correlations experimentally is to fit  $g(x)$  with the same generalized exponentials of 3.4. In this way we can recover the spatially averaged correlation between states 4.2 (8.4) lattice sites apart as  $A1/A0$  ( $A2/A0$ ). As in the analysis of the local shape, also here, the finite imaging resolution limits our analysis to three neighboring states, and it follows that  $g(4.2d)$  ( $g(8.4d)$ ) saturates at a value around 0.6 (0.3). Experimental results are reported in Fig.3.6.

In the localized regime the correlation is finite but small. Atoms occupy independent neighboring localized states. As  $E_{int}$  is increased, the correlation features quite a broad crossover towards larger values, signaling that coherence is progressively established locally over distances of first  $4.2d$  and then  $8.4d$ . The position of this crossover is in good agreement with the prediction of the simple disorder screening argument, from which we expect the center of the crossover to occur when  $E_{int}$  is comparable to the standard deviation of energies in the lowest miniband (dashed lines in the picture).

We can now consider together the behavior of the correlation between neighboring state and the phase fluctuations analyzed in the previous section, in order to have a more complete picture of the properties of the system for increasing interactions. The system crosses a large crossover region of only partial coherence indicated by a large  $g(4.2d)$  but also relatively large phase fluctuations  $\Delta\phi$ . This is consistent with the formation of locally coherent fragments expected for a Bose glass. Ultimately, the features of a single extended, fully coherent state, i.e. a BEC, are seen for  $E_{int}$  comparable to, or larger than, the full width of the lowest “miniband”. In this region of parameters in fact  $g(4.2)$  and  $g(8.4)$  approach their maximum values and the phase fluctuation is reduced to the background value.

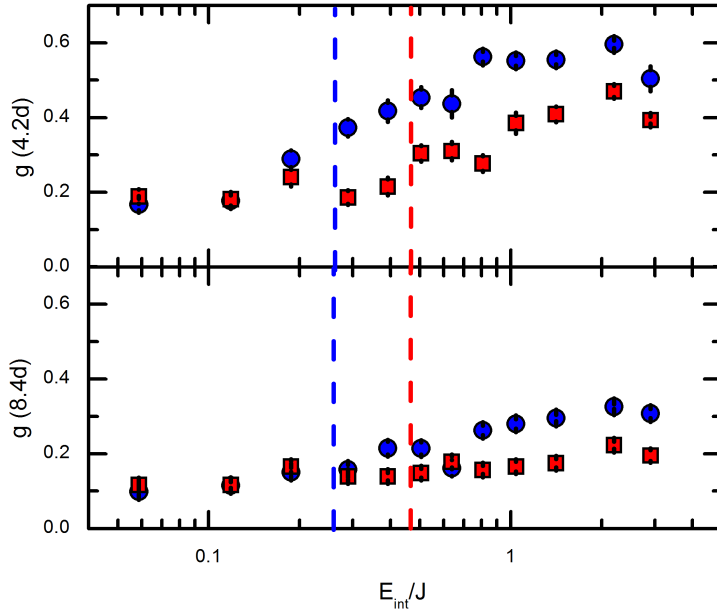


Figure 3.6: The spatially averaged correlation function  $g(x)$  is extracted from the Fourier transform of the momentum distribution itself, and fits with three generalized exponential functions evaluate  $g(x)$  at  $4.2d$  (a) and  $8.4d$  (b). The blue circles are for  $\Delta/J = 6.2$  and the red squares for  $\Delta/J = 9.5$ . The error bars denote the standard error of the mean. The correlation at  $4.2d$  starts to increase when the interaction energy is comparable with the standard deviation of the energies in the first miniband (indicated by the dashed lines). This indicates the presence of coherent fragment larger than a single state.

### Shape of the correlation function

More information about the extent and decay of the spatially averaged correlation function can be gained by examining the Fourier transform of the momentum distribution at larger distances. Though the detailed structure is not resolvable, making the data there unsuited for the analysis described above, we can extract information about the general shape of  $g(x)$ . The data are then fitted with the following function:

$$g_{fit}(x) = \left[ \sum_{j=0}^4 \exp\left(-\left|\frac{jD}{l_g}\right|^\beta\right) \cdot \exp\left(-\left|\frac{x-jD}{L_s}\right|^\alpha\right) \right] \cdot \frac{1 + B\cos(k_1x)}{1 + B} \quad (3.7)$$

where  $\beta$  is the correlation exponent and  $L_g$  is the correlation length. This describes the sum of five generalized exponential functions spaced by  $D$ , with amplitudes determined by the global shape of the correlation function.

The overall behavior of the correlation function is shown in Fig.3.7. The correlation length  $L_g$  increases at larger interaction energy to values larger than the mean separation of states ( $4.2d$ ). It saturates at values around  $6d$ , consistent

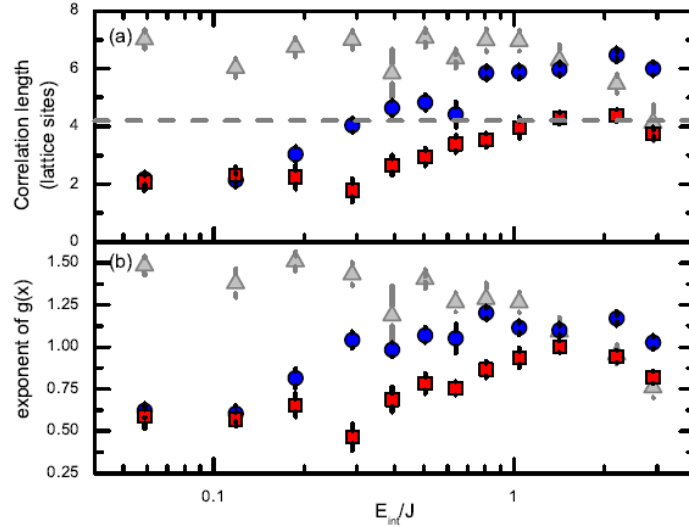


Figure 3.7: Decay of the correlation function. (a) Correlation length; (b) exponent of the generalized exponential function. Also in this figure the blue circles are for  $\Delta/J = 6.2$  and the red squares for  $\Delta/J = 9.5$ . The gray triangles are for a single lattice ( $s_1 = 5.7$ ), fitted to a single generalized exponential function. The dashed line denotes the average separation of states,  $4.2d$ . The error bars denote the standard error of the mean.

with the imaging resolution, for both quasiperiodic and single lattice potentials<sup>4</sup>. The increase in correlation length shows that the average size of fragments found in the fragmented BEC regime increases with  $E_{int}$  until only a single fragment describes the system as in the regular lattice case.

The exponent  $\beta$  of  $g(x)$  is seen to increase from values of about 0.5 to values slightly larger than 1. While such an increase is qualitatively expected, the values of  $\beta$  are not in agreement with expectations from theory. For a 3D Bose gas at zero temperature, we expect a transition from exponential decay ( $\beta = 1$ ) in the insulating regime [1] to a shape of the correlation function given by the confining potential,  $\beta = 2$  in our case. However in our analysis, any finite thermal component artificially reduces the exponent by increasing the values of the Fourier transform at small  $x$ -values. Indeed, we observe an exponent of 1.5 or less even in the single lattice potential, for which the system is superfluid. In the quasiperiodic lattice, the exponent approaches that of the single lattice potential for large values of the interaction energy. If we look at the plot it is possible to note a decrease

<sup>4</sup>We note that the atoms are trapped in a harmonic confinement, the correlation function itself, in this case features a decay due to the atomic density profile even when the system is fully coherent. For example the degree of coherence, defined as  $\tilde{g}(x', x+x') = G(x', x+x')/(\sqrt{\rho(x')}\sqrt{\rho(x+x')})$ , is often used in substitution to the normal definition of the first order correlation function when inhomogeneous systems are taken into account.

in  $L_g$  and  $\beta$  at the largest values of  $E_{int}$ . This can presumably be explained by an experimental imperfection: the interaction energy is probably not completely removed from the system during the initial stage of expansion from the lattice. This would lead to a broader peak in the momentum distribution and therefore a narrower shape at short distances in the correlation function.

In recent theoretical works on disordered bosonic systems, the change in shape and in extension of the correlation function in one dimension at  $T = 0$  from exponential decay to algebraic decay has been used to distinguish the Bose glass from the superfluid phase [53, 54, 55]. These theoretical investigations have the advantage of being able to consider large system sizes, where a jump in the extension of the correlation function  $G(x_0, x)$  is an indication that fragments form, leading moreover to an exponential decay of  $g(x)$  in the Bose glass regime. In the experiment, the correlation function can only be recovered for smaller distances, due to the finite imaging resolution and system size. Fragments with sizes larger than approximately  $2D$  cannot be distinguished from the superfluid. In this sense, the evolution of the correlation function can give information about the crossover from the Anderson glass to the fragmented BEC (where the correlation length starts to increase), but cannot quantify the crossover to the superfluid. The use of a higher resolution imaging system and eventually larger system sizes might enable the observation of the correlation function at larger distances. The crossover from fragmented BEC to superfluid might then be experimentally quantified.

## 3.2 Subdiffusive expansion in the disordered lattice

In the previous section we have presented an extensive study on the ground state of a gas of bosonic atoms in a disordered lattice. We have analyzed in detail the transition from a disorder localized state to an extended coherent state driven by a weak interaction. Interactions are able to screen the effect of disorder and create a coherent state which has similar properties compared to the superfluid phase of a Bose gas in a regular lattice.

The natural question to pose now is about the transport properties of such a system. A localized system is in fact expected to be characterized by the absence of transport since it is in an insulating phase. On the contrary an extended Bose Einstein condensate in a regular lattice is known to be in a conducting phase where atoms are free to move from site to site. What about a disordered interacting system? This question can be posed in two complementary ways. Can atoms move across the disordered lattice by tunneling from state to state

thanks to the coupling given by interaction? Can an initially localized wavepacket spread in a disordered potential when a non-linearity is added in the system? We experimentally addressed this problem and in the following we report about our results [56].

In particular we study the expansion of the bosonic cloud in the disordered lattice when the initial longitudinal harmonic confinement is removed. This procedure causes a big perturbation in the system which is suddenly carried out of equilibrium. We observe that a non interacting gas does not expand, confirming the localized nature of the single-particle states. By adding a controlled interaction we observe instead a slow increase of the cloud size, which follows a subdiffusive law in agreement with theoretical models and numerical simulations.

### Measured time-evolution of the width

The experimental procedure we employ to study the transport dynamics of our system is similar to the one used to investigate the ground state even if they differ in few essential points. The condensate of about  $5 \times 10^4$  atoms is produced in the crossed optical trap at the scattering length  $a = 280a_0$ . The trap potential has a radial (axial) frequency of  $2\pi \times 50$  (70)Hz. We first load the interacting condensate into the quasiperiodic lattice with a constant  $\Delta/J \sim 3$ ; the lattice beams give an additional radial confinement and the final radial frequency is  $\omega_r = 2\pi \times 70$ Hz. At a given time  $t = 0$  the optical trap is suddenly switched off, allowing the sample to expand along the lattice; at the same time,  $\Delta$  and  $a$  are tuned to their final values within 10 ms, and kept there during the evolution. The experimental sequence is sketched in Fig.3.8. We note that, conversely to the experiment devoted to the study of the ground state, here the system is prepared always in the same conditions and the final values of disorder and interaction are set during few ms in a non-adiabatic way. For this reason we do not expect to occupy only the states in the lowest miniband of the quasiperiodic lattice but to populate in a more homogeneous way all the states which lie under the envelope of the initial density profile.

The initial interaction energy per particle is estimated as in Eq.(3.1). Also in this case we have an uncertainty on the estimate of the number of the initially occupied lattice sites and therefore on  $N$ . We calculate that the initial distribution occupies on average  $20 \pm 7$  sites; this translates into a 35% uncertainty on  $E_{int}$ .

After the opening of the trapping potential we follow the evolution of the atomic distribution along the disordered lattice. A first qualitative characterization of the effect of repulsive interactions on the transport capability of the system

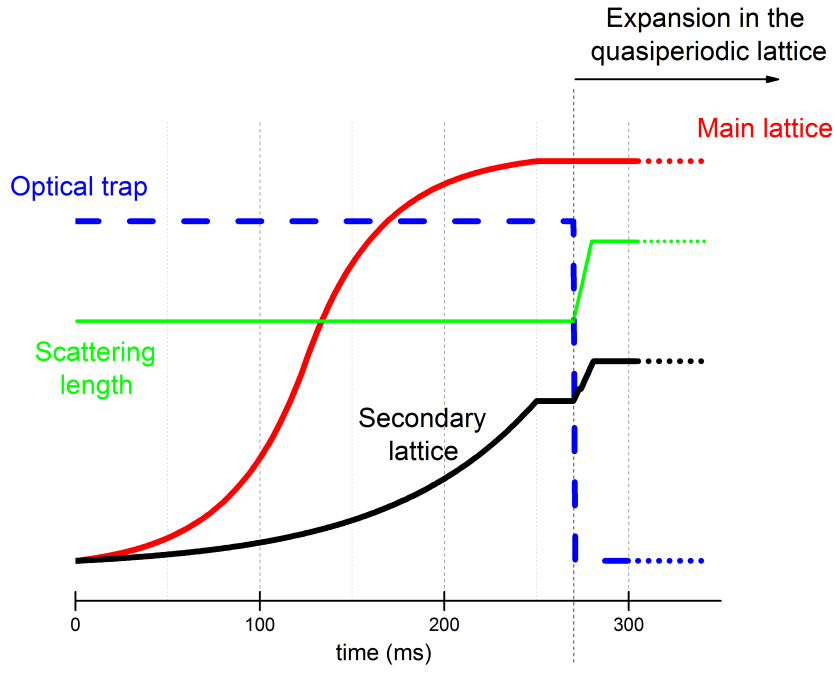


Figure 3.8: Experimental sequence for the diffusion experiments.

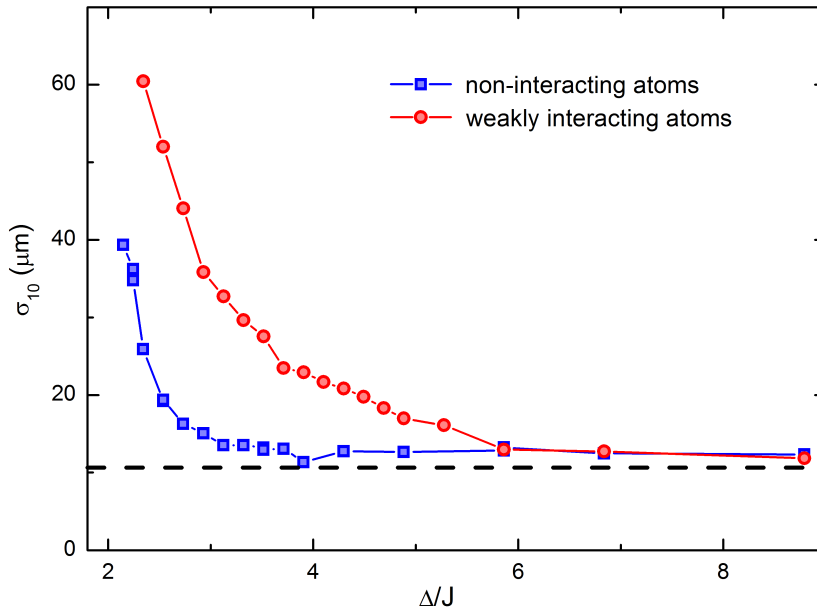


Figure 3.9: Axial width of the cloud after 10 seconds of evolution in the quasiperiodic lattice in the non interacting case (blue squares) and for initial interaction energy  $E_{int} = 1.5J$  (red circles). The dashed line shows the initial size of the cloud.

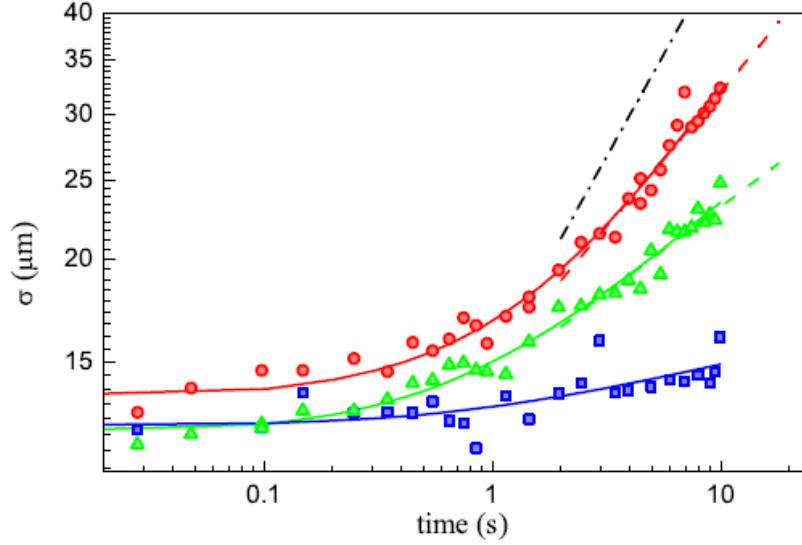


Figure 3.10: Time evolution of the width  $\sigma$  for different initial interaction energies:  $E_{int} = 0$  (blue squares),  $E_{int} = 1.8J$  (green triangles), and  $E_{int} = 2.3J$  (red circles). Solid lines are fits with Eq.(3.9). The dashed lines show the fitted asymptotic behavior, while the dash-dotted line shows the expected behavior for normal diffusion. The slow expansion of the non-interacting sample is due to technical noise. The lattice parameters are  $J/h = 180\text{Hz}$  and  $\Delta/J = 4.9$ .

can be given by comparing the width of the cloud after 10s of evolution with the initial one. The final size of the cloud  $\sigma_{10}$  versus the disorder strength  $\Delta/J$  is plotted in Fig.3.9. We measure the width of the radially-integrated spatial distribution  $n(x)$  by in-situ absorption imaging (see sec.2.5.1 for details). The width of the distribution is calculated as the square root of its second moment<sup>5</sup>:

$$\sigma = \sqrt{\int x^2 n(x) dx}. \quad (3.8)$$

In absence of interaction, we observe than for value of the disorder larger than  $\Delta/J = 2$ , where the eigenstate of the system are expected to be localized over a few lattice sites, expansion is gradually suppressed and for  $\Delta/J > 3$  we are no more able to appreciate any expansion on the timescale of the experiment. If we add some repulsive interaction, we still observe a crossover between an expanding and a non-expanding system, but the crossover position is shifted to larger value of  $\Delta/J$ , i.e. a lager disorder is needed to prevent the observation of an expansion over 10 seconds. This indicates that a localized non-interacting system is turned into a non-localized system by the interaction.

<sup>5</sup>Here  $\int n(x) = 1$ .

In order to characterize the expansion of the interacting atoms for  $\Delta/J > 2$ , we have also performed a systematic study of the time evolution of  $\sigma$  for increasing times, up to  $t = 10$ s. In Fig.3.10 we show for instance the time evolution of  $\sigma$  for a fixed value of the disorder  $\Delta/J = 5$  and three different values of the initial interaction energy  $E_{int}$ . In absence of interaction the system is localized and the width essentially does not change in time. Only a very small expansion can be observed, presumably due to the noise intrinsically present in the experiment. The noise is mostly provided by the vibrations of the retroreflecting mirror of the lattice beams. An extensive characterization of the noise-induced delocalization will be given in the next section. The introduction of a repulsive interaction allows the wave-packet to expand: the expansion is however not ballistic as it is for a non-interacting superfluid below the localization threshold, since its velocity decreases with time. Note that the expansion is very slow if compared with the characteristic time given by the tunneling energy of the primary lattice ( $J/h \sim 5$ ms for  $s_1 = 7$  as in figure). To model the expansion dynamics we fit the measured evolution with the solution of a generalized diffusion equation:

$$\sigma(t) = \sigma_0 \left(1 + \frac{t}{t_0}\right)^\alpha \quad (3.9)$$

Here  $\sigma_0$  is the initial width,  $t_0$  is an ‘‘activation time’’ and  $\alpha$  is the expansion exponent. Ballistic expansion would correspond to  $\alpha = 1$  and normal diffusion to  $\alpha = 0.5$ . By fitting the experimental data we instead extract exponents  $\alpha \approx 0.2 - 0.4$ . This indicates a subdiffusive expansion. The results of a systematic study on the coefficient  $\alpha$  for different values of initial interaction energy  $E_{int}$  and disorder strength are report in Fig.3.11. In the following we will show that Eq.(3.9), with three fitting parameters, is expected to correctly model the overall behavior from short times to the asymptotic regime  $t \gg t_0$ . The initial size at that point does not play a role in the expansion, two parameters in the fitting procedure are enough and the expansions shows a linear behavior in the log-log scale. However, in order to decrease the uncertainty on the parameters and to extract information also from the measurements at shorter times, we chose to fit also the data taken for  $t < t_0$  using the three parameters fitting function. This gives us also the possibility to confirm that the asymptotic regime has been reached by comparing the fitted  $t_0$  with the maximum observation time. The characteristic value for the activation time  $t_0$  is indeed around one second (except for the non-interacting case, where it is larger), i.e. one order of magnitude smaller than the maximum observation time. This indicates that the asymptotic behavior is achieved for approximately one decade. Note also that by fitting only the data

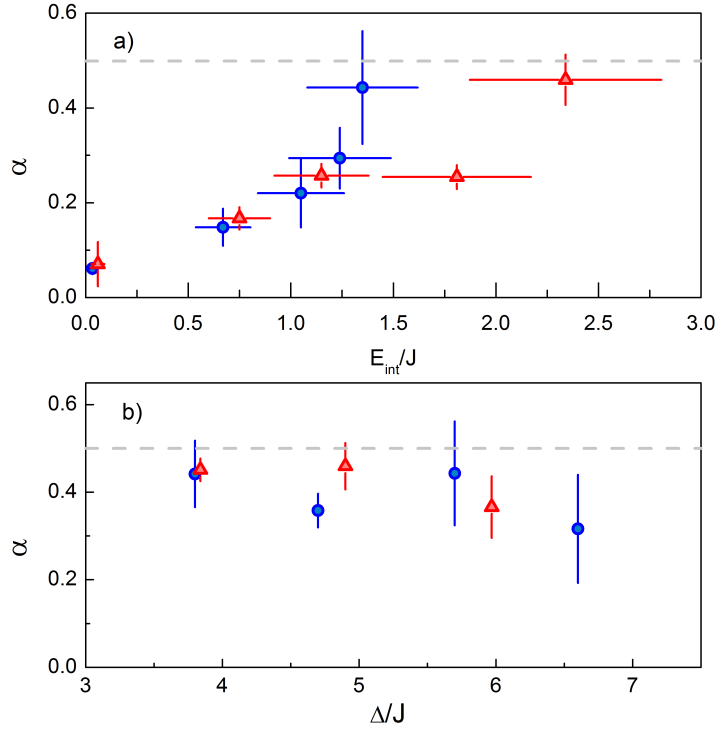


Figure 3.11: Expansion exponents  $\alpha$  for two different values of the primary lattice height ( $J/h \simeq 180$ Hz for the red triangles and  $J/h \simeq 300$ Hz for the blue squares). In (a) the disorder strength is fixed to  $\Delta/J = 5$  and the initial interaction energy  $E_{int}$  is varied. In (b)  $E_{int} \simeq 2$  and  $\Delta/J$  is varied. The fitted exponent is always smaller than 0.5 (dashed gray line), indicating a subdiffusive behavior.

points for  $t > t_0$  with the asymptotic form of Eq.(3.9), as shown by dashed lines in Fig.3.10, we obtain results in good agreement with what we extract from our fitting procedure.

The dynamics of a wavepacket in a disordered potential in presence of a non-linearity has been the subject of many theoretical predictions and debate based on numerical simulations over the last 20 years starting from the first results published by Shepelyansky in 1993 [57]. He has been the first to numerically obtain that non-linearity prevents localization leading to a subdiffusive dynamics of an initially localized wavefunction. However, our data are the first experimental evidence of such a subdiffusive expansion.

The observed subdiffusion confirms the microscopic mechanism of the expansion expected for an interacting disordered system where all the single-particle states are localized. Interaction breaks the orthogonality of the states and allows the transfer of population between neighboring states. Since the transfer rate depends on  $E_{int}$ , the velocity of expansion decreases as the sample expands and

becomes less dense. Various authors have built models for the expansion that relate the transfer rate to the variation of the width [57]. We now review these results presenting a heuristic model for our system based on a perturbative approach, which qualitatively justifies the observed subdiffusion. We also compare our results with the solution of a non-linear diffusion equation which, according to some authors [58], could be used to describe the behavior of a system like ours.

### 3.2.1 Perturbative model

We present in this section a heuristic model which aims to link the macroscopic subdiffusive expansion of the atomic cloud in the disordered potential with the microscopic interaction assisted hopping of atoms between single-particle localized states.

Let us start by considering the localized eigenstates of the 1D single-particle problem,  $\varphi_i$ , labeled by the site index  $i$ . These states have individual energies  $\epsilon_i$  with typical separation  $\delta E \approx \Delta$  and a characteristic localization length  $\xi \approx d/\ln(\Delta/2J)$ . A schematic representation of the axial states along one quasiperiod of the quasiperiodic lattice is shown in Fig.3.12. We consider the interaction term in the second quantization Hamiltonian for a bosonic gas of cold atoms (Eq.(1.1)) as the perturbative term in the single particle problem:

$$\hat{H}_{int} = \hat{H}' = \frac{g}{2} \int dx \hat{\psi}^\dagger(x) \hat{\psi}^\dagger(x) \hat{\psi}(x) \hat{\psi}(x) \quad \text{with} \quad g = \frac{4\pi\hbar^2 a}{m}. \quad (3.10)$$

In chapter 1 we deduced the Bose Hubbard Hamiltonian by decomposing the wavefunction  $\hat{\psi}(x)$  over the basis of the Wannier functions, here, instead, we choose  $\varphi_i$ , which are orthogonal and normalized to unity:

$$\hat{\psi}(x) = \sum_i \hat{a}_i \varphi_i(x), \quad (3.11)$$

being  $a_i$  the bosonic destruction operator at site  $i$ . In general, four states can be coupled by the interaction. It can be seen that the dominant contribution in the expansion process is the one in which two particles are moved from two states  $i$  and  $j$  with occupation  $N$  to two initially empty states  $k$  and  $l$ . Here  $N$  is again the mean number of atoms per occupied state in the initial distribution, which is related to the width  $\sigma$  by the relation  $N = N_{tot}/\sigma$ . The off-diagonal term of the interaction Hamiltonian for this process has the form:

$$V'_{ijkl} = \frac{g}{2} N I_{ijkl} \quad \text{with} \quad I_{ijkl} = \int \varphi_l^*(x) \varphi_k^*(x) \varphi_j(x) \varphi_i(x) dx. \quad (3.12)$$

From perturbation theory we know that this kind of process can happen at asymptotic times only if the energy is conserved, i.e.  $\Delta E = |\epsilon_i + \epsilon_j - \epsilon_k - \epsilon_l| = 0$ . In a

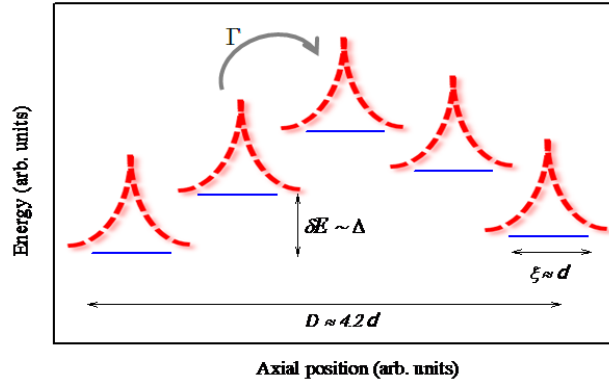


Figure 3.12: Cartoon of the axial states along one quasiperiod of the quasiperiodic lattice. The localization length of the localized single particle eigenstates is of the order of the lattice spacing  $d$  and the mean separation in energy between neighboring states is of the order of  $\Delta$ .

disordered system it is impossible to have perfect energy matching of the states. Anyway, if the transition rate for the process is large enough, even a finite energy difference might not be resolved and the transition can take place. As discussed for example in [59, 60] the appropriate energy conservation requirement is actually

$$|V'_{ijkl}| > \Delta E. \quad (3.13)$$

The transfer rate associated to this microscopic process is:

$$\Gamma_{ijkl} = \frac{2\pi}{\hbar} \frac{|V'_{ijkl}|^2}{\Delta E} \quad (3.14)$$

From Eq.(3.12) one sees that the coupling term  $|V'_{ijkl}|$  is essentially the interaction energy per particle  $E_{int}$  times an overlap integral  $I \approx \exp(-L/\xi)$ , where  $L$  is the mean separation between the four states. We can therefore conclude that the macroscopic expansion of the system will be determined by all the microscopic processes between states that are laying within a few localization lengths from each other.

We can distinguish two different regimes of expansion. The first one occurs when the initial interaction energy is sufficiently large to provide that all the strongest couplings of each localized state to the other states within one localization length are active. This regime is reached when  $E_{int} > \delta E$ . Here one can define a macroscopic rate  $\Gamma = \langle \Gamma_{ijkl} \rangle$ , where the symbol  $\langle \dots \rangle$  denotes an average over the system extension. From Eq.(3.12) and Eq.(3.14) we obtain that the transfer rate from state to state  $\Gamma \propto (gN)^2 \propto \sigma^{-2}$ . The second regime occurs when the interaction energy is weaker,  $E_{int} < \delta E$ . In this case only a reduced number

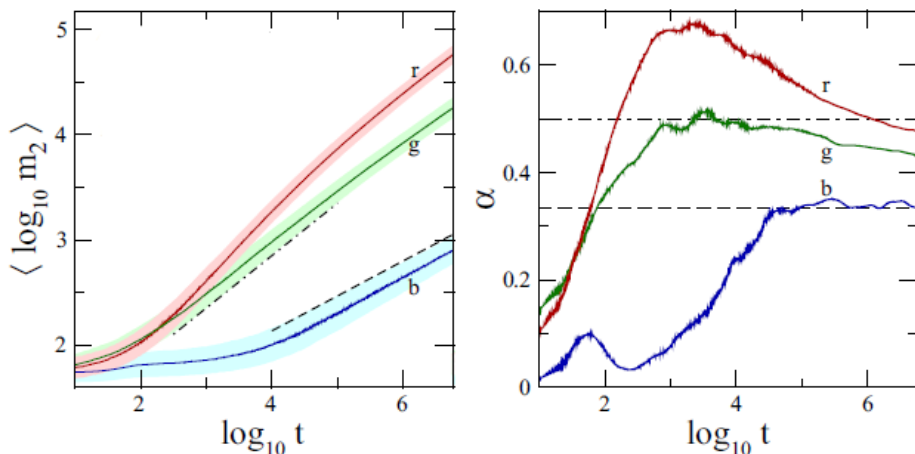


Figure 3.13: Numerical simulations for the expansion in random system in presence of non-linearity [61]. Log-Log plot of the time evolution of the second moment of the distribution (left) and of the instantaneous diffusion exponent  $\alpha$  (right) for three different value of the strength of the non-linear term (we note that the exponent here reported is twice what we usually consider since  $\sigma = \sqrt{m_2}$ ). When  $E_{int} > \delta E$  (green line) the diffusion exponent is expected to be 0.5, when  $E_{int} < \delta E$ , (blue line) 0.33. A transition between the two regimes can be seen in the green curve which tends to smaller value for longer times.

of microscopic transitions are activated by interaction, and the rate  $\Gamma$  has thus an additional dependence on  $E_{int}$  and scales faster with the width<sup>6</sup>.

We can now relate  $\Gamma$  to a rate of change of the width of the distribution itself. In the case in which the expansion is assumed to be instantaneously diffusive, as it is usually done to describe a lattice with random disorder [62], the diffusion coefficient is essentially  $\Gamma$  itself, and in the first regime ( $E_{int} > \delta E$ ) one obtains:

$$\frac{d\sigma^2}{dt} \propto \sigma^{-2}. \quad (3.15)$$

More in general we can write an equation of motion for the width of the distribution of the form:  $d\sigma/dt = C\sigma^{-p}$ , where  $p$  is a positive rational number and  $C$  is a constant which takes into account all the terms that do not depend directly on  $\sigma$ . The integration of this equation with the initial condition  $\sigma(0) = \sigma_0$  leads to:

$$\sigma(t) = \sigma_0 \left( 1 + \frac{C}{\alpha \sigma_0^{1/\alpha} t} \right)^\alpha, \quad (3.16)$$

with  $\alpha = 1/(p + 1)$ . Note that the fitting Eq.(3.9) is derived from this. From Eq.(3.15) we get  $p = 3$ , and thus we obtain  $\alpha = 0.25$ . In the random disorder

<sup>6</sup>According to some authors working in the quantum chaos field, these two regimes can be called *strong chaos* and *weak chaos* regime [61].

case, 0.25 is therefore the maximum value of  $\alpha$  that one should expect from the perturbative approach traced so far. The exponent  $\alpha$  is also expected to be smaller when the system enters the regime in which  $E_{int}$  is no more enough to couple all the possible states. These expectations are consistent with the results of the extensive numerical simulations of disordered lattices based on the *Discrete Non-Linear Schrödinger Equation* (DNLSE) or similar models. One example is shown in Fig.3.13.

### Quasiperiodic disorder: role of the spatial correlation

So far we have shown a general perturbation approach to the problem, treating our system like a randomly disordered lattice. We can now consider more in detail the effect of the quasiperiodic disorder used in our experiment. We need indeed to justify our observation of exponents as large as 0.4, therefore definitely larger than the maximum value expected for random disorder. As we will see, larger values of alpha can be justified if one considers the spatial correlation of the disorder in a quasiperiodic lattice.

In this sense it is instructive to numerically calculate the quantity  $|V'_{ikk}|/\Delta E$  in the quasiperiodic lattice, for various spatial separations between the two states. Fig.3.14 shows for example the calculations for transitions between doublets of states. It is clear that the largest coupling is achieved on average for states that are separated by one quasiperiod  $D = d/(\beta - 1)$ . This result is a consequence of the peculiar spatial correlation of the eigenstates in the quasiperiodic lattice. The large coupling of states separated by one quasiperiod suggests that in the expansion might have a more coherent nature than in the case of a random disorder. The expansion in this case would be dominated by sequential hopping between states close in energy and separated by  $D$ . It is instructive to rewrite Eq.(3.15) by assuming that the rate  $\Gamma$  represents an instantaneous velocity instead of an instantaneous diffusion coefficient. In this case one obtains:

$$\frac{d\sigma}{dt} \propto \Gamma \propto \sigma^{-2}. \quad (3.17)$$

This equation gives an expansion exponent  $\alpha = 1/3$  in the time evolution of the width expressed by Eq.(3.16) or equivalently by Eq.(3.9).

This is valid for the strong regime of large interactions. We can also give an estimate on how much the exponent should decrease in the regime of weaker interactions. For example, we numerically evaluated the behavior of the coupling between doublets of states for our quasiperiodic lattice with  $\Delta/J = 3.5$ , which correspond to  $\delta E \approx 3J$ . We followed the analysis presented in [59, 60, 61, 62, 63]

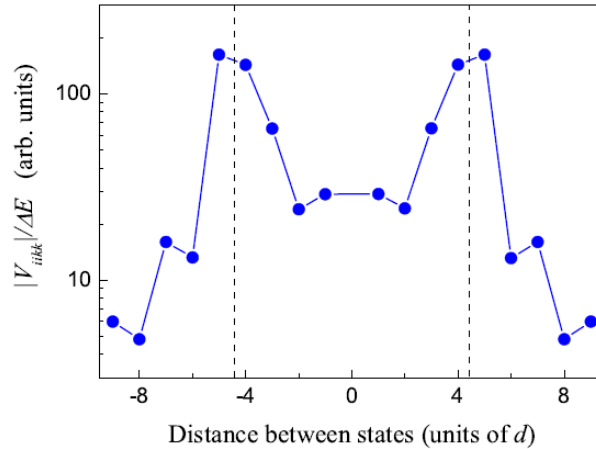


Figure 3.14: Calculated mean coupling for doublets of states in the quasiperiodic lattice versus the distance between the state. The dominant couplings are those between states that sit one quasiperiod,  $D \approx 4.2d$ , apart.

and we selected the strongest coupling  $|V'_{iik}|/\Delta E_{ik}$  for each initial state  $i$ . We then calculated the probability to have such coupling active for a varying interaction energy. Finally we averaged this result over many initial states along the lattice. As shown in Fig.3.15, we find that the normalized rate is about constant above a certain interaction energy,  $E_{int} > \delta E$ , while it decreases for decreasing interaction energy. If we consider an inverse linear dependence, we get that the rate  $\Gamma$  scales as  $N^3 \propto \sigma^{-3}$ , since  $E_{int} \propto N$ . This changes the expansion exponent in the equation of motion for  $\sigma$ . For example, in the case of a coherent expansion we supposed to occur in the quasiperiodic case, one obtains

$$\frac{d\sigma}{dt} \propto \sigma^{-3} \quad \Rightarrow \quad \sigma \propto t^{1/4}. \quad (3.18)$$

In conclusion we have shown that assuming a more coherent expansion in the quasiperiodic lattice than in the pure random case, the expansion exponent  $\alpha$  is expected to be  $1/3$  in the regime of larger interaction, where each initial state can be couple by interaction to at least another state. For smaller interaction energy, the exponent is smaller and close to  $1/4$ . These value of  $\alpha$  are larger than the one found in the random case and closer to what we measure in the experiment. Furthermore, numerical simulations performed on the quasiperiodic potential confirm these expectation [64].

This heuristic model, and in particular the assumption of a more coherent process for a quasiperiodic disorder, are far from being a rigorous way to describe the complex dynamics of such a system and derive the correct value of the expansion exponent. Nevertheless it gives a hint to the microscopic processes ruled

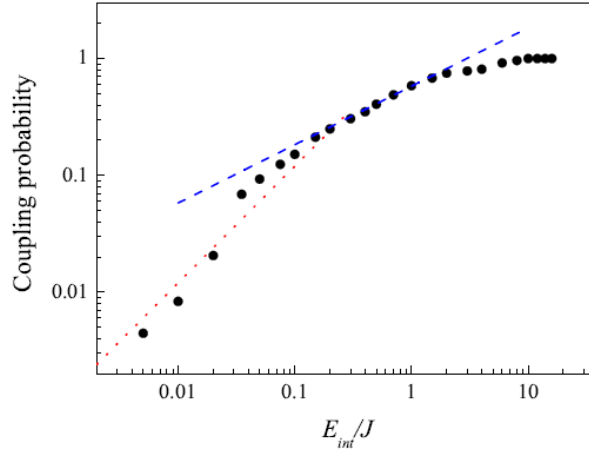


Figure 3.15: Calculated probability of coupling for doublets of states in a quasiperiodic lattice with  $\Delta = 3.5J$ . When the interaction energy is large enough the probability is 1. This means that all the couplings are active and therefore each initial state can be coupled at least with another state. For smaller interaction energies this probability has a strong dependence on  $E_{int}$  itself. The dashed and dotted lines are a guide for the eye for decay proportional to  $\sqrt{E_{int}}$  and  $E_{int}$  respectively.

by non-linearity which determine the expansion and finds general results in good agreement with both simulation and experiment.

### 3.2.2 Numerical simulations for the quasiperiodic potential

Numerical simulations of the spreading of a wavefunction in disordered potentials in presence of non-linearities have been extensively performed for random disorder. However, it is also possible to simulate also the quasiperiodic situation. In particular, a one dimensional DNLSE [64] has been used by our theory colleagues to simulate the expansion of a wavepacket for the same lattice parameters as in the experiment. We now briefly introduce the DNLSE and discuss the numerical results in comparison with the experimental data.

The evolution of non-interacting system in a one dimensional quasiperiodic potential is described by the Aubry-André model, which is obtained from the Schrödinger equation by expanding the single-particle wave function  $\psi(x)$  over a set of Wannier states as in the Bose-Hubbard model. The Wannier functions are maximally localized at the minima of the primary lattice in the lowest Bloch band and they are all identical. In the presence of interactions between the atoms, one can instead use a mean field approach and start from the Gross-Pitaevskii

equation:

$$i\hbar \frac{\partial \psi}{\partial t} = -\frac{\hbar^2}{2m} \frac{\partial^2 \psi}{\partial x^2} + V(x)\psi + gN_{tot}|\psi|^2\psi, \quad (3.19)$$

here  $\psi(x)$  is normalized in order to have  $\int |\psi(x)|^2 dx = 1$ . Using the same procedure as in the non-interacting case and decomposing  $\psi(x)$  over the Wannier functions  $|\psi(x)\rangle = \sum_i \psi_i |w_i\rangle$ , one gets a generalized Aubry-André model which includes an additional non-linear term that represents the mean-field interaction [36]. The interaction term in the Hamiltonian is

$$H_{int} = \frac{\beta}{2} \sum_i c_i^4 \quad \text{with} \quad \beta = gN_{tot} \int |w(x)|^4 dx, \quad (3.20)$$

where  $N_{tot}$  is the total number of particle in the system and  $\psi_i$  is a complex variable whose modulus square gives the probability of finding a particle at the lattice site  $i$ . To get the right normalization we have that  $\sum_i |\psi_i|^2 = 1$ .

Expression 3.20 gives the interaction energy per particle. In order to compare the experimental finding with the numerical one we have to relate the interaction coupling  $\beta$  with the estimate of the mean interaction energy per particle that we defined for the experiment. To do this some assumptions have to be made. First of all we have to apply this one dimensional equation to the three dimensional condensate of the experiment. We can assume that the three dimensional wavefunction can be separated into a radial and an axial part  $\psi = \phi_r \phi_x$ . Making the approximation that the radial shape of the condensate does not change during the expansion, we can include  $\int |\phi_r|^4$  in the  $\beta$  constant. This is not rigorously true since the radial shape of the interacting condensate depends on the interaction energy itself, which decreases as the sample expands<sup>7</sup>. Furthermore we can approximate both the radial wavefunction and the axial Wannier function with gaussian functions. We then remind that we defined  $N$  as the average atom number per occupied state. We can then get  $N_{tot} \approx n_{site} N$ , where  $n_{site}$  is the number of average occupied lattice sites. Under this assumptions, reminding the definition of  $E_{int}$  given in Eq.(3.1) we obtain:

$$\beta \approx 2 E_{int} n_{site}. \quad (3.21)$$

We note that, while  $E_{int}$  decreases during the expansion of the sample,  $\beta$  is constant. In the experiment we initially occupied around 20 sites; this means that a typical value of the initial interaction energy for the experiment reported in this thesis,  $E_{int} = 2J$ , correspond to  $\beta \sim 80J$ .

<sup>7</sup>A variation in the radial shape of the condensate is also given by a radial heating which occurs during the expansion. We will discuss about the role of this heating in the axial dynamics in the next section.

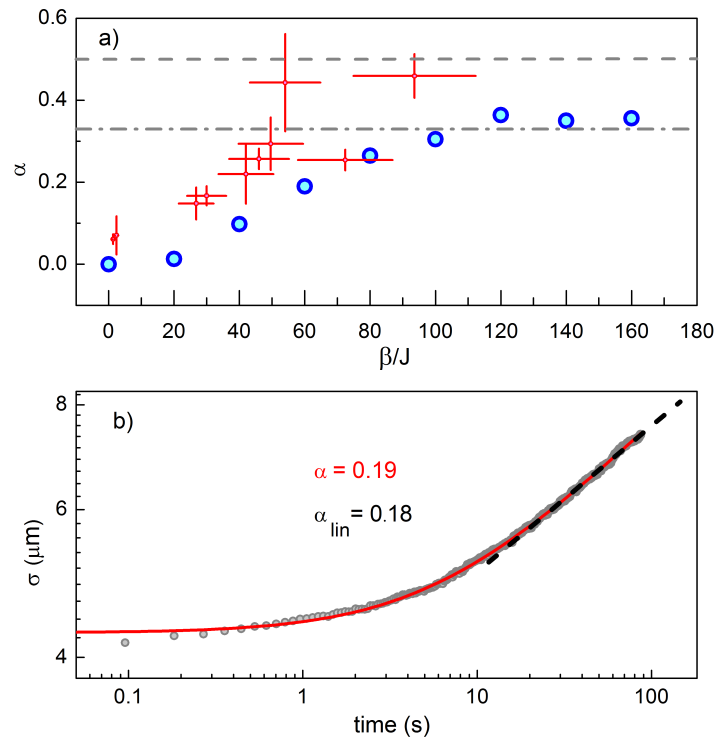


Figure 3.16: Mean field simulations of the expansion in the quasiperiodic lattice. Panel (a) shows the dependence of the expansion exponent  $\alpha$  on the interaction coupling term  $\beta$ . The red crosses are the experimental results. The dashed gray lines indicate respectively the normal diffusion exponent (0.5) and the exponent found from a perturbative approach, supposing a coherent expansion (1/3). Panel (b) shows the time evolution of the width of the distribution for  $\Delta/J = 5$  and  $\beta = 80$ . Fits with the same Eq.(3.9) used for the experiment (red solid line), or with a linear behavior in the asymptotic regime (black dashed line), give very similar results for the exponent  $\alpha$ .

In Fig.3.16 we show some results of the numerical simulations. The time evolution of the width of the distribution is fitted either with the fitting Eq.(3.9) as in the experiment, or with a line in log-log scale neglecting the first part of the expansion. The two fitting procedure give very similar values for the expansion exponent  $\alpha$ . The exponent increases for increasing  $\beta$  and approaches a saturation value around 0.35. This value is definitely larger than  $1/4$ , which is the value for the random disorder case, and similar to  $1/3$  that is the value obtained from the perturbative approach assuming a coherent expansion. The numerical results are in qualitatively agreement with the experimental ones. However we note that the exponent extracted from the experimental data are typically larger than the numerical one. This is probably due to the temporal noise that, as already pointed out, is intrinsically present in the experiment and not in the simulation. We also note that the saturation value of  $\alpha$  is reached in the experiment for smaller value of the interaction energy than in the simulation. Furthermore the activation time in the simulations is much longer than in the experiment. A smaller initial size and a longer simulated expansion is in fact needed in order to get an expansion comparable with the experimental one. These discrepancies are due to the finite temperature of the atomic sample in the experiment and to the presence of the radial degrees of freedom which are not taken into account in the simulations. In the next section we give a justification to this statement with a better characterization of the effect of the finite temperature and of the radial degrees of freedom on the axial expansion.

### 3.2.3 Finite temperature and radial degrees of freedom effect

An important feature of the experimental system is the presence of the radial degrees of freedom, something that is absent in all numerical simulations and models developed so far. The radial confinement is harmonic since it is provided by the gaussian laser beams which create the optical lattice. The radial quantum for the experimental parameters is  $\hbar\omega_r \approx J/2$ , about one order of magnitude smaller than the typical average energy difference between axial states  $\delta E$ . Therefore several radial states might be populated in presence of the interaction which couples the various degrees of freedom and is typically of the order of  $J$ . A cartoon of the axial and radial states for our quasiperiodic lattice is shown in Fig.3.17.

The presence of the radial degrees of freedom in the experiment can be taken into account in the perturbative model introduced in the previous section modeling the effect on the microscopic hopping dynamics. There are two main effects of the radial excitations to be considered:

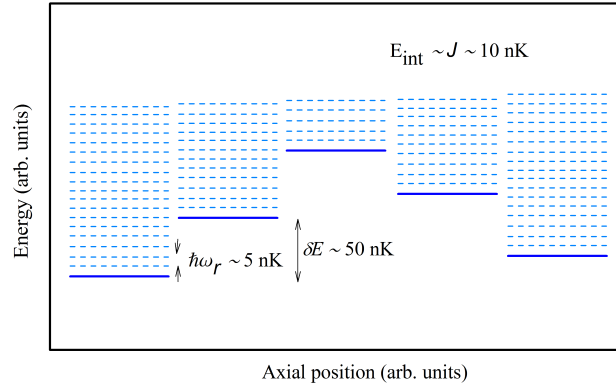


Figure 3.17: Schematic representation of the energy spectrum of the axial states along one quasiperiod of the quasiperiodic lattice (continuous lines) together with the relative radial states (dashed lines).

1) The 4-states overlap integral  $I_{ijkl}$  in Eq.(3.12) must be modified to include also the radial plane:

$$I_{ijkl} = \int \varphi_l^* \varphi_k^* \varphi_j \varphi_i dx \int \varphi_{rl}^* \varphi_{rk}^* \varphi_{rj} \varphi_{ri} d^2r \quad (3.22)$$

An increasing radial excitation of the system therefore results in a broadening of the radial wavefunctions, with a consequent decrease of  $I_{ijkl}$  and the associated coupling term  $|V'_{ijkl}|$ . This could decrease the expansion exponent.

2) The possibility of populating excited radial modes softens the energy conservation requirement, since, as we have already observed, the radial level separation  $\hbar\omega_r$  is smaller than the characteristic energy spacing of the quasiperiodic lattice  $\delta E$  (by approximately one order of magnitude in the present experiment). This implies that axial states that could not be coupled because of a too small  $E_{int}$  in a 1D system, might be at least partially coupled in presence of a radial excitation since the energy mismatch between axial states is reduced by the presence of the radial states. This increases the number of active coupling for a given  $E_{int}$  with respect to the pure 1D situation and could therefore give a larger expansion exponent.

The relative magnitude of these two competing effect is difficult to estimate and could influence the axial expansion, and in particular the value of  $\alpha$ , in opposite ways. We can indeed conceive two possible limits for the radial temperature. When  $k_B T_r < \hbar\omega_r$  the excited radial population is negligible, and one has effectively a 1D problem. In our case  $\hbar\omega_r/k_B \approx 5\text{nK}$ : this temperature is very small, close to the minimum temperature achievable in the Bose-Einstein condensate. Anyway, this limit cannot be achieved as a stationary state, since the thermalization of the axial and radial degrees of freedom, which occurs in the case of an

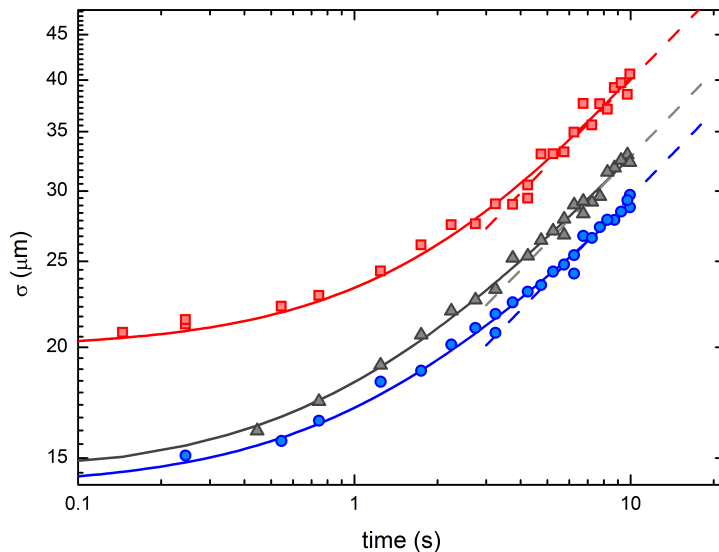


Figure 3.18: The time evolution of the width for the three data-set shows the effect of the finite radial temperature. The scattering length and the mean temperature in the three cases are respectively:  $a = 100 a_0$  and  $T_r = 60$  nK for the blue circles,  $a = 400 a_0$  and  $T_r = 60$  nK for the gray triangles and  $a = 400 a_0$  and  $T_r = 200$  nK for the red squares. When the radial temperature is lower the expansion is slower even in the case in which the interaction energy is bigger than in the high- $T_r$  data-set. The continuous lines are fits with Eq.(3.9) while the dashed lines are the fits to the asymptotic behavior. The fitted exponents are:  $\alpha = 0.32(2)$  for the blue circles,  $\alpha = 0.34(2)$  for the gray triangles and  $\alpha = 0.40(5)$  for the red squares. The lattice parameters are  $J/h = 290$  Hz and  $\Delta/J = 3.9$ .

interacting sample, will rapidly bring the radial temperature to a minimum value of the order of  $T_r \approx \delta E/k_b \approx 50$  nK. Conversely, when  $k_B T_r \gg \delta E$ , many radial states are excited. In this limit the energy mismatch that must be compensated by the coupling terms to provide the axial hopping, is no longer of the order of  $\delta E$ , but it becomes of the order  $\hbar\omega_r$ . The critical  $E_{int}$  to reach the regime of large interaction will therefore be  $\hbar\omega_r$ . The experiment is performed in an intermediate regime of temperature,  $k_B T_r \approx \delta E$ , where we can expect that the critical energy for the strongly interacting regime lays somewhere in between  $\delta E$  and  $\approx \hbar\omega_r$ . This expectation is confirmed by the comparison between the experimental and numerical energy dependence of the exponent  $\alpha$  as discussed above and shown in Fig.3.16.

To experimentally check the relative magnitude of the two competing effects of the presence of the radial modes, we have compared the evolution of interacting samples at low radial temperature  $T_r$  with those of samples with the same  $g$ , but with a larger  $T_r$  prepared via controlled parametric heating. The typical observation is reported in Fig.3.18: the expansion of the high- $T_r$  sample is faster,

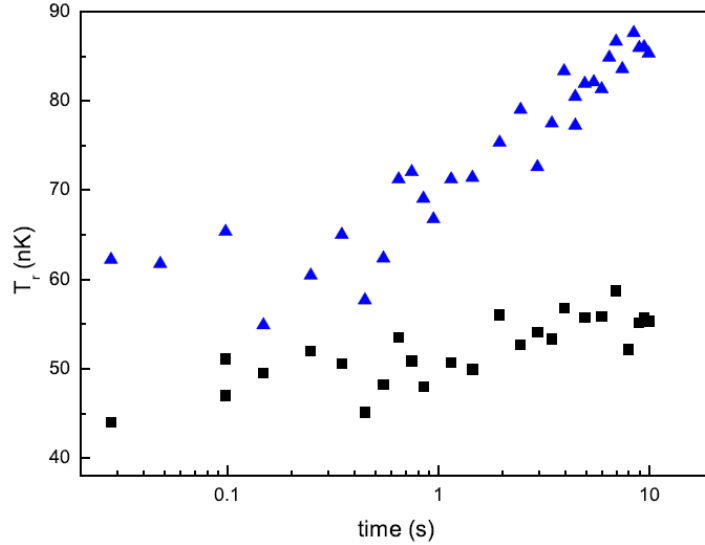


Figure 3.19: Time evolution of the radial temperature for a non-interacting sample (black squares) and for an interacting one (Blue triangles).

despite a reduction of  $E_{int}$  by approximately a factor 2, indicating that the second effect dominates. Raising the temperature therefore helps the coupling of a larger number of states by the interaction. In order to separate out the effect of the reduced  $E_{int}$  at the larger  $T_r$ , we have also measured the time evolution of the sample at low  $T_r$  in which a similar  $E_{int}$  was achieved by reducing  $g$ . This measurement shows a slower expansion, as expected since now the reduced  $E_{int}$  is not compensated by an increased coupling efficiency.

We stress that for non-interacting samples we do not observe any dependence of the axial dynamics on the radial temperature: samples prepared via controlled parametric heating at different radial temperatures never show expansion in absence of interaction<sup>8</sup>. This experimental test confirm the secondary role of the radial modes in the subdiffusion. Nevertheless when interaction is added in the system, the finite temperature and the presence of the radial degrees of freedom influence the axial dynamics. The expansion is in fact faster than in the 1D situation and in particular the activation time is smaller. This allows the observation of subdiffusive expansion over the experimental time scale (10 seconds). Numerical 1D simulations require much longer evolution time for initial size of the distribution, lattice and interaction parameters comparable with the experimental ones.

From a study of the radial momentum distribution of the expanding samples we also detect a radial heating during the 10s evolution time for samples that

<sup>8</sup>This is valid until the temperature is not high enough to populate the second band of the lattice where the eigenstates are not localized

are initially prepared as Bose-Einstein condensate, i.e. at the lowest measurable temperatures,  $T_r \leq 50\text{nK}$ . The typical evolution is reported in Fig.3.19. In absence of interaction we see a slow heating with a rate of the order of 1-3 nK/s, presumably due to pointing or amplitude noise on the lattice beams. The interacting samples show instead a larger initial  $T_r \sim \delta E/k_B$ , which presumably arises from a thermalization of the axial and radial degrees of freedom. The following heating during the full evolution time is typically 3-5 nK/s, hence larger than the one of non-interacting samples. This excess heating presumably arises from the axial noise to the radial degrees of freedom mediated by interaction. This noise, as mentioned before, also cause a slow expansion in the non-interacting sample. This noise might be due to variations in the laser wavelengths and to vibrations of the retro-reflecting mirror that creates the standing waves, which result in a spatial movement of the two lattices and a consequent excitation of the axial dynamics even in the case of orthogonal localized states, as we will discuss in the next section.

Finally we note that the maximum temperature that can be reached in the experiment while preserving a single-band dynamics is of the order of 200nK. For higher temperatures we see a clear excitation of the second band of the quasiperiodic lattice, whose single-particle eigenstates are not localized for the range of parameters we explored. This excitation is detected as the appearance of rapidly moving tails in the density distribution and as a fast decreasing of the number of atoms during the evolution.

### 3.2.4 Time evolution of the density profiles

So far we have studied in detail the time evolution of the width of the spatial distribution of a wavepacket expanding in a disordered potential in presence of non-linearities. We have shown how theory, numerical simulations and the experimental results presented in this thesis, agree in demonstrating the subdiffusive nature of the expansion. More information about the spreading of the wavepacket is given by the evolution of the shape of the spatial distribution. In the experiment we have the possibility to characterize this evolution, since the in situ images we take directly represent the density distribution of the atomic cloud.

Since the coupling between localized states is larger at the center of the sample, where the atom number per site  $N$  and therefore the interaction energy is larger, we can expect a faster expansion in the center than in the tails of the distribution. This translates in the appearance of a flat region in the central part of the distribution as already predicted by Shepelyansky in the first work on the topic [57]. In

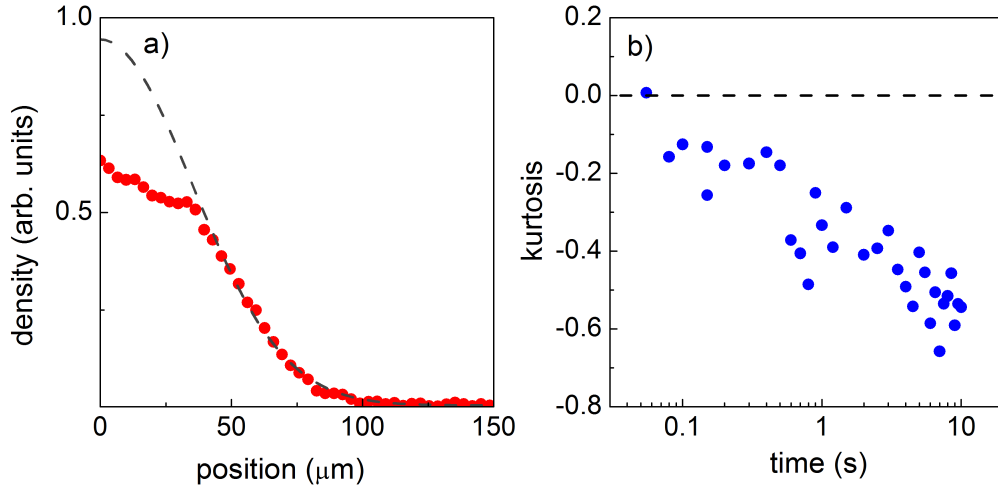


Figure 3.20: a) Density profile of the interacting atomic cloud ( $E_{int} \approx 2J$ ) after 10 seconds of expansion in the disordered lattice. The distribution shows a clear flat-top shape. Dashed line is a Gaussian fit of the tail. b) Evolution in time of the kurtosis of the density distribution for the interacting atoms.

the experiment this behavior is clearly visible in the typical shape of the atomic cloud at long expansion times as shown in Fig.3.20. Initially the atomic cloud has a Gaussian profile since it is prepared in a harmonic trap. The flat-top shape gradually emerges during the expansion as can be seen in the typical evolution of the kurtosis of the distribution:

$$\gamma = \frac{\int x^4 n(x) dx}{\sigma^4} - 3. \quad (3.23)$$

By definition  $\gamma = 0$  for a Gaussian distribution.

An analogous change of shape is predicted by general models of non-linear diffusive systems. In the following we introduce a *non-linear diffusion equation* that correctly describes the behavior of many physical systems in which the diffusion coefficient results not to be constant during the evolution. This kind of equation is used for example to describe the dynamics of a classical fluids in a porous medium. We compare the solutions of such equation with the experimental results.

### Non-linear diffusion equation

The evolution of a diffusive system is described by the well known diffusive equation.

$$\frac{\partial n(x, t)}{\partial t} = D \frac{\partial^2 n(x, t)}{\partial x^2} \quad (3.24)$$

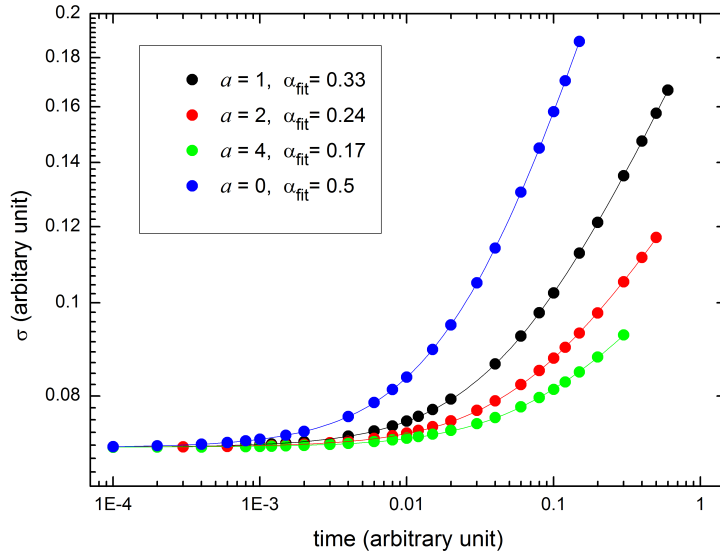


Figure 3.21: Time evolution of the width of the numerical solution of the non-linear diffusive Eq.(3.27) for different values of the exponent  $a$ . Lines are fit with the usual fitting formula Eq.(3.9). The fitted expansion exponent  $\alpha$  is in good agreement with the relation:  $\alpha = 1/(2 + a)$ .

If we take as initial condition a Gaussian distribution of width  $\sigma_0$  normalized to 1, the solution of the equation at any time remains a Gaussian of the form:

$$n(x, t) = \frac{1}{\sqrt{2\pi}\sqrt{\sigma_0^2 + 2Dt}} e^{-\frac{x^2}{2(\sigma_0^2 + 2Dt)}} \quad (3.25)$$

the time-evolution of the width of the distribution is therefore given by:

$$\sigma(t) = \sqrt{\sigma_0^2 + 2Dt} \quad (3.26)$$

This expression is of the same form of Eqs.(3.9) and (3.16) with the expansion exponent  $\alpha = 0.5$ , as expected.

It is possible to generalize the diffusion equation in such a way that it can describe the behavior of non-linear systems. Different non-linear diffusion equations exist in literature according to the detail of the non-linear process that one wants to describe. In our case the expansion can not be described by the regular diffusion equation since the diffusion coefficient, as we discussed above, is not constant but it depends on the local interaction energy which allows the coupling between different states. This interaction energy is not homogeneous across the distribution and is not constant in time. One can then imagine to replace the diffusion coefficient  $D$  of Eq.(3.24) with an effective diffusion coefficient proportional to the density profile to some power  $a$ :

$$\frac{\partial n(x, t)}{\partial t} = \frac{\partial}{\partial x} D_0 n^a(x, t) \frac{\partial n(x, t)}{\partial x} \quad (3.27)$$

The asymptotic solution of this equation is [65]:

$$n(x, t) \propto \begin{cases} t^{1/(2+a)} \left(1 - \frac{x^2}{x_0^2}\right)^{1/a}, & \text{for } x < x_0 \\ 0, & \text{for } x > x_0 \end{cases} \quad (3.28)$$

The front of the diffusion  $x_0$  has the following time dependence:

$$x_0 \propto \sqrt{\frac{2+a}{a}} t^{1/(2+a)} \quad (3.29)$$

This means that the number of occupied sites and hence the width of the distribution, i.e. the square root of its second moment, also evolve as:

$$\sigma(t) \propto t^{1/(2+a)}. \quad (3.30)$$

The relation between  $a$  and the expansion exponent in Eqs. 3.9 and 3.16 is thus given by the simple relation  $\alpha = 1/(2+a)$ .

The self-similar solution (3.28) is valid only for asymptotic times. We then numerically solved the non-linear diffusion Eq.(3.27) taking a Gaussian distribution as initial condition. The time evolution of the square root of the second moment of the numerical solution is plotted in Fig.3.21. Fitting the points with Eq.(3.9), we get expansion exponents in good agreement with (3.30).

The shape of the distribution evolves from a Gaussian to the asymptotic solution during the expansion. We tried to fit the numerical solution with an expression of the same form as the asymptotic one, leaving the spatial exponent  $1/a_{fit}$  as a free parameter. In Fig.3.22 we show on the left the numerical results of the non-linear diffusion equation for three different evolution times, fitted with the asymptotic solution. The initial Gaussian distribution is well fitted with an exponent  $1/a_{fit} \gg 1$ . One gets  $1/a_{fit} = 1/a$  when the asymptotic regime is reached. For intermediates evolution time the tails of the distribution are not perfectly fitted. However the discrepancy between the numerical solution and the fit is only at a level that might not be experimentally resolved. We can conclude that, for our aim, the asymptotic solution with a free exponent is a good approximation for the solution of the non-linear diffusion equation at any time.

The evolution of the fitted exponent during the expansion is shown in Fig.3.23. We can see that the shape of the distribution rapidly changes in the first stages of the expansion and the asymptotic value for the exponent is already reached when the width of the distribution is approximately 1.2 times the initial one. In the experiment, when the interaction energy is large enough, the final size of the cloud is as large as twice the initial one. We can therefore expect, for the longer evolution times, to have reached the asymptotic regime.

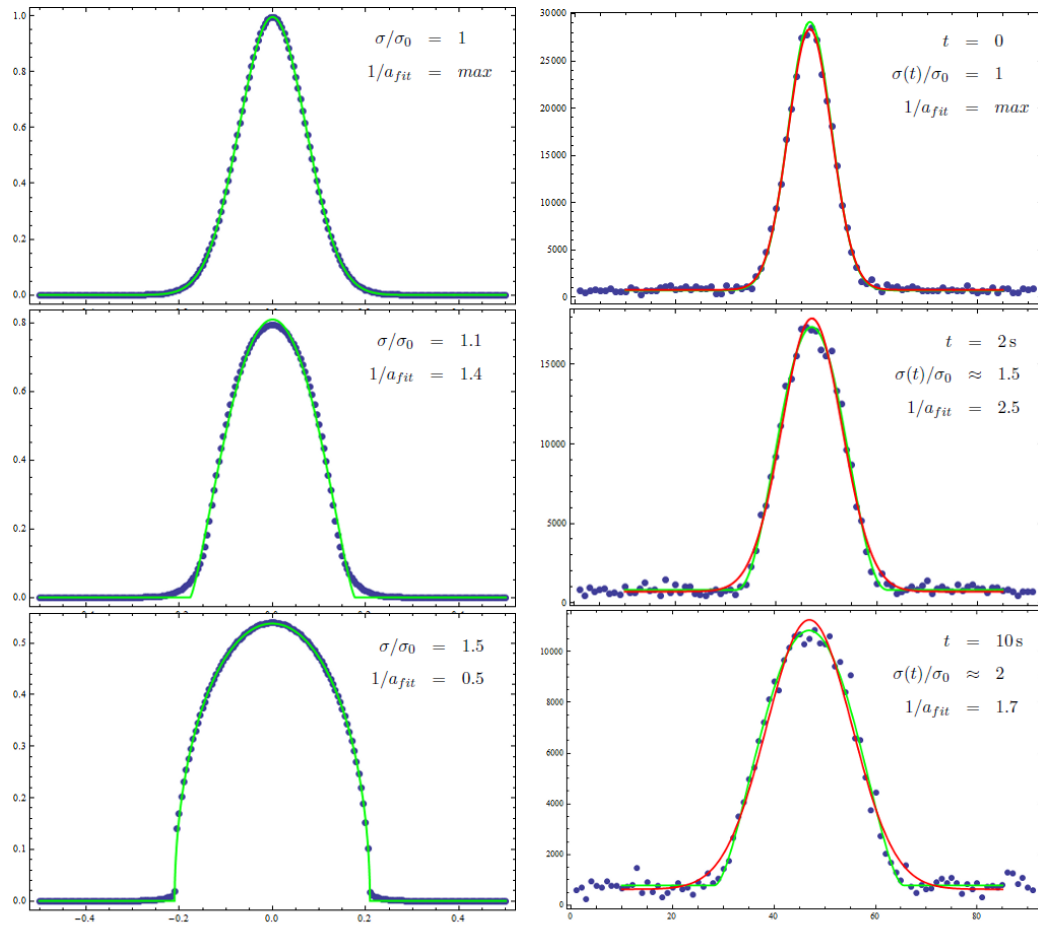


Figure 3.22: Density profiles of the numerical solution of the non-linear diffusion equation with  $a = 2$  (left) and of the experimental atomic distributions (right). Green lines are fits with the asymptotic solution 3.28, red lines are fit with a Gaussian.

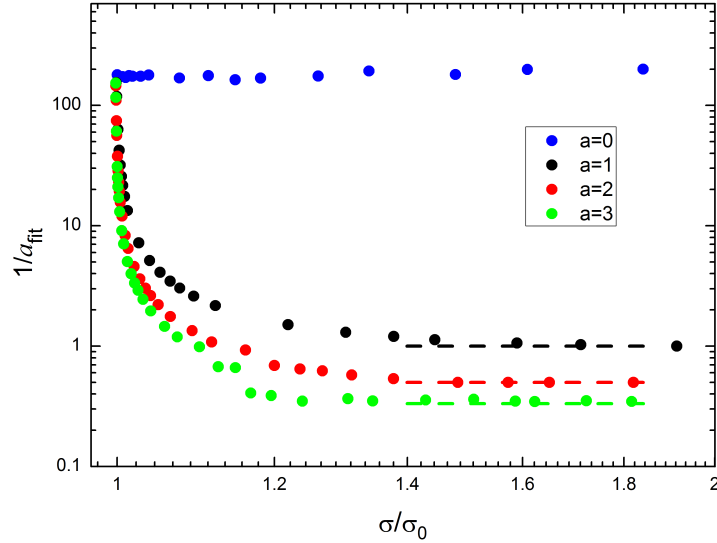


Figure 3.23: The numerical solution of the non-linear diffusion equation (3.27) is fitted with the asymptotic solution 3.28 leaving the spatial exponent  $1/a_{fit}$  as a free parameter. The graph shows the evolution of  $1/a_{fit}$  during the expansion for different values of the coefficient  $a$ . The fit fixes the maximum value of the exponent to 200, where the solution is a good approximation of a gaussian distribution. The asymptotic value  $1/a$  is reached when the width of the distribution is about 1.2 times the initial one.

We perform the same fitting procedure for the experimental data. Results are shown on the right in Fig.3.22 and in Fig.3.24. As soon as the size of the cloud increases with respect to the initial one, i.e. for expansion times larger than the activation time  $t_0$ , data are better fitted with the solution of the non-linear diffusion equation than with a Gaussian. We note that when the interaction energy is too strong, heating processes during the expansion cause a non-negligible transfer of atoms in the second band of the lattice where the single particle eigenstate are not localized. These atoms are thus free to move across the lattice causing a faster expansion of the tails of the distribution that comes back to be well fitted by a Gaussian. Furthermore the presence of this non-localized atoms also causes an effective faster increase of the width. We have to take care of neglecting these points in fitting the time evolution of the width in order to avoid an overestimation of the expansion exponent  $\alpha$ .

The time evolution of the fitted exponent  $1/a_{fit}$  shows the same qualitatively behavior as the numerical solution. We compare the experimental results with the numerical results for  $a = 2$ , that is the expected value of  $a$  for a subdiffusive expansion in a random system. The asymptotic value is significantly different. Furthermore we do not see any difference in the asymptotic spatial exponent  $1/a_{fit}$

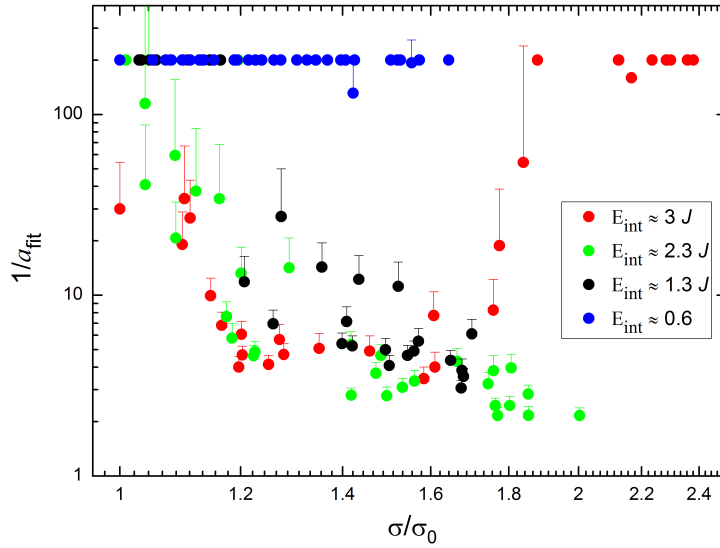


Figure 3.24: Experimental data for different values of the initial interaction energy are fitted with the solution of the non-linear diffusion equation. The evolution of the spatial exponent  $1/a_{fit}$  during the expansion is shown in the graph. When the interaction energy is not strong enough (blue points) we do not appreciate any change in the shape of the atomic distribution. On the other hand, when the interaction energy is too strong (red points) we detect the effect of the presence of atoms in the second band of the lattice as explained in the text.

for different interaction energy, i.e. for different expansion exponents  $\alpha$ . This is due to the finite resolution of the imaging system. We are in fact not able to resolve sharp edges of the density distribution. In order to compare the numerical solution with the experimental results we have to take this limitation into account. In Fig.3.25 we compare a set of experimental data with the numerical solution of the non-linear diffusion equation with  $a = 2$  convolved with a Gaussian of the same width as the measured spatial resolution of our imaging system ( $12 \mu m$ ). With this correction we see a better agreement of the Non-linear diffusive equation model with the experiment.

In conclusion we have experimentally verified that the evolution of the shape of the distribution during the subdiffusive expansion is in qualitative agreement with the solution of a general non-linear diffusion equation of the form (3.27). The study of the evolution of the profiles potentially provide a more complete characterization of the expansion with respect to the study of the evolution of the width alone. The finite resolution of the imaging system unfortunately does not allow us to resolve the difference between the solution of non-linear diffusion equations with different  $a$ .

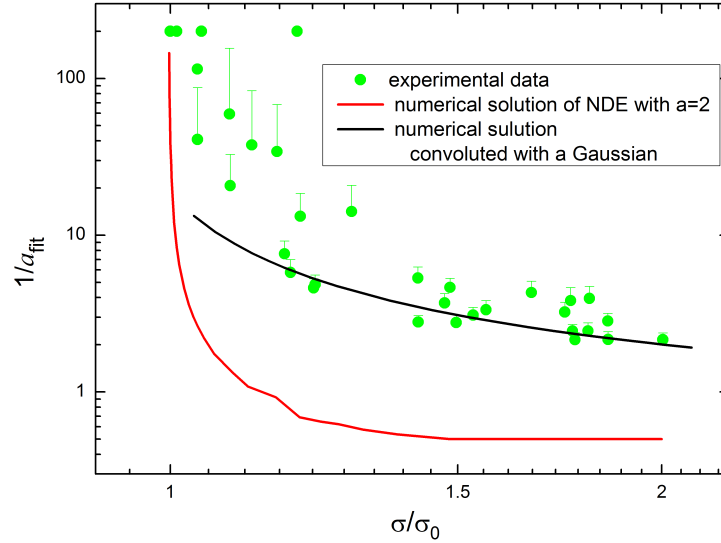


Figure 3.25: Evolution of the spatial exponent  $1/a_{fit}$  for experimental data with  $a = 500a_0$  (green points), for the numerical solution of the non-linear diffusion equation with  $a=2$  (red line) and for the numerical solution convolved with a Gaussian to simulate the effect of the finite imaging resolution of the experiment (black line).

### 3.3 Noise-induced delocalization

In the previous section we have already outlined some consequences of the intrinsic presence of noise in our experimental system. We have seen that noise is a source of heating for the atoms and, more interestingly, that a slow expansion in the disordered lattice, driven by noise, can be observed even in absence of interaction. Actually noise has been recognized to have an important role in disordered systems and in particular its delocalizing effect is well-known [66]. More generally speaking, noise can have a strong impact on the behavior of quantum systems and, while the importance of a full understanding of its role has been recognized since many decades, mainly theoretical studies have been performed so far. The problem with experiments is that the noise is typically already present in the system and, while it can often be fully characterized, it can hardly be controlled.

We employed our experimental setup to characterized the delocalization of the disordered localized system induced by noise [67]. Furthermore we investigate the interplay of noise and interaction in the expansion dynamics of the atomic cloud in the disordered lattice. In our case, with the word “noise” we intend a random in time modification of the lattice potential. In this sense a source of noise is the shaking of the lattice caused by fast variation of the frequency or of the power of the laser beams as well as by vibration of the retroreflecting mirror or rapid

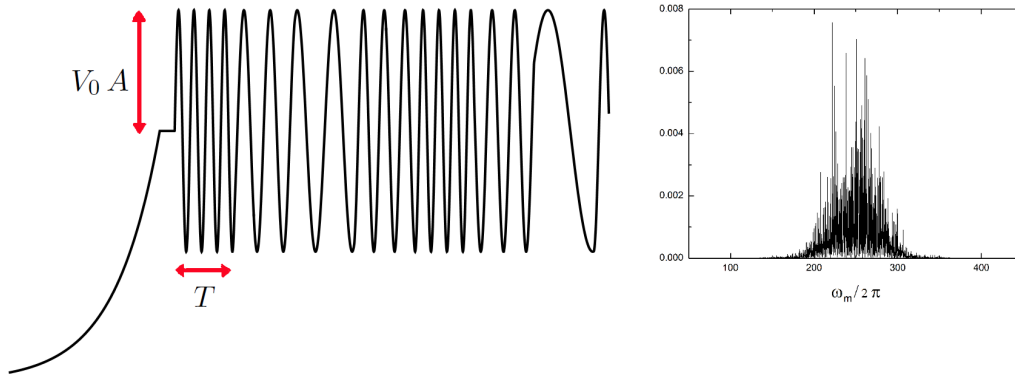


Figure 3.26: Schematic of the noisy modulation of the power of the secondary lattice after the loading and its power spectrum.

pointing movements. This is what we call “intrinsic noise”. We took care to reduce as much as possible these sources of noise. The lasers we use to create the quasiperiodic lattice have in fact a narrow linewidth and the power of the beams on the condensate is actively stabilized. Nevertheless some intrinsic noise is unavoidable and its effect has been already outlined. However it is possible to add in the system a controlled non-equilibrium noise by a proper active modulation of the lattice potential.

We study the impact of such controlled noise on the expansion dynamics of the atoms. We find that noise breaks the single-particle localization and induces a diffusive expansion dynamics. The combination of noise and repulsive interactions with variable strengths gives instead rise to an anomalous diffusion with variable expansion exponent  $\alpha$ .

### Experimental procedures

We adiabatically prepare a non-interacting Bose-Einstein condensate in the quasiperiodic potential with  $\Delta/J \approx 3$ . During the loading of the lattices we slowly vary the scattering length from the value we usually employ during the evaporation, around  $280 a_0$ , to almost zero. The final axial frequency is around  $2\pi \times 70\text{Hz}$ . At a certain time we suddenly switch off the axial confinement and within few ms we change the disorder strength to its final value. During the subsequent evolution of the non-interacting cloud in the quasiperiodic potential we modulate the amplitude of the secondary lattice in a noisy way and we detect by in situ absorption images the width of the cloud for increasing times up to 10 seconds.

The strategy we chose to introduce noise into the system without causing a direct excitation of the higher bands of the lattice or of the radial modes is to

apply a sinusoidal amplitude modulation of the disorder. The time dependent potential given by the secondary lattice results to be of the form:

$$V_2(t) = V_0 (1 + A \sin(\omega_m t + \phi_m)). \quad (3.31)$$

The frequency of the modulation  $\omega_m$  is randomly varied with time step  $T$  in a proper interval,  $\omega_m/2\pi \in [200 \text{ Hz}, 300 \text{ Hz}]$ . The phase  $\phi_m$  is adjusted in order to preserve the continuity of the modulation and the sign of its first derivative. The width of the effective power spectrum during 10 s, with  $T=10 \text{ ms}$  is essentially the entire frequency interval<sup>9</sup> as shown in Fig.3.26.

### 3.3.1 Non-interacting diffusive expansion

The time evolution of the width of the non-interacting atomic cloud in the disorder noisy potential is shown in Fig.3.27. We observe that a sufficiently large noise amplitude  $A$  results in an evident expansion of an initially localized sample. To analyze the nature of such expansion, we fit the time-evolution of the width  $\sigma$  with Eq.(3.9) as we did to characterize the interaction induced dynamics. We typically reach the asymptotic regime of expansion for approximately one decade. The typical value of the fitted expansion exponent is  $\alpha = 0.45(5)$ , which is consistent with normal diffusion. In the asymptotic regime  $\sigma$  thus evolves as:

$$\sigma^2 \sim D t \quad (3.32)$$

The diffusion coefficient is related to the fit parameters by the relation  $D = \sigma_0^2/t_0$ . Diffusive expansion is actually the kind of dynamics that is predicted for a white-noise source from first-principle considerations. For example, the diffusion can be seen as the result of incoherent hopping between the single-particle localized states<sup>10</sup>. The accepted idea is that the noise induced hopping is totally analogous to the classical Brownian motion of particles in a scattering environment.

The statement that the noise induced dynamics has a diffusive nature is also confirmed by the fact that the spatial profile of the atomic cloud remains a Gaussian during the expansion. As pointed out in sec.3.2.4 a Gaussian distribution is the solution of the normal diffusive equation with a constant diffusion coefficient at any time.

---

<sup>9</sup>A proper Fourier analysis of the noise signal shows that for  $T < 1/(2\pi\omega_m) \simeq 5 \text{ ms}$  the effective power spectrum shrinks.

<sup>10</sup>Such an effects already has been observed in a few atomic systems, such as in atom-optics realization of the kicked rotor [68].

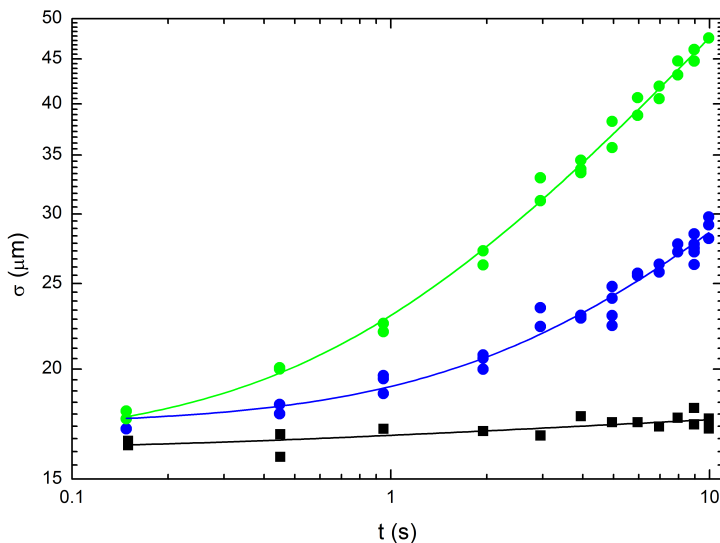


Figure 3.27: Time evolution of the non-interacting system in the quasiperiodic lattice with  $\Delta/J = 6$  for various values of the noise amplitude. For  $A = 0$  the system is localized (black). For  $A = 0.54$  (blue) and  $A = 0.9$  (green) the system exhibits normal diffusion. Lines are fits with Eq.(3.9): the fitted exponent  $\alpha$  is compatible with 0.5.

As in the case of the interaction induced delocalization, a one-dimensional DNLSSE has been used to simulate our system. Numerical simulations confirm that the diffusion exponent  $\alpha$  is independent on the amplitude noise, i.e. the noise induced expansion is diffusive for any value of  $A$ .

The dependence of the diffusion coefficient on the noise and the lattice parameter is not trivial. As for the interaction induced expansion, also in the case of noise, we can apply a similar perturbative approach. Here the perturbative term of the Hamiltonian (1.1) is of the form:

$$H' = \int dx \hat{\psi}^\dagger (A V_0(x) \sin(\omega_m t + \phi_m)) \hat{\psi} \quad \text{where} \quad V_0(x) = \frac{\Delta}{J} \cos(2\pi\beta x + \phi) \quad (3.33)$$

The transfer rate  $\Gamma$ , and thence the diffusion coefficient in this case are constant in time since the perturbative term strength does not depend on the width of the system and therefore does not vary during the expansion. The quasiperiodic nature of the disorder is expected not to influence the expansion dynamics since, conversely to the interaction induced delocalization, the process now is not sensitive to the ordering of the energies level across the lattice. From simplified perturbative arguments  $\Gamma$  is expected to be proportional to  $A^2 (\Delta/J)^2$  multiplied by an overlap integral that, neglecting the time evolution term, is of the form:

$$I_{ij} = \left| \int \varphi_j^*(x) \cos(2\pi\beta x + \phi) \varphi_i(x) \right|^2, \quad (3.34)$$

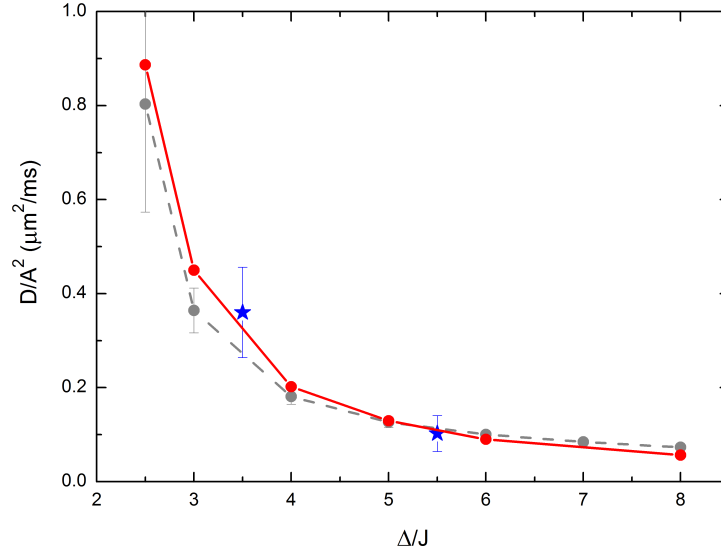


Figure 3.28: Dependence of  $D/A^2$  on  $\Delta/J$  in the regime where the perturbative approach applies. Red points refer to numerical simulations, blue stars to experiment. The perturbative approach results, shown by the dashed gray line, are to be in good approximation proportional to the numerical results.

where  $\varphi_i(x)$  is the single particle eigenfunction centered at the  $i$ -th lattice site. To get the diffusion coefficient we have to multiply the rate  $\Gamma$  by the square of a length scale; since the hopping happens between localized states, we expect that the proper length scale is the localization length of the single particle states  $\xi \sim d/\ln(\Delta/2J)$ . This is valid as far as  $\xi > d$ , where  $d$  is the lattice spacing. For higher degree of localization the scale becomes  $d$  itself. Summarizing, if we follow a perturbative approach and  $\xi > d$ , the diffusion coefficient results to have this proportionality:

$$D \propto A^2 f(\Delta/J), \quad \text{where} \quad f(\Delta/J) = (\Delta/J)^2 I_{ij} \xi^2. \quad (3.35)$$

In Fig.3.28, we show some numerical and experimental results in the regime where this approach applies and we find a good agreement between experiments, simulations and perturbative calculations. Nevertheless, when the noise strength is too strong, the perturbative approach fails. Indeed, a theoretical analysis, in a kicked rotor system [69], predicts that when the noise amplitude is large compared to the degree of localization, the dependence of the diffusion coefficient on  $A$  and  $\xi$  is of the kind:  $D \propto A^2 + \xi^2$ . A systematic characterization of the dynamic expansion in the disorder potential for different values of noise amplitude and lattice parameters is presently being performed. Preliminary results confirm the predicted dependence also in our system.

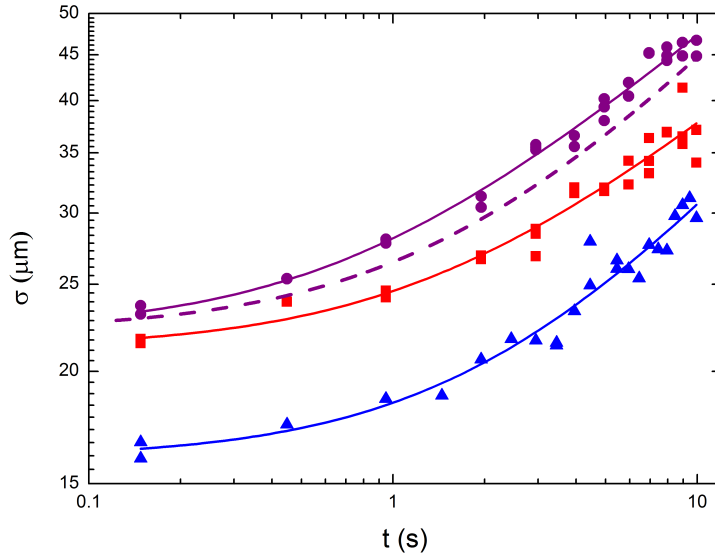


Figure 3.29: Time evolution of the width of a system with  $\Delta/J = 4$ . The blue triangles show the expansion of a non-interacting sample in presence of noise ( $A=0.6$ ). The red squares refer to a static interacting sample ( $E_{int} \simeq 0.8J$ ). Purple circles combine the two effects. Solid lines are fits with the fitting formula (3.9) whereas the dashed line is the numerical solution of Eq.(3.36) with the initial condition fixed by the fit.

### 3.3.2 Combined effect of noise and weak interactions

We have so far presented the study of two independent effects that cause destruction of disorder induced localization and consequently dynamic expansion: weakly repulsive interaction and noise. We can now wonder what happens when we combine the two effects.

With similar experimental procedures as the ones summarized before, we also investigate the expansion of the atomic cloud in presence of both repulsive interaction and noise. We observe that the combination of the two effects always produces a faster expansion than the two individual sources of delocalization. The expansion exponent fitted for data up to ten seconds of expansion time, is however typically intermediate between the ones due to noise and interactions alone. This suggests that the two delocalizing mechanisms might cooperate additively. One example of these observations is shown in Fig.3.29, where one clearly sees the faster expansion caused by the cooperation between noise and interactions.

We studied how such anomalous diffusion depends on the two relevant controlled parameters, i.e. the interaction energy  $E_{int}$  and the noise amplitude  $A$ . Fig.3.31 provides a summary of our observations. Results are extracted from fits of the experimental data with the usual fitting formula (3.9). For a fix value of

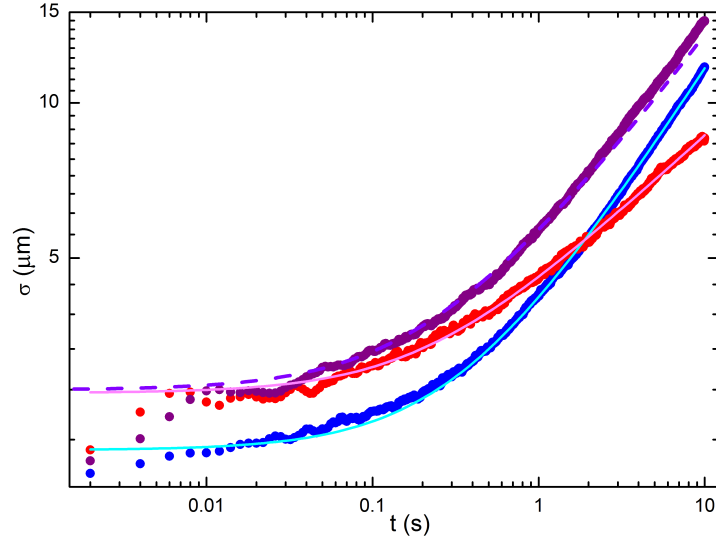


Figure 3.30: Numerical simulation of the time evolution of the width of a system with  $\Delta/J = 2.5$ . The blue data show the expansion of a non-interacting sample in presence of noise ( $A=0.4$ ). The red data refer to a static interacting sample ( $\beta = 40$ ). Purple data combine the two effects. Solid lines are fits with the fitting formula (3.9) whereas the dashed line is the numerical solution of Eq.(3.36).

the noise amplitude, the measured exponent features a crossover. In the non-interacting case the expansion is ruled only by noise and thus  $\alpha = 0.5$ . When the interaction energy increases, the value of the exponent approaches the one of the static interacting case  $\alpha \approx 0.3$ . We can define a generalized activation time  $t^*$ , defined as  $\sigma(t^*) = \sqrt{2}\sigma_0$ . It is a measure of the inverse of the diffusion coefficient.  $t^*$  decreases as either  $A$  or  $E_{int}$  increase, indicating a faster expansion.

If we suppose an additive cooperation of the two effects a more correct analysis can be performed in the following way. We first determine from the fit the diffusion coefficient  $D_{noise}$  due to noise alone, and the generalized diffusion coefficient  $\tilde{D}_{int} = (\sigma_0/t_0^\alpha)^2$  due to interaction alone. We then evaluate numerically the solution of the combined diffusion equation:

$$\frac{d\sigma}{dt} = \frac{D_{noise}}{2\sigma} + \alpha \tilde{D}_{int}^{1/2\alpha} \sigma^{1-1/\alpha} \quad (3.36)$$

and we compare it with the experimental and numerical data for the combined noise and interaction. The good agreement, shown in Figs.3.29-3.30, supports the idea of cooperation. The underlying idea of this model is that the hopping between localized states is now induced by both noise and interactions. These two mechanism are independent on each other.

As already discussed, while in the case of noise the hopping rate is constant over time, in the case of interaction the rate is density dependent and therefore

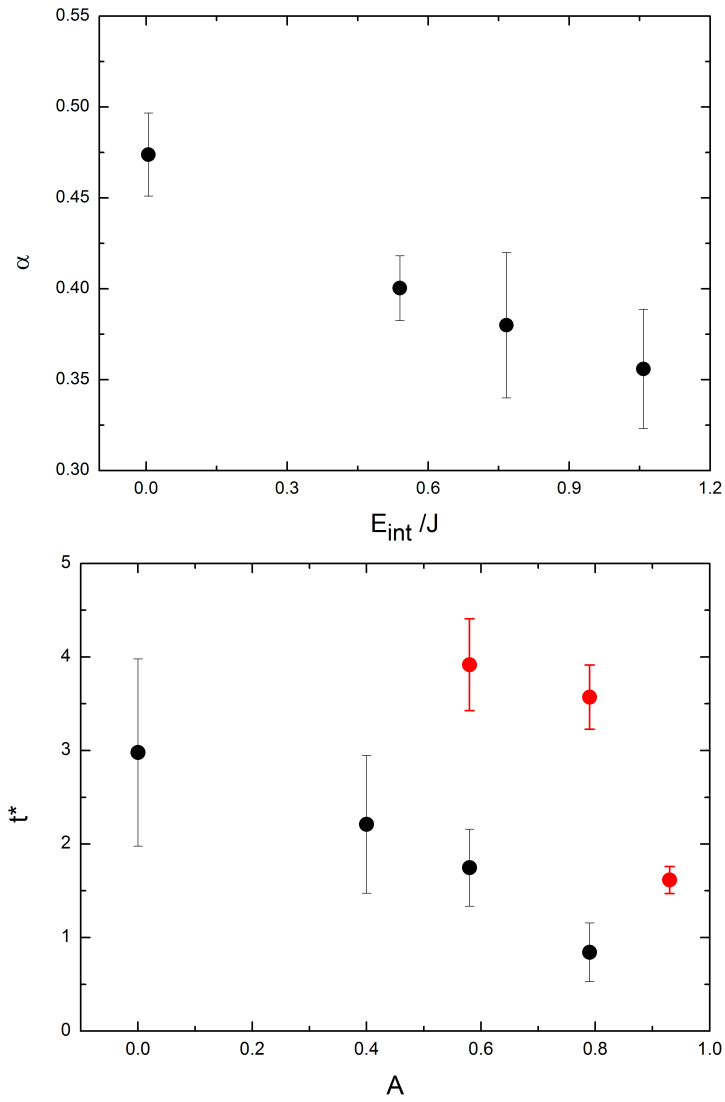


Figure 3.31: Top: Expansion exponent vs the initial interaction energy, for a fixed noise amplitude  $A = 0.4$ . Bottom: Generalized activation time  $t^*$  vs the noise amplitude for a non-interacting sample (red points) and for a fixed value of initial interaction energy  $E_{int} = 0.8J$

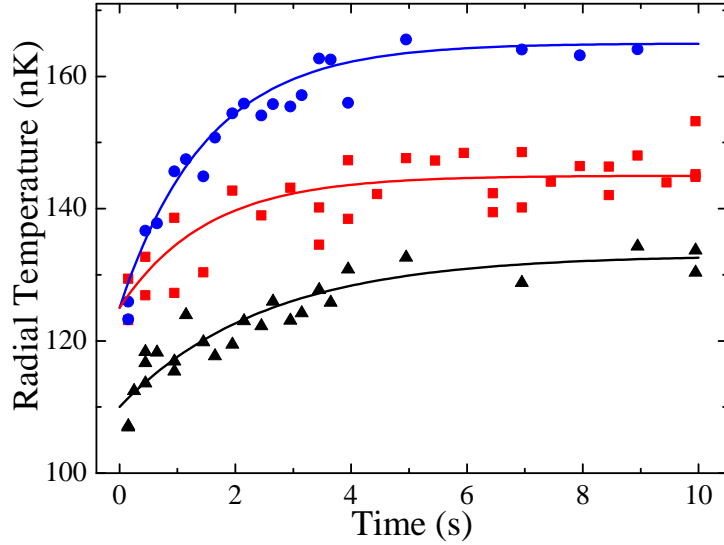


Figure 3.32: Time evolution of the radial temperature for a non-interacting system in presence of noise with  $A=0.8$  (red squares), for a static interacting system with  $E_{int} \simeq 0.8J$  (black triangles) and in presence of both noise and interactions (blue points). Lines are guides for the eyes.

tends to drop to zero as the sample expands. We therefore expect a long-time crossover to a regime where the interactions effects are negligible, and the system diffuses normally. We have not observed this crossover in the experiment, in agreement with a crossover time exceeding 10 s that we derive from the solution of the combined diffusion equation. The results showed in Fig.3.31 give just an indication of the behavior of the system in the transient regime in which both interaction and noise give their contribution in the expansion.

We note that the agreement of the numerical data with the solution of Eq.(3.36) is very good whereas the experimental expansion is faster. This is due to the presence of the radial modes that are not taken into account in the simulation. During the expansion the system heats up as we can see, in presence of interaction, from the time evolution of the radial temperature in Fig.3.32. The presence of noise causes an increase of the total energy of the system (this has also been confirmed by the numerical simulations), which translates in an increase of the temperature. In a pure one-dimensional case, as in the simulations, the energy is limited by the width of the band. As discussed in sec.3.2.3, because of the presence of the radial modes, an increasing temperature during the expansion affect the dynamics leading to a faster expansion. We experimentally verified that the larger is the heating, the larger is the disagreement between the measurement and the solution of Eq.(3.36).



## Chapter 4

# Experimental investigation of strongly-interacting bosons in a disordered lattice

In order to complete the study of the interplay between disorder and interaction in a bosonic system, after the study of weakly-interacting atoms presented in the previous chapter, we also moved our experimental investigation to the strongly-correlated regime. Here new interesting and complex quantum phases are predicted but few experimental observations are available. In this chapter we describe our preliminary results in the strongly-interacting regime. The experimental results are compatible with the observation of the predicted strongly-interacting Bose glass phase even if further measurements and analysis are still in progress.

In sec.4.1 we give a brief description of how we prepare one dimensional systems in which the interaction energy can be larger than the kinetic one ( $U > J$ ). Thanks to the high degree of independent tunability of the interaction energy and of the disordered strength over a large range, we have been able to trace a complete and complex  $\Delta-U$  phase diagram. This diagram, as measured through the correlation length of the system, shows a complex structure with different insulating and non-insulating regions. We show and comment this phase diagram in sec.4.2. We then report on the measurements of the transport capability (sec.4.3) and of the excitation spectrum of the system (sec.4.4) in different regions of the phase diagram.

## 4.1 Experimental realization of the one-dimensional system with tunable interactions

The study of the weakly interacting regime reported in the previous chapter has been performed by loading a one-dimensional quasiperiodic lattice on a three dimensional condensate. This technique fails when one wants to reach interaction energies  $U$  larger than the tunneling energy  $J$ . To investigate also the strongly interacting regime, we therefore load the condensate in a tight two-dimensional lattice, creating an array of independent quasi-one-dimensional systems. The quasiperiodic potential is then aligned along the longitudinal axis of these “tubes”, as schematically represented in Fig.2.11.

The temporal sequence for the optical lattices loading is shown in Fig.4.1. A condensate of about 40 000 atoms is prepared in the optical trap with a scattering length  $a = 280a_0$ . The optical trap is kept constant in intensity during the entire sequence with an average trap frequency  $\omega \simeq 2\pi \times 50\text{Hz}$  (not shown in the figure). Before starting the lattices loading, the scattering length is tuned in 50 ms to the value  $a_{load}$ . This value of the scattering length determines the size of the condensate at the moment in which the lattices are loaded and therefore also the number of populated tubes, the number of atoms in each tube, and subsequently in each lattice site. The two-dimensional tight lattice is then loaded with S-shaped ramps lasting 400 ms; when it is strong enough to avoid tunneling from tube to tube during the loading process, also the quasiperiodic lattice is ramped up. The final value of the two horizontal lattices is about  $s_{\hat{x}} = s_{\hat{y}} = 30$ . In the last part of the loading procedure, the scattering length is set with a slow ramp to its final value  $a_{meas}$  and kept there for the rest of the experiment. This value of  $a$  determines  $U$ , the interaction energy of the atoms according to Eq.(1.18). We calculate  $U$  from a Gaussian approximation of the Wannier function as:

$$U = g \frac{1}{(2\pi)^{3/2} a_{tube}^2 a_{latt}}, \quad (4.1)$$

where  $a_{tube}$  and  $a_{latt}$  are the harmonic oscillator lengths calculated from the harmonic approximation of the lattice wells with Eqs.(2.6-2.7), in the tight confined radial direction and in the axial direction of the tube, respectively.

An accurate estimation of the distribution of the atoms in the one-dimensional tubes and in the lattice is important for a reliable characterization of the experimental system and for a comparison with theory. In particular it is necessary, though not trivial, to estimate the number of atoms per lattice site to get, for example, the theoretical value for the superfluid-Mott insulator transition. A

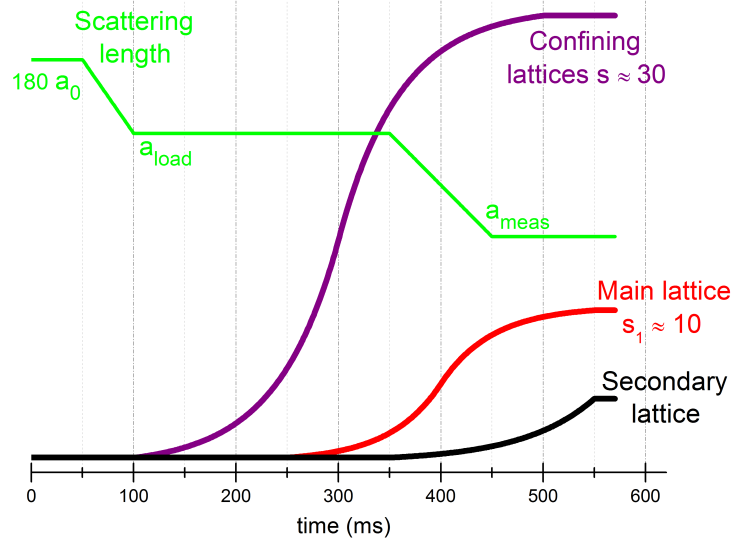


Figure 4.1: Experimental sequences for the loading of the condensate in the lattices.

first rough calculation can be done in the following way<sup>1</sup>. We first consider a three-dimensional Thomas-Fermi distribution for the interacting condensate in the optical trap. Let us consider a cylindrical symmetry and call  $R_r$  and  $R_z$  the Thomas-Fermi radii of the condensate along the radial and axial direction. Integrating the distribution along the vertical direction we get that the number of atoms per tube can be described by  $N_{tube} = N_{max} [1 - (r/R_r)^2]^{3/2}$ , where  $N_{max} = (5/2)N_{tot}d^2/\pi R_r^2$  is the number of atoms in the central tube and  $d = \lambda/2$  is the spacing of the tubes. Let us now consider what happens inside a single tube. Here the radial confinement is very strong, the transverse level spacing is large and atoms occupy only the groundstate. The system becomes effectively one dimensional. In particular the interparticle interaction in the longitudinal direction modifies, and we have to replace the three-dimensional s-wave scattering length  $a$ , by an effective one-dimensional scattering length defined as [72]:

$$a_{1D} = -\frac{a_r^2}{2a} \left[ 1 - C \left( \frac{a}{a_r} \right) \right], \quad (4.2)$$

where  $a_r$  is the harmonic oscillator length along the radial direction of the tubes and  $C = 1.4603\dots$  is a constant. If the atomic density is not low enough to enter the Tonks-Girardeau regime, the axial density distribution remains a Thomas Fermi-inverted parabola as in the three-dimensional case. The Thomas-Fermi distribution in one-dimension takes this form:

$$n(z) = n_{TF}^0 \left( 1 - \frac{z^2}{R_{TF}^2} \right), \quad (4.3)$$

<sup>1</sup>Similar calculations have been also considered for example in [70, 71, 46]

where  $n_{TF}^0 = [(9/64)N_{tube}^2(m\omega_z/\hbar)^2|a_{1D}|]^{1/3}$ , and

$$R_{TF} = \left[ \frac{3N_{tube}(\hbar/m\omega_z)^2}{|a_{1D}|} \right]^{1/3}. \quad (4.4)$$

To calculate the longitudinal harmonic frequency  $\omega_z$  we take into account the confinement induced by the optical trap beams and by the lattices beams.

The experiments reported in the following refer to two different situations. For a first set of measurements  $a_{load} = 20a_0$ . Following the calculations summarized above and averaging the atomic distributions in the tube, we estimate an average atom number per tube of 150. In a second set  $a_{load} = 190a_0$ , the average atom number per tube in this condition reduces and is approximately 60. The number of particle per lattice sites depends on the interaction energy determined by  $a_{meas}$ .

It is very important for a good characterization of the different quantum phases of the system to have a very cold sample. The thermal energy has in fact not to dominate over the other energies of the system. Too large temperatures mask the physics related to the interplay between disorder and interaction we are interested to study. Indeed, very interesting physics could arise from the study of the role of temperature in disordered systems and, although this kind of experimental investigation could be possible in future experiments on our apparatus, this is out of the aims of this thesis. For example the recently theoretically predicted temperature-induced metal-insulator transition [59] could be experimentally investigated. A good control over the temperature is however fundamentally important also in present experiments specially if we want to investigate correlation properties. Furthermore the most part of the many theoretical works on the topic considers the  $T = 0$  condition and for a comparison with our experimental results we need a very cold sample. For these reasons we concentrated our efforts in minimizing the heating during the experimental preparation of the sample. First of all the alignment of the lattices on the position of the condensate resulted to be very critical. Furthermore we optimize the duration and the shape of the ramps for the lattices and for the scattering length in order to minimize the heating. An active power stabilization of the lattices is also necessary to avoid heating during the loading and the measurements.

A good measurement of the temperature in the lattice is not trivial. However we obtain a first rough estimation in the following way. Starting from the condensate in the optical trap we ramp up the lattices following the procedure above described. With symmetrical ramps we then decrease the lattices potential down to zero and we measure the temperature of the atoms in the optical trap from time of flight images. We then have to make some assumptions in order to get

the temperature of the atoms in the lattice. First of all we assume that ramping up and ramping down the lattices heat up the system by the same amount and, therefore, that the entropy in the lattice is half than the one measured at the end. If we then assume that the loading process is isentropic, we can estimate the temperature in the lattice by rescaling the measured temperature with the known modification of the potential. For example the axial frequency in the tubes is approximately twice the one in the optical trap, because of the confinement induced by the two tight lattices beams. Furthermore the presence of the lattice potential is taken into account by considering the effective mass instead of the atomic mass. These considerations should be reasonable for a superfluid in a regular lattice, but possibly fails in the other situations and the estimation of the temperature is even more complex. In the presence of the quasiperiodic lattice, for example, the lattice band structure is modified and therefore also the effective mass. Starting from an initial temperature of the condensate in the trap of approximately 15 nK, typical estimated value of temperature are  $T \simeq 25 - 35$  nK.

## 4.2 Correlation measurements

In Fig.3.1 we showed a  $\Delta - U$  phase diagram of the width of the momentum distribution traced in a previous work in our group [15]. We note that the maximum interaction energy reached in that experiment was of the order of the tunneling energy  $J$ , far from being strong enough to allow the system to enter the Mott insulator regime. In a first experiment performed with the new experimental configuration described in the previous section, we repeated the momentum distribution measurements being now able to trace a complete  $\Delta - U$  phase diagram. Furthermore from the analysis of the Fourier transform of the momentum distribution we extract the correlation length of the atomic wavefunction and we obtain the phase diagram for this quantity too.

### 4.2.1 Analysis of the momentum distributions

The experimental procedure for the momentum distribution measurements is quite easy and not too different from the one used to investigate the weakly interacting sample. The momentum distribution of the atoms trapped in the one-dimensional (disordered) tubes is in fact simply obtained by imaging the atoms after a free expansion of 16 ms from the trapping potential which is suddenly switched off. From the analysis of the momentum distribution and of its Fourier transform we can measure the correlation length of the atomic wavefunction. In the superfluid

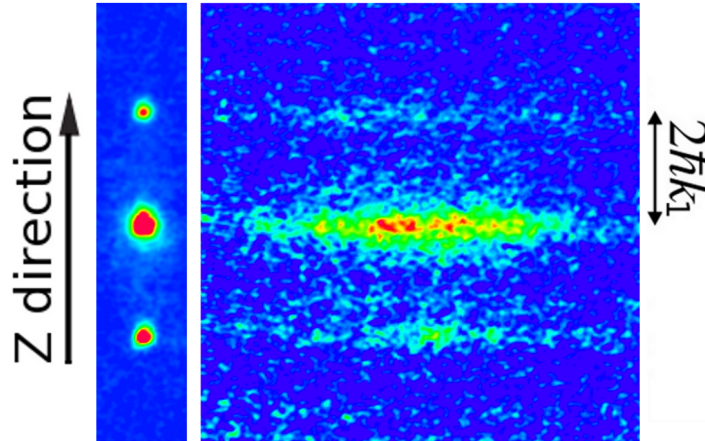


Figure 4.2: Momentum distribution of a superfluid atomic sample in a lattice aligned along the  $\hat{z}$  direction. The picture on the left refers to atoms in a single three-dimensional tube, the picture on the right refers to atoms in an array of quasi one-dimensional tubes

phases the (Wannier) wavefunctions centered in each lattice site are phase-locked to each other and interfere giving rise to sharp peaks in the density distribution. The distance between the peaks corresponds to the sized of the Brilluin zone in the momentum space, that is  $2\pi\hbar/d = 2\hbar k_1$ , being  $d = \lambda_1/2$  the lattice spacing. On the contrary, insulating phases are characterized by the absence of coherence between atoms sitting in different lattice sites which results in the broadening of the momentum distribution.

In Fig.4.2 we compare the momentum distribution of two superfluid samples in a lattice. On the left, we show the momentum distribution of atoms trapped in a one dimensional lattice aligned on a three dimensional condensate, i.e. the configuration we used for the experiments in the weakly interacting regime reported in the previous section. On the right, the image refers to atoms trapped in the two-dimensional array of one-dimensional tubes obtained with two tight lattices along the  $\hat{x}$  and  $\hat{y}$  direction. A shallower lattice is instead align along the  $\hat{z}$  direction where the atoms are in the superfluid phase. Along the  $\hat{z}$  direction the two momentum distributions coincide since they both refers to superfluid atoms in a lattice. Horizontally the atoms showed in the first image are trapped in a single (three dimensional) tube and we do not observe any structure in this direction. The stripes in the second image are instead a clear evidence of the absence of phase coherence between the wavefunctions belonging to the different tubes created by the two-dimensional tight lattice and are thus a confirmation of the fact that atoms are trapped in an array of one-dimensional systems independent from each other.

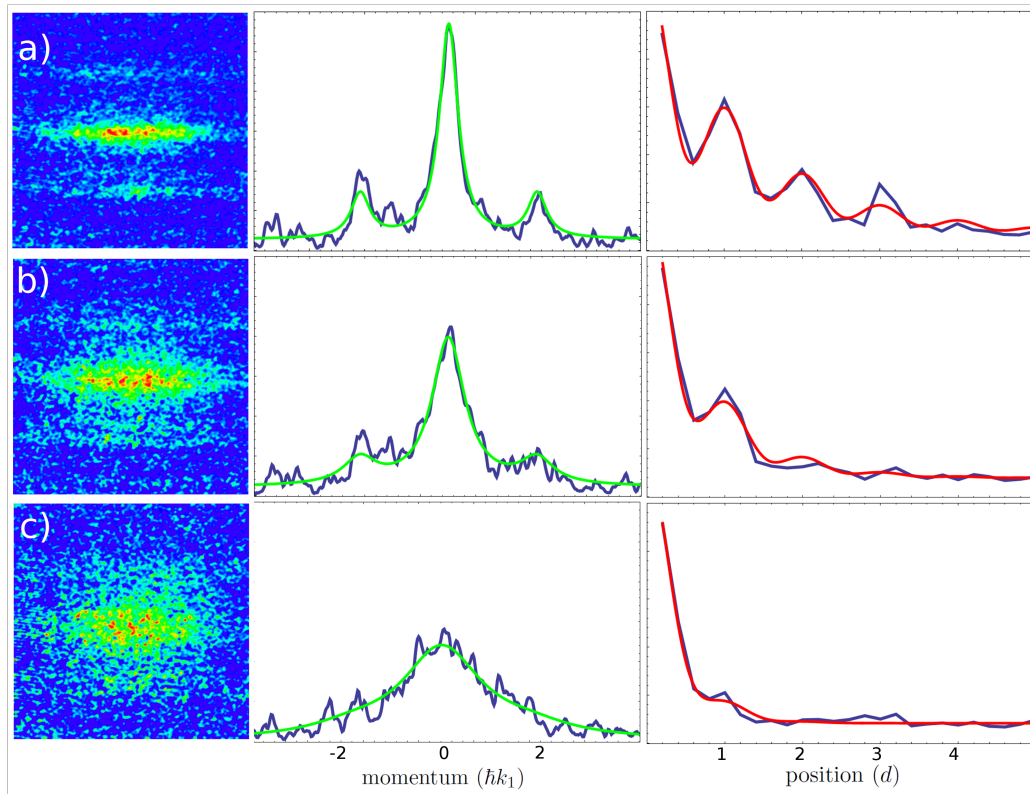


Figure 4.3: Analysis of the time of flight imaging for a non interacting sample in a clean lattice (a), and in the quasiperiodic lattice with  $\Delta/J = 8$  (b) and  $\Delta/J = 12$  (c). The radially integrated momentum distribution images are fitted with three Lorentzian peaks. The Fourier transform, which gives the correlation function, is fitted with a sinusoidally modulated exponential decay.

The Fourier transform of the momentum distribution gives the spatially average correlation function according to Eq.(3.6). For a uniform non-interacting gas in one-dimension the mean square fluctuations of the phase of the atomic wavefunction can be calculated following [47]. They are expected to feature a linear diverge for large separation  $x$ :

$$\langle [\Delta\phi(x)]^2 \rangle = \frac{mkT}{n_{1D}\hbar^2}|x|, \quad (4.5)$$

where  $n_{1D} = N/L$  is the number of particles per unit length. Thus the correlation function decays exponentially,

$$\rho(x) \simeq n_{1D}e^{-|x|/2L_\phi}, \quad (4.6)$$

with correlation length

$$L_\phi = \frac{n_{1D}\hbar^2}{mk_B T}. \quad (4.7)$$

For an infinite system a condensate is obtained only for  $T = 0$ . In finite systems, the phase is well correlated throughout the system, which thus behaves as a true condensate, provided the linear dimension of the system  $L$  is less than  $L_\phi$ . This implies that:

$$T \ll \frac{T_{1D}}{N}, \quad (4.8)$$

where we define  $T_{1D} = \frac{\hbar^2 n_{1D}^2}{mk_B}$ . In a trap, the region with larger density dominates and the effective correlation length is larger and can be estimate as  $L_\phi/0.67$  [73, 74]. The momentum distribution of a trapped one-dimensional gas at finite temperature, which is the Fourier transform of the correlation function, is therefore a Lorentzian distribution whose width is inversely proportional to the correlation length:

$$P(p) \propto \frac{1}{p^2 + \left(\frac{0.67\hbar}{L_\phi}\right)^2}. \quad (4.9)$$

In the experiment we study atoms in one dimensional lattices. The presence of the lattice along the one-dimensional system also affects the correlation properties of the system. In particular, a more proper estimation of the correlation length has to be taken into account the reduce mass of the atom in the periodical potential [46]. In order to calculate  $L_\phi$  for our system we substitute  $m$  with  $m^* = 2\hbar^2/J\lambda^2$  in Eq.(4.7).

The time of flight images of the atomic cloud are analyzed as shown in Fig.4.3. The radially integrated momentum distribution is fitted with three Lorentzian peaks  $2\hbar k_1$  apart from each other. Its Fourier transform, the correlation function, is instead fitted with an exponential decay, which is periodically modulated by

the presence of the lattice potential. The period of the sinusoidal modulation is  $d = \lambda_1/2$ . The values of correlation length extracted from the two fitting procedures are in good agreement.

### 4.2.2 $\Delta - U$ Phase diagram

The analysis of the atomic momentum distribution for various values of the disorder strength and of the interaction energy gives the possibility to characterize the crossover between superfluid and insulating phases. Narrow peaks in the momentum distribution and large correlation lengths are indication of a superfluid phase, whereas, on the contrary, an insulating phase is characterized by broad peaks and short correlation length. Besides the disorder induced insulating phase (Anderson glass), the new experimental configuration allows us to access also the interacting induced one (Mott insulator) and to trace a full phase diagram.

The density of the sample during the measurements is typically large and, in average, more than 3 atoms populate the same lattice site. To avoid three-body losses, the atoms are kept only for a short time (few tens of ms) in the three-dimensional lattice before opening the trapping potentials and taking the time of flight image.

Let us starting by considering the non-interacting case. In Fig.4.4 we show the measured correlation length for a non-interacting system. We repeat the same measurement for the two different value of  $a_{load}$  which correspond to two different atomic densities in the tubes. When we increase the disorder strength the correlation length decreases indicating the crossover from a superfluid to a disorder-induced localized system. For  $\Delta/J > 2$  the system has localized eigenfunction with localization length  $\xi = 1/\ln(\Delta/2J)$ . The value of the measured correlation length is close to the one expected for the localized wavefunction shown in the figure by the dashed gray line. In the clean lattice the correlation length is expected to be the one calculated by Eq.(4.7), considering the effective mass of the atoms in the lattice. Actually if we estimate the temperature and the atomic density as previously described, we get a larger value of  $L_\phi$ . According to the calculation, for the two different densities, we obtain in fact  $L_\phi \simeq 2.5, 5$ . The smaller measured value can be due to an underestimation of the temperature and an overestimation of the density. The measured value of  $L_\phi$  approaches the calculated one when we consider a superfluid interacting sample indicating a more reliable estimation of the density and of the temperature. For example if we consider the density estimated for  $U/J = 3$  we get a correlation length smaller than 2 lattice sites.

In Fig.4.5 we compare the measured evolution of the correlation length  $L_\phi$  for

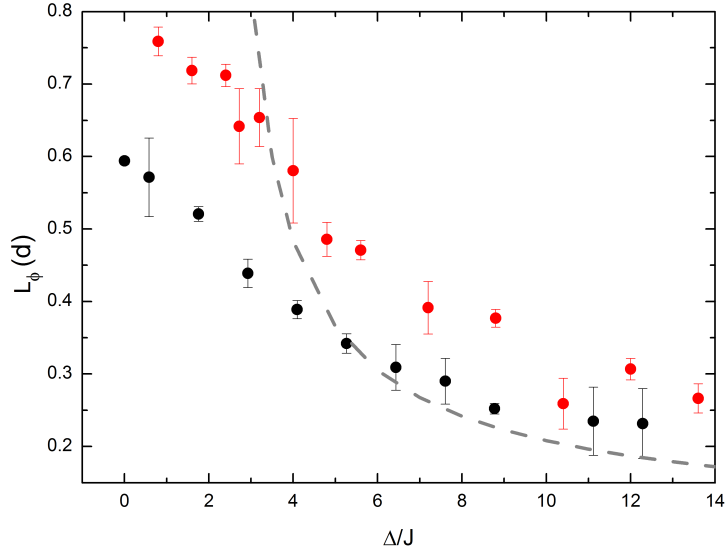


Figure 4.4: Measured correlation lengths of the non-interacting system for increasing value of  $\Delta/J$ . Red (black) points refer to the situation in which  $a_{load} = 20(190)$  and the average atom number per tube is 150 (60). The dashed line indicates the correlation length of a localized wavefunction with localization length  $\xi = 1/\ln(\Delta/2J)$ .

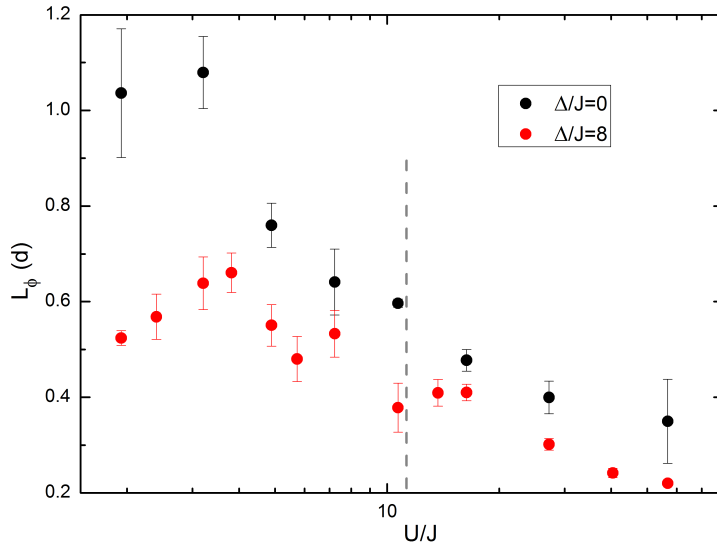


Figure 4.5: Measured correlation lengths for increasing  $U/J$  and in the quasiperiodic lattice with  $\Delta/J = 8$  and  $\Delta/J = 12$ .

increasing interaction energies in a clean lattice and in a disordered one ( $\Delta/J = 8$ ). In the clean case ( $\Delta/J = 0$ ), we observe, as expected, a decreasing of the correlation length for increasing  $U/J$  which corresponds to a transition from a superfluid to an insulating phase. The transition is not sharp and well defined but it is spread over a wide range of  $U/J$  and it can be more properly called crossover. The reason is that the system is not homogeneous neither along the tubes nor in the density of the different tubes. As discussed in section 1.4 the transition to a Mott insulator (MI) state occur at a  $n$ -dependent critical value of  $U/J$  that in the one-dimensional case can be calculated with Eq.(1.27). The transition to MI domains with a small occupancy  $n$  occurs at lower interaction values than those required to enter MI domains with higher  $n$ . The center of the crossover coincides with the calculated critical value for the interaction energy considering the calculated mean site occupation  $\bar{n} \simeq 5$ :  $(U/J)_c \simeq 11$ . The dashed line in the picture indicates such value of interaction.

In the disordered case, the non-interacting correlation length is smaller than in the clean case. For weak interacting energies it increases indicating the crossover from the localized Anderson glass phase to the superfluid phase passing through the weakly interacting Bose phase. Keeping increasing the interaction strength,  $L_\phi$  decreases again. It is interesting to note that in this regime of interactions (before the fully localization induced by the interaction) the disorder system has a smaller localization length with respect to the clean lattice. This is an indication of a cooperation of disorder and interaction in creating an insulating phase conversely to what happens in the weakly interaction regime. The decrease of the correlation length for large interaction in the disordered lattice is compatible with the fact that the system enters the insulating Bose glass phase.

We repeated the momentum distribution measurement and analysis for various values of the disorder  $\Delta/J$ , ranging from 0 to 20, and of the interaction energy  $U/J$ , ranging from 0 to 80. By interpolating the experimental results we can trace the phase diagrams of Fig.4.6 for both the width of the momentum distribution (calculated as the rms of the momentum distribution central peak) and the correlation length. By referring to the rms plot we can qualitatively describe the phase changes occurring in the atomic system. At small disorders and small interactions, the momentum distribution is narrow (blue zone), and the system is in a superfluid (SF) phase. At larger disorder and interaction the momentum distribution progressively broadens (green, yellow and red zones) meaning that the system is more and more insulating. We can recognize in the phase diagram the different quantum regimes described in the first chapter of this thesis. In an ordered system

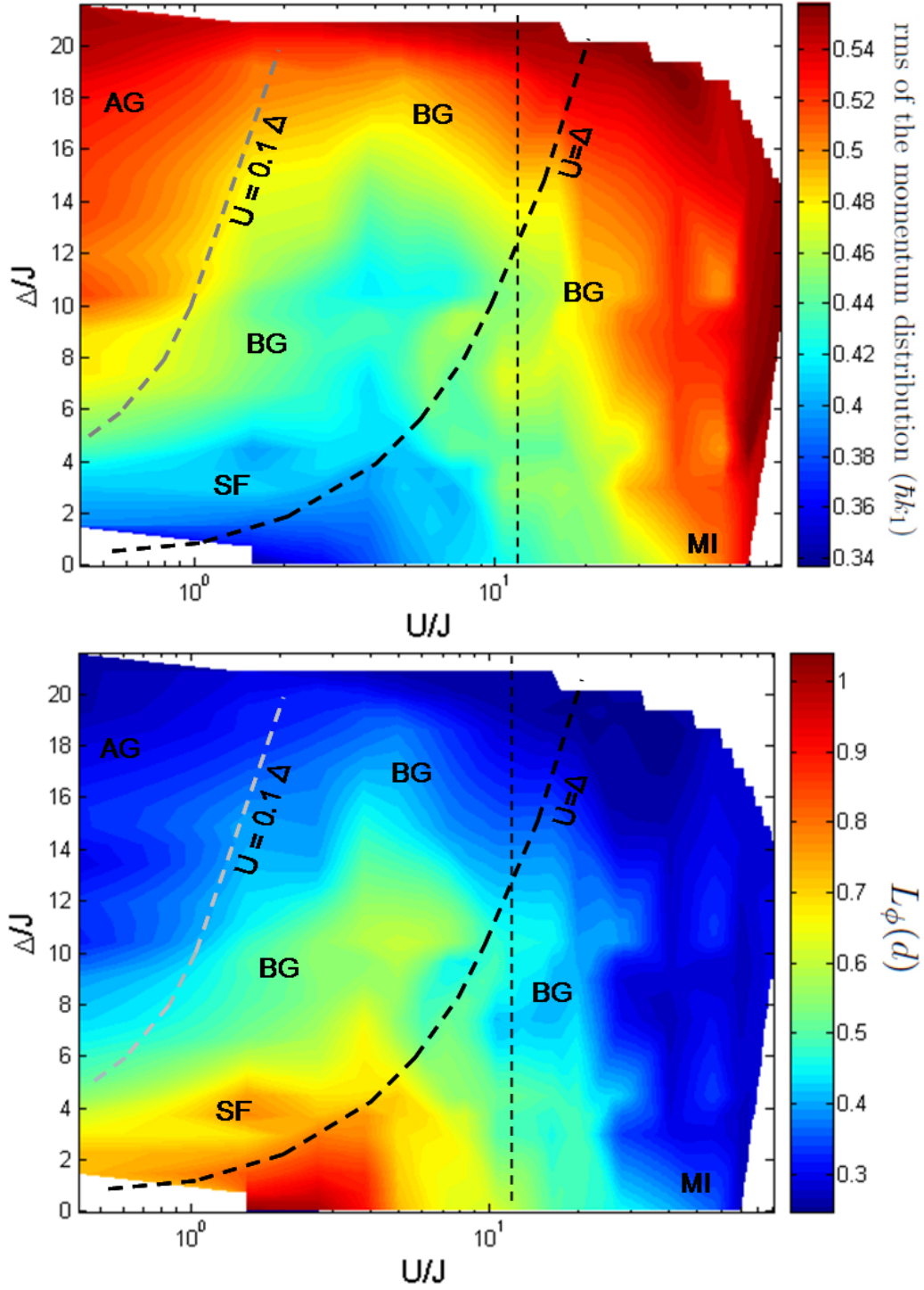


Figure 4.6: Phase diagrams. Top: rms of the momentum distribution central peak. Bottom: Correlation length  $L_\phi$  extracted from the fit of the Fourier transform of the momentum distribution. With BG we label the zone of the phase diagram where we expect a Bose glass phase.

( $\Delta/J = 0$ ), as already mentioned, the system undergoes a crossover from a SF to a MI phase as the interaction becomes sufficiently large. The vertical dashed line on the diagram indicates the calculated critical value of interaction energy  $(U/J)_c$  for the transition to MI for a one-dimensional system with occupancy  $n = 5$ .

An analogous crossover from superfluid to insulator is also observed in the non-interacting case ( $U/J \simeq 0$ ). For increasing disorder amplitude  $\Delta/J$  the system enters in fact the disorder-induced localized Anderson glass (AL) phase. For weak interaction energies, as expected, for a given  $\Delta/J$  value and increasing  $U/J$  (i.e. moving along a horizontal line in the phase diagram) the system delocalizes. According to the discussed screening arguments (sec.1.3), the AG-SF crossover occurs at an interaction energy  $U = 0.1\Delta$ , which is the full width of the first “miniband” of the quasiperiodic lattice (sec.2.3.1). The dashed gray line on the phase-diagram indicates such a value<sup>2</sup>.

Let us now come to the most recently debated and still poorly experimentally explored zone of the phase diagram: the strongly correlated disordered system. If we keep increasing the interaction for a given disorder, we observe that, after an intermediate coherent zone, the momentum distribution starts to broaden again. Interestingly, this broadening happens for smaller values of interaction energy than in the clean case. This can also be appreciated if one fixes a given  $U/J$  values and moves vertically on the phase-diagram increasing the disorder: the momentum distribution width increases indicating a more insulating state. In this zone of the phase diagram, where a disordered insulating phase is observed even though the interaction is not yet strong enough to induce localization by itself, the system has the expected behavior of a Bose glass.

Even if the weakly interacting and the strongly interacting Bose glass show the same glassy features, the roles played by disorder and interactions in the two cases are pretty different. In the weakly interacting regime, interactions and disorder have competing effects: interactions serve to smooth the disordered potential and create a more coherent state. Conversely, in the strongly correlated regime, they cooperate in creating an insulating phase. One possible mechanism we can imagine, for example, in the region close to the Mott insulator, is that inhomogeneities introduced in the system by the disorder potential help the system to reach in

<sup>2</sup>Since the crossover from the localized to the superfluid system occurs over a large range of interaction energy, it is difficult to fix a transition value for the interaction energy. However the full width of the first “miniband”,  $0.1\Delta$ , seems to be a reasonable estimation. In previous experiments in our group [15, 51] we observed the transition for smaller values of the interaction energy. In that case, however, the presence of populated higher radial modes could have shifted the transition towards smaller values of interactions

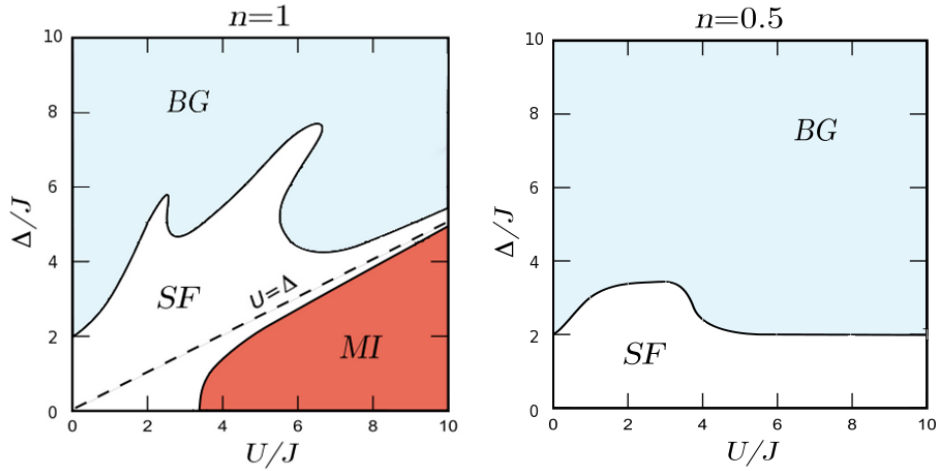


Figure 4.7:  $\Delta - U$  phase diagrams obtained by numerically solving the Bose-Hubbard problem for an occupancy  $n = 1$  (left) and  $n = 0.5$  (right). The dashed line in the phase diagram on the left shows [34].

certain region the commensurate filling necessary for the Mott-insulator to form, acting as local traps. This would break the superfluid into smaller pieces.

The presence of a Bose glass phase has to be confirmed by other measurements aimed to investigate the transport capability and the excitation spectrum of the system. Preliminary measurements of these kinds are reported in the next sections.

### Theoretical phase diagram

The  $\Delta - U$  phase diagram for atoms in a quasiperiodic potential has been also traced in theoretical works [34, 35], numerically solving the Bose-Hubbard problem. Referring to Fig.4.7 we note that, besides the MI and the SF phases, a unique glassy phase, indicated as Bose glass (BG), is present for large disorder amplitudes. The weakly interacting glassy phase studied in the previous chapter and the strongly interacting one we intend to investigate here, present in fact the same features. Both phases are globally insulating though they are characterized by the presence of superfluid zones. This fact results in a finite compressibility of the system and in a gapless excitation spectrum.

We also note that the phase diagram shows different quantum phases according to the occupancy of the lattice sites. Since an integer occupancy is required for the Mott insulator to form, in the case  $n = 0.5$  showed in the right of the picture for example, only the SF and the BG phases exist. These phase diagram are traced for a single homogeneous one-dimensional system. The experimental situation, as already pointed out, is by far more complex. The experimental system is in fact

composed by several (few hundreds) one dimensional inhomogeneous systems with different atomic densities. Different phases can thus coexist in the system according to the local chemical potential. The experimental phase diagram results to be a “combination” of different theoretical phase diagrams with different occupancies of the lattice sites and the theoretical sharp transitions become crossover between different phases.

### 4.3 Transport measurements

A confirmation of the insulating or conducting (superfluid) nature of the different phases can be obtained by transport measurements. Measurements of this kind are expected to be less sensitive to the finite temperature of the experimental system and to the possible variations of the temperature across the phase diagram. To evaluate the transport capability of the system we apply an impulse on the condensate in the lattice and we measure the momentum transferred to the atoms. In insulator phases the system dissipate the energy that does not translates in momentum [75]. A similar experiment to study a strongly interacting disordered system has been performed by Pasienski *et al.* [22].

Transport measurements are performed in the same experimental conditions as the correlation measurements reported in the phase diagrams in Fig.4.6. The experimental procedure is also similar except that the harmonic vertical confinement induced by the optical trap beams is switched off  $300\mu\text{s}$  before the lattices potentials. The sudden change of the vertical potential applies an impulse on the condensate. We then evaluate the momentum transferred to the atoms,  $\Delta p$ , by measuring the displacement of the central peak of the momentum distribution as shown in Fig.4.8. When the system is in a superfluid phase we transferred momentum is around  $0.32 \hbar k_1$ . This value approaches zero when the system enters an insulating phase. In the superfluid system we can also appreciate an unbalance in the high of the lateral peaks.

We repeat this measurement for increasing values of the interaction energy  $U/J$  for the clean lattice and for two values of disorder ( $\Delta/J = 8$  and  $\Delta/J = 12$ ) i.e. moving along three horizontal lines in the phase diagram. The results are reported in panel a) of Fig.4.9. The interpretation of these data is similar to what already discussed for the correlation measurements and gives a confirmation of the results. In the clean case the system undergoes a crossover from a conducting to an insulating phase by increasing the interaction. The center of the crossover is around the calculated critical interaction energy for the transition to a Mott

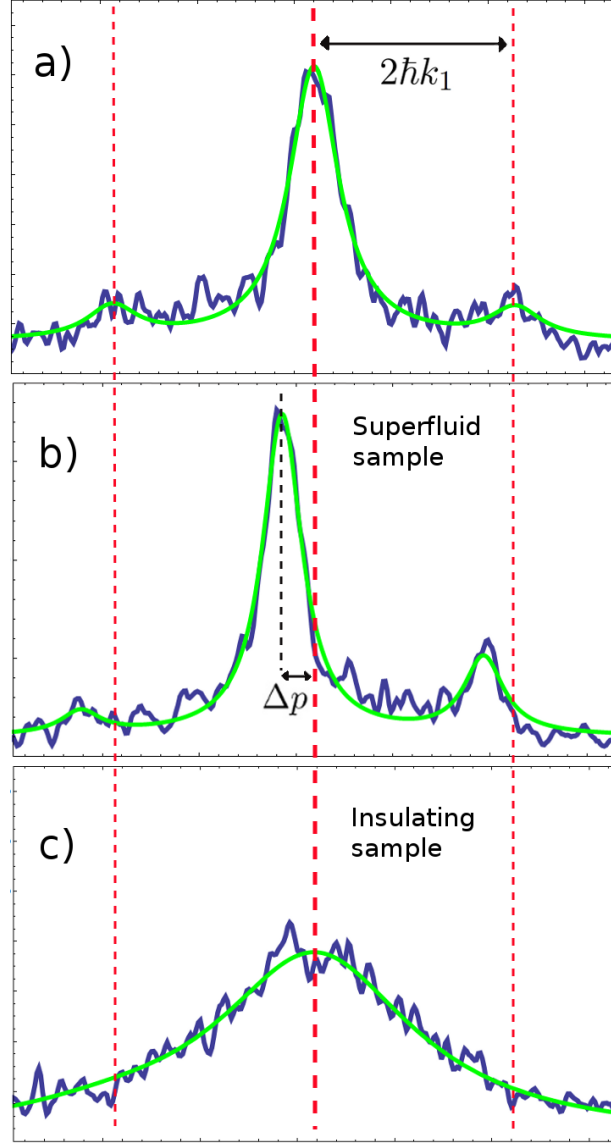


Figure 4.8: Analysis of the transport measurements. Figure a) shows the momentum distribution of a superfluid sample when the optical trap confinement is simultaneously switched off with the lattices potentials. We take the central peak position as a reference. Figure b) shows the momentum distribution of a superfluid sample ( $\Delta/J = 0$  and  $U/J = 0$ ) and figure c) of an insulating sample ( $\Delta/J = 0$ ,  $U/J = 70$ ) when the optical trap is switched off  $300\mu\text{s}$  before the lattices. The applied impulse translates into a transferred momentum  $\Delta p$  in the superfluid case and the position of the central peak moves. In the insulating case, on the contrary, the peak, besides broadening, stays centered at the same position as the reference one.

insulator phase considering an occupation density of 5 atoms per lattice site. The momentum distribution peaks in fact progressively broaden and the transferred momentum vanishes. The applied impulse does not transfer almost any momentum to the atoms for  $U/J \geq 80$  and the system is in a completely insulating phase.

In the two disordered cases, for very small  $U/J$ , the system is in an insulator state (Anderson glass) and the transferred momentum  $\Delta p$  is small. Increasing the interaction energy we observe that  $\Delta p$  first increases, indicating the crossover from the Anderson glass to the superfluid, and then decreases again demonstrating the presence of a crossover to a new disordered insulating phase. Increasing the disordered strength generally leads to greater dissipation, confirming the presence of an insulating disordered phase for interaction energies that are not large enough, in a clean lattice, to lead the system in a Mott insulator state.

In panel b) of Fig.4.9 we plot the dependence of the rms of the momentum distribution on the interaction energy. In the clean lattice case, when the system is superfluid, the rms after the applied impulse is the same as the one of the unperturbed system. Interestingly we note that we do not detect any difference in the width of the distribution in the two disordered cases. This is probably due to the fact that the dissipation of the applied impulse causes an increase of the temperature, that translates into a larger momentum distribution, even when the system is not completely insulating.

The transport measurements together with the correlation measurements give a clear indication of the insulation nature of the system in a range of parameters where it can not be neither an Anderson glass or a weakly interacting Bose glass, because of the strong interaction energy between particles, nor a Mott insulator since the interaction alone is not strong enough to induce localization. The measurement of a gapless excitation spectrum of the system in this zone of the phase diagram would give the confirmation of the presence of superfluid islands in a globally insulating sample, i.e. of a Bose glass.

## 4.4 Excitation spectra measurements

In this section we present preliminary measurements of the excitation spectrum of our system. As briefly discussed in sec.1.4 and 1.5 we expect that in a superfluid gas any amount of energy can be transferred into the system. Conversely in a Mott insulating phase the lowest possible excitation is at energy  $U$ . The excitation spectrum of a Mott insulator is thus characterized by a gap at low energies whereas

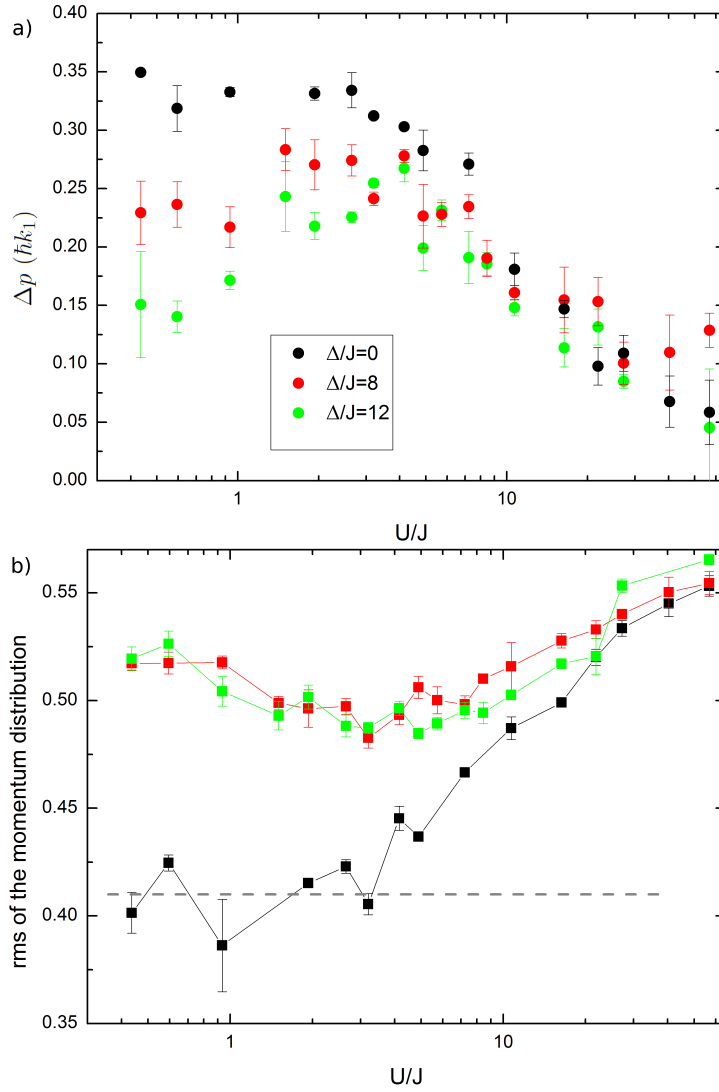


Figure 4.9: Transferred momentum  $\Delta p$  (a) and rms of the momentum distribution (b) after an applied impulse vs  $U/J$ . Three sets of data refer to three different value of the disorder:  $\Delta/J = 0$ ,  $\Delta/J = 8$  and  $\Delta/J = 12$ . The dashed gray line in panel b) indicate the rms of the momentum distribution of system when no impulse is applied.

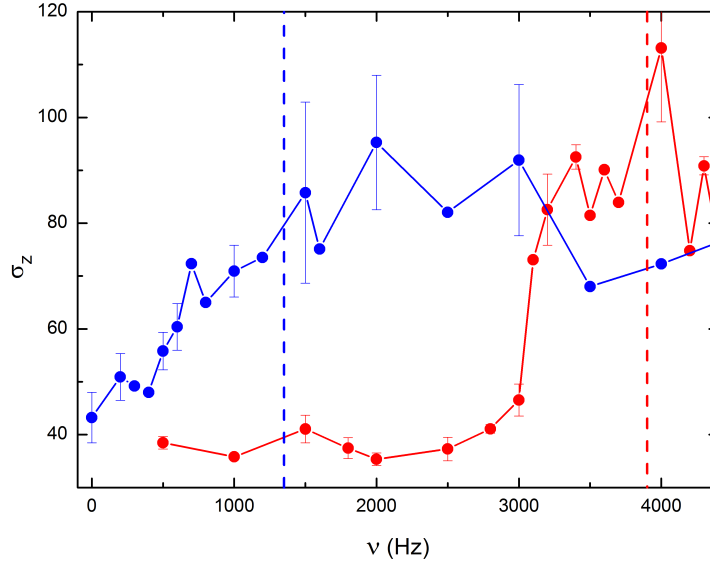


Figure 4.10: Excitation spectra of a superfluid gas ( $\Delta/J = 0$  and  $U/J \simeq 15$ ) and of a Mott-insulator ( $\Delta/J = 0$  and  $U/J \simeq 50$ ). Excitations are detected from a double component Gaussian fit of the atomic cloud after expansion as an increase in the size of the thermal component. Dashed lines indicate the value of the interaction energy  $U$ .

the superfluid excitation spectrum is gapless. A gas in the Bose glass phase, even though it is globally insulating, is characterized by the presence of superfluid islands. The excitation spectrum of a Bose glass is thus expected to be gapless as the superfluid one.

Experimentally the excitation spectrum of the one-dimensional gases is measured with the following procedure. A sinusoidal modulation of the main lattice height  $s_1$ , with frequency  $\nu$  and amplitude 20%, stimulates the resonant production of excitation with energy  $h\nu$ . We detect the excitations produced after 200 ms of modulation by decreasing to zero, with exponential ramps lasting 300 ms, the intensities of the confining lattices and of the quasiperiodic lattice. At the same time we increase the optical trap confinement in order to keep trapped also the atoms heated by the excitation. We then take images of the atomic cloud after 16 ms of free expansion from the optical trap and we fit them with a bimodal Gaussian distribution. Excitations are detected either by the decreasing of the condensed fraction or by the increasing of the size of the thermal component, since both effects indicate an increase of the thermal energy of the system. To avoid three body losses during the modulation of the lattice, for these measurements we use  $a_{load} = 190$  in order to have a lower density along the tubes.

In a first experiment, whose results are shown in Fig.4.10, we consider atoms in a clean lattice ( $\Delta = 0$ ). We compare the excitation spectra of the system for two

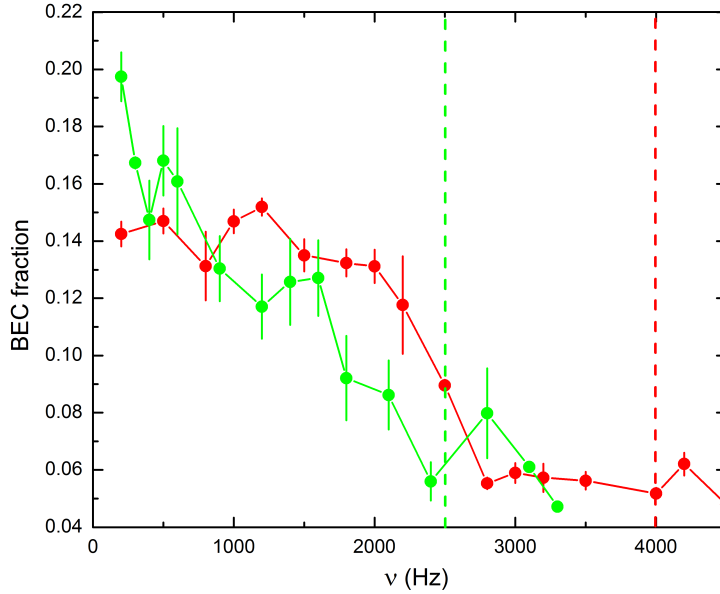


Figure 4.11: Excitation spectra of a Mott insulator ( $\Delta/J = 0$  and  $U/J \simeq 50$ ) and of a Bose glass ( $\Delta/J = 7$  and  $U/J \simeq 30$ ). Excitations are detected from a double component Gaussian fit of the atomic cloud after expansion as an decrease in the condensed fraction. Dashed lines indicate the value of the interaction energy  $U$ .

different values of the interaction energy;  $U/J \simeq 15$  and  $U/J \simeq 50$ . For the lower interaction strength the gas is in the superfluid phase and the modulation of the lattice causes excitation at any frequency. On the contrary, when  $U/J$  is larger, modulations under a certain frequency do not excite the system indicating a Mott-insulator state. The minimum energy needed to excite the system is expected to be  $U$  (see sec.1.4). This reference value for the energy is indicated in the figure with dashed lines for the two cases.

In a second experiment, shown in Fig.4.11, we compare the excitation spectra of the system in the Mott insulator phase ( $\Delta/J = 0$  and  $U/J \simeq 50$ ) with the one of a disordered interacting system ( $\Delta/J = 7$  and  $U/J \simeq 30$ ). The value of interaction energy for the disordered system has been chosen in order to have a comparable value of the correlation length  $L_\phi$  in the two situations.  $L_\phi$  has been measured from the momentum distribution analysis as previously described. The disordered system spectrum shows the same characteristic as the spectrum of a superfluid gas. The system is in fact excited for any value of the modulation frequency.

In conclusion, we have shown that, for a certain range of large interactions and disorder, the system is insulating since it has a short coherence length as a Mott insulator or an Anderson glass, although it has a gapless excitation spectrum like

a superfluid. We note that the disorder strength is however not strong enough to dominate the behavior of the system and in particular we have  $\Delta < U$ . In this range of the parameter we have thus observed the presence of a Bose glass phase.



# Conclusions

In conclusion, in this thesis we have studied bosonic atoms in a quasiperiodical one-dimensional lattice investigating the ground state properties and the transport of such a system in both regimes of weak and strong interactions. Experiments with cold atoms in general have demonstrated their capability to give responses to open questions in the field of the physics of disorder thanks to the possibility that they offer to tune all the important parameters of the physical system in a controlled way. The experiments reported in this thesis are an example of the contribution given by quantum gases experiments.

Disorder has been recognized to have a dominating role in determining many physical phenomena. The complex and intriguing physics of disordered systems has been attracting an increasing interest not only in the quantum gases community but in many different fields. From condensed matter physics to optics from statistical mechanics to biophysics, the study of disordered induced phenomena is, for sure, still open and in evolution.

More in details in this thesis, in the weakly interacting regime, we characterized the crossover from the disordered induced localized phase (Anderson glass) to the superfluid phase, passing through an intermediate glassy phase (weakly interacting Bose glass). We measured, in particular, the local shape of the wavefunction and its correlation length when we vary the interaction energy. We also studied the transport induced in the disordered system either by a weak interaction between atoms or by a temporal noise on the potential. We gave the first experimental evidence of the subdiffusive expansion of a wavepacket in a disordered medium in presence of non-linearities. We also provide a first investigation of the combined effect of noise and interaction on the dynamical delocalization.

In the strongly correlated regime we performed measurements of the correlation length, of the transport properties and of the excitation spectrum of the system. We provided the first full experimental phase diagram which shows a complex structure with different insulating and non-insulating regions for a wide range of

disorder and interaction. These experiments aim to experimentally characterize the theoretically predicted strongly interacting Bose glass phase.

Many questions remain open and have to be addressed in the future. For example, one important point to be clarified is the role of the spatial correlations of the disordered potential in both the transport dynamics and in the ground-state properties. In this sense it might be interesting to shape potentials with tunable spatial correlation length, both perturbing a periodical lattice and in free space. To do this, speckle potentials or holographic potentials created by spatial light modulators might be used. With these kinds of potentials one might also investigate the barely explored topic of disorder physics in two and three dimensions. In fact, the most part of the experiments, have been so far performed in one-dimension and also the theoretical works are mostly devoted to the study of one-dimensional systems. Another interesting issue is the role of the finite temperature in disordered systems. Also in this case from the theoretical side few results are available [59], and the experimental investigation has just started. Another line of interesting research is the physics of disorder induced by impurities. This is a common situation in condensed matter systems and can be simulated in cold atoms experiments by quantum mixtures [76, 77, 78].

Grazie a Giovanni Modugno per l'attenzione che mi ha dato in questi anni e per avermi permesso di svolgere il lavoro che ho presentato in questa tesi. Lo ringrazio per la sua così evidente passione per la fisica e la ricerca.

Grazie al Prof. Inguscio e a tutti i colleghi del *Quantum gases group* del LENS. Lavorare in un gruppo così ricco di persone competenti ed entusiaste è stato molto arricchente e stimolante. Ringrazio tutti per le discussioni e i consigli, oltre che per il materiale prestato, in particolare Chiara Fort, Nicole Fabbri, Giacomo Lamporesi e Manuele Landini.

Un grazie speciale alle persone con cui ho lavorato in laboratorio. Grazie a Giacomo Roati, Ben Deissler e Matteo Zaccanti. Un grazie davvero sentito a Chiara D'Errico e Luca Tanzi con cui ho condiviso la maggior parte del lavoro che ho presentato in questa tesi. Grazie a Chiara per la disponibilità e l'amicizia, anche al di fuori del laboratorio, che mi ha dimostrato dal primo momento in cui ho messo piede al LENS. E grazie a Luca per la sua serenità e per il sostegno, forse alle volte anche involontario, che mi ha dato in questi anni. Grazie anche a Lorenzo Gori, da poco arrivato alla BEC 2, ma il cui contributo è già grande. Mi rendo conto della fortuna che ho a lavorare con tre persone che apprezzo e stimo come loro.

Ringrazio poi gli amici teorici per le utili discussioni: Marco Moratti, Marco Larcher e Filippo Caruso. Le simulazioni numeriche riportate in questa tesi sono opera loro.

Grazie inoltre al Prof. Bagnato, a Sergio Muniz, Jorge Seman, Patricia Castilho e Jackson Poveda. Le tre settimane in laboratorio con loro a São Carlos son state un'esperienza breve, ma per me davvero importante.

Grazie a Italia e Valeria per l'amicizia consolidata da tre anni di convivenza. Grazie anche ad Andrea, Francesco, agli amici della scuola di ballo Salsacaliente e della banda musicale di Sesto per tutti i momenti di divertimento e amicizia che ho vissuto con loro in questi anni. Grazie infine a tutti gli amici "lombardi" e alla mia famiglia, perché ci sono sempre.

Dedico questa tesi al mio papà, oltre che alla mia mamma e a Francesca, con un affetto che va aldilà di ogni distanza.



# Bibliography

- [1] M. P. A. Fisher, P. B. Weichman, G. Grinstein and D. S. Fisher, *Boson localization and the superfluid-insulator transition*, Phys. Rev. B **40**, 546-570 (1989)
- [2] D. Jaksch, C. Bruder, J. I. Cirac, C. W. Gardiner and P. Zoller, *Cold Bosonic Atoms in Optical Lattices*, Phys. rev. Lett. **81**, 3108 (1998)
- [3] P. W. Anderson, *Absence of Diffusion in Certain Random Lattices*, Phys. Rev. **109**, 1492 (1958)
- [4] R. Dalichaouch, J. P. Armstrong, S. Schultz, P. M. Platzman and S. L. McCall, *Microwave localization by two-dimensional random scattering*, Nature **354**, 53 (1991)
- [5] D. S. Wiersma, P. Bartolini, A. Lagendijk and R. Righini, *Localization of light in a disordered medium*, Nature **390**, 671 (1997)
- [6] T. Schwartz, G. Bartal, S. Fishman and M. Segev, *Transport and Anderson localization in disordered two-dimensional photonic lattices*, Nature **446**, 52 (2006).
- [7] Y. Lahini, A. Avidan, F. Pozzi, M. Sorel, R. Morandotti, D. N. Christodoulides and Y. Silberberg, *Anderson Localization and Non-linearity in One-Dimensional Disordered Photonic Lattices*, Phys. Rev. Lett. **100**, 013906 (2008).
- [8] A. Aspect and M. Inguscio, *Anderson localization of ultracold atoms*, Physics Today **62**, 8, 30 (2009)
- [9] J. Billy, V. Josse, Z. Zuo, A. Bernard, B. Hambrecht, P. Lugan, D. Clément, L. Sanchez-Palencia, P. Bouyer, A. Aspect, *Direct observation of Anderson localization of matter waves in a controlled disorder*, Nature **453**, 891 (2008)

- 
- [10] G. Roati, C. D’Errico, L. Fallani, M. Fattori, C. Fort, M. Zaccanti, G. Modugno, M. Modugno, and M. Inguscio, *Anderson localization of a non-interacting Bose-Einstein condensate*, Nature **453**, 895 (2008)
- [11] C. D’Errico, *Anderson localization of a weakly interacting Bose-Einstein condensate*, PhD Thesis, University of Florence (2009).
- [12] F. Jendrzejewski, A. Bernard, K. Müller, P. Cheinet, V. Josse, M. Piraud, L. Pezzé, L. Sanchez-Palencia, A. Aspect and P. Bouyer, *Three-dimensional localization of ultracold atoms in an optical disordered potential*, arXiv:1108.0137v2
- [13] S. S. Kondov, W. R. McGehee, J. J. Zirbel, B. DeMarco, *Three-Dimensional Anderson Localization of Ultracold Fermionic Matter*, arXiv:1105.5368v1
- [14] D. K. K. Lee and J. M. F. Gunn, *Bosons in a random potential: condensation and screening in a dense limit*, J. Phys.: Condens. Matter **2**, 7753-7768 (1990)
- [15] B. Deissler, M. Zaccanti, G. Roati, C. D’Errico, M. Fattori, M. Modugno, G. Modugno and M. Inguscio, *Delocalization of a disordered bosonic system by repulsive interactions*, Nature Phys. **6**, 354 (2010)
- [16] M. Greiner, O. Mandel, T. Esslinger, T. W. Hansch and I. Bloch, *Quantum phase transition from a superfluid to a Mott insulator in a gas of ultracold atoms*, Nature **415**, 39 (2002)
- [17] M. J. Mark, E. Haller, K. Lauber, J. G. Danzl, A. J. Daley, and H.C. Nägerl *Precision Measurements on a Tunable Mott Insulator of Ultracold Atoms*, arXiv:1107.1803v1
- [18] T. Stöferle, H. Moritz, C. Schori, M. Köhl and T. Esslinger, *Transition from a Strongly Interacting 1D Superfluid to a Mott Insulator*, Phys. Rev. Lett. **92**, 130403 (2004)
- [19] W. S. Bakr, A. Peng, M. E. Tai, R. Ma, J. Simon, J. I. Gillen, S. Folling, L. Pollet, and M. Greiner, *Probing the Superfluid to Mott Insulator Transition at the Single Atom Level*, Science **329**, 547 (2010)
- [20] J. F. Sherson, C. Weitenberg, M. Endres, M. Cheneau, I. Bloch and S. Kuhr *Single-atom-resolved fluorescence imaging of an atomic Mott insulator* Nature **467**, 68 (2010)

- 
- [21] L. Fallani, J. E. Lye, V. Guarrera, C. Fort, and M. Inguscio, *Ultracold Atoms in a Disordered Crystal of Light: Towards a Bose Glass*, Phys. Rev. Lett. **98**, 130404 (2007)
- [22] M. Pasienski, D. McKay, M. White and B. DeMarco *A disordered insulator in an optical lattice*, Nature Phys. **6**, 677 (2010)
- [23] M. White, M. Pasienski, D. McKay, S. Q. Zhou, D. Ceperley and B. DeMarco *Strongly interacting Bosons in a Disordered Optical Lattice*, Phys. Rev. Lett. **102**, 055301 (2009)
- [24] R. Grimm, M. Weidemüller, and Y. B. Ovchinnikov, *Optical dipole traps for neutral atoms*, Advances in Atomic, Molecular and Optical Physics **42**, 95 (2000).
- [25] M. Modugno, *Teoria dei condensati di Bose-Einstein* Appunti del corso di Fenomeni Quantistici Macroscopici, Universit degli studi di Firenze
- [26] K. Sheshadri, H. R. Krishnamurthy, R. Pandit and T. V. Ramakrishnan, *Superfluid and Insulating Phases in an Interacting-Boson Model: Mean-Field Theory and the RPA*, Europhys. Lett. **22**, 257 (1993)
- [27] P. L. Gould, G. A. Ruff and D. E. Pritchard, *Diffraction of atoms by light: The near-resonant Kapitza-Dirac effect*, Phys. Rev. Lett. **56**, 827 (1986)
- [28] H. Feshbach, *A Unified Theory of Nuclear Reactions*, Ann. Phys. **5**, 357 (1958).  
H. Feshbach, *A Unified Theory of Nuclear Reactions. II*, Ann. Phys. **19**, 287 (1962).
- [29] U. Fano, *Sullo spettro di assorbimento dei gas nobili presso il limite dello spettro d'arco*, Nuovo Cimento **12**, 156 (1935).
- [30] C. Chin, R. Grimm, P. Julienne, E. Tiesinga, *Feshbach resonances in ultracold gases*, Rev. Mod. Phys. **82**, 1225-1286 (2010)
- [31] A. J. Moerdijk, B. J. Verhaar and A. Axelsson, *Resonances in ultracold collisions of  ${}^6\text{Li}$ ,  ${}^7\text{Li}$ , and  ${}^{23}\text{Na}$* , Phys. Rev. A **51**, 48524861 (1995)
- [32] C. D'Errico, M. Zaccanti, M. Fattori, G. Roati, M. Inguscio, G. Modugno and A. Simoni, *Feshbach resonances in ultracold  ${}^{39}\text{K}$* , New J. Phys. **9**, 223 (2007).

- 
- [33] J. W. Goodman, *Speckle Phenomena in Optics: Theory and Applications*, Roberts and Company Publishers, (2007).
- [34] G. Roux, T. Barthel, I. P. McCulloch, C. Kollath, U. Schollwöck and T. Giamarchi, *Quasiperiodic Bose-Hubbard model and localization in one-dimensional cold atomic gases*, Phys. Rev. A **78**, 023628 (2008)
- [35] X. Deng, R. Citro, A. Minguzzi and E. Orignac, *Phase diagram and momentum distribution of an interacting Bose gas in a bichromatic lattice*, Phys. Rev. A **78**, 023606 (2008)
- [36] M. Modugno *Exponential localization in one-dimensional quasi-periodic optical lattice*, New J. Phys. **11**, 033023 (2009)
- [37] P. Lugan, A. Aspect, L. Sanchez-Palencia, D. Delande, B. Grémaud, C. A. Müller, C. Miniatura, *One-dimensional Anderson localization in certain correlated random potentials*, Phys. Rev. A **80**, 023605 (2009)
- [38] M. Landini, *A tunable Bose-Einstein condensate for quantum interferometry*, PhD Thesis, University of Trento (2012)
- [39] G. Roati, *Quantum degenerate Potassium-Rubidium mixtures*, PhD Thesis, University of Trento (2003).
- [40] F. Ferlaino, *Atomic Fermi gases in an optical lattice*, PhD Thesis, University of Florence (2004).
- [41] E. de Mirandes, *Bloch oscillations of ultracold atoms*, PhD thesis, University of Florence (2005).
- [42] C. D'Errico, *Osservazione di Risonanze di Fano-Feshbach in miscele atomiche K-Rb*, Master Thesis, University of Florence (2005).
- [43] M. Zaccanti, *Tuning of the interactions in ultracold K-Rb quantum gases*, PhD thesis, University of Florence (2007).
- [44] M. Girardeau, *Relationship between Systems of Impenetrable Bosons and Fermions in One Dimension*, J. Math. Phys. **1**, 516 (1960).
- [45] E. H. Lieb, W. Liniger, *Exact Analysis of an Interacting Bose Gas. The General Solution and the Ground State*, Phys. Rev. **130**, 1605 (1963).

- 
- [46] B. Paredes, A. Widera, V. Murg, O. Mandel, S. Fölling, I. Cirac, G. V. Shlyapnikov, T. W. Hänsch and I. Bloch, *Tonks-Girardeau gas of ultracold atoms in an optical lattice*, Nature **429**, 277 (2004)
- [47] C. J. Pethick, H. Smith, *Bose-Einstein condensation in Dilute Gases*, Cambridge University Press (2001).
- [48] B. Damski, J. Zakrzewski, L. Santon, P. Zoller and M. Lewenstein, *Atomic Bose and Anderson glasses in optical lattices*, Phys. Rev. Lett. **91**, 080403 (2003)
- [49] T. Giamarchi and H. J. Schulz, *Anderson localization and interactions in one dimensional metals*, Phys. Rev. B **37**, 325-340 (1988)
- [50] P. Lugan, D. Clément, P. Bouyer, A. Aspect, M. Lewenstein, and L. Sanchez-Palencia, *Ultracold Bose Gases in 1D Disorder: From Lifshits Glass to Bose-Einstein Condensate*, Phys. Rev. Lett. **98**, 170403 (2007)
- [51] B. Deissler, E. Lucioni, M. Modugno, G. Roati, L. Tanzi, M. Zaccanti, M. Inguscio and G. Modugno, *Correlation function of weakly interacting bosons in a disordered lattice*, New J. Phys. **13**, 023020 (2011)
- [52] F. Dalfovo, S. Giorgini, L. Pitaevskii and S. Stringari, *Theory of Bose-Einstein condensation in trapped gases*, Rev. Mod. Phys. **71**, 463 (1999)
- [53] L. Fontanesi, M. Wouters and V. Savona, *Superfluid to Bose-Glass Transition in a 1D Weakly Interacting Bose Gas*, Phys. Rev. Lett. **103**, 030403 (2009)
- [54] L. Fontanesi, M. Wouters and V. Savona, *Mean-field phase diagram of the one-dimensional Bose gas in a disorder potential*, Phys. Rev. A **81**, 053603 (2010)
- [55] A. Cetoli and E. Lundh, *Correlations and superfluidity of a one-dimensional Bose gas in a quasiperiodic potential*, Phys. Rev. A **81**, 063635 (2010)
- [56] E. Lucioni, B. Deissler, L. Tanzi, G. Roati, M. Zaccanti, M. Modugno, M. Larcher, F. Dalfovo, M. Inguscio and G. Modugno, *Observation of Subdiffusion in a Disordered Interacting System*, Phys. Rev. Lett. **106**, 230403 (2011)
- [57] D. L. Shepelyansky, *Delocalization of Quantum Chaos by Weak Nonlinearity*, Phys. Rev. Lett. **70**, 1787 (1993)
- [58] M. Mulansky and A. S. Pikovsky *Spreading in Disordered Lattices with Different Nonlinearities*, Europhys. Lett. **90**, 10015 (2010)

- [59] I. L. Aleiner, B. L. Altshuler and G. V. Shlyapnikov, *A finite-temperature phase transition for disordered weakly interacting bosons in one dimension*, Nat. Phys. **6**, 900 (2010)
- [60] B. L. Altshuler, Y. Gefen, A. Kamenev and L. S. Levitov, *Quasiparticle Lifetime in a Finite System: A Nonperturbative Approach*, Phys. Rev. Lett. **78**, 2803 (1997)
- [61] T. V. Laptjeva, J. D. Bodyfelt, D. O. Krimer, Ch. Skokos and S. Flach, *The crossover from strong to weak chaos for nonlinear waves in disordered systems*, Europhys. Lett. **91**, 30001 (2010)
- [62] S. Flach, D.O. Krimer, C. Skokos, *Universal Spreading of Wave Packets in Disordered Nonlinear Systems*, Phys. Rev. Lett. **102**, 024101 (2009)
- [63] D. O. Krimer, S. Flach, *Statistics of wave interactions in nonlinear disordered systems*, Phys. Rev. E **82**, 046221 (2010)
- [64] M. Larcher, F. Dalfovo and M. Modugno, *Effects of interaction on the diffusion of atomic matter waves in one-dimensional quasiperiodic potentials*, Phys. Rev. A **80**, 053606 (2009)
- [65] B. Tuck, *Some explicit solutions to the non-linear diffusion equation*, Journ. of Phys. D: Appl. Phys. **9**, no. 11, 1559-1569 (1976).
- [66] F. Sagues, J. M. Sancho, J. Garcia-Ojalvo, *Spatiotemporal order out of noise*, Rev. Mod. Phys. **79**, 829 (2007)
- [67] C. D'Errico *et al.*, *Experimental interplay of noise and interaction in Anderson localization suppression*, in preparation
- [68] D. A. Steck, V. Milner, W. H. Oskay and M. G. Raizen, *Quantitative study of amplitude noise effects on dynamical localization*, Phys. Rev. E **62**, 34613475 (2000)
- [69] E. Ott, T. M. Antonsen and J. D. Hanson, *Effect of Noise on Time-Dependent Quantum Chaos*, Phys. Rev. Lett. **53**, 2187 (1984)
- [70] P. Pedri, L. Pitaevskii, S. Stringari, C. Fort, S. Burger, F. S. Cataliotti, P. Maddaloni, F. Minardi and M. Inguscio, *Expansion of a Coherent Array of Bose-Einstein Condensates*, Phys. Rev. Lett. **87**, 220401 (2001)

- 
- [71] B. Laburthe Tolra, K.M. OHara, J. H. Huckans, W. D. Phillips, S. L. Rolston, and J. V. Porto, *Observation of Reduced Three-Body Recombination in a Correlated 1D Degenerate Bose Gas*, Phys. Rev. Lett. **92**, 190401 (2004)
- [72] V. Dunjko, V. Lorent and M. Olshanii, *Bosons in Cigar-Shaped Traps: Thomas-Fermi Regime, Tonks-Girardeau Regime, and In Between*, Phys. Rev. Lett. **86**, 5413 (2001)
- [73] S. Richard, F. Gerbier, J. H. Thywissen, M. Hugbart, P. Bouyer and A. Aspect, *Momentum Spectroscopy of 1D Phase Fluctuations in Bose-Einstein Condensates*, Phys. Rev. Lett. **91**, 010405 (2003)
- [74] F. Gerbier, J. H. Thywissen, S. Richard, M. Hugbart, P. Bouyer and A. Aspect, *Momentum Distribution and Correlation Function of quasicondensates in elongated traps.*, Phys. Rev. A **67**, 051602(R) (2003)
- [75] A. Polkovnikov, E. Altman, E. Demler, B. Halperin and M. D. Lukin, *Decay of superfluid currents in a moving system of strongly interacting bosons*, Phys. Rev. A **71**, 063613 (2005)
- [76] U. Gavish and Y. Castin, *Matter-Wave Localization in Disordered Cold Atom Lattices*, Phys. Rev. Lett. **95**, 020401 (2005).
- [77] M. Antezza, Y. Castin and D. Hutchinson, *Quantitative study of two- and three-dimensional strong localization of matter waves by atomic scatterers*, Phys. Rev. A **82**, 043602 (2010).
- [78] J. Stasińska, P. Massignan, M. Bishop, J. Wehr, A. Sanpera and M. Lewenstein, *Glass to superfluid transition in dirty bosons on a lattice*, arXiv:1111.3494v1 (2011)